INNER RING FATIGUE ANALYSIS OF ROLLING ELEMENT BEARINGS

A THESIS SUBMITTED TO
THE GRADUATE SCHOOL OF NATURAL AND APPLIED SCIENCES
OF
MIDDLE EAST TECHNICAL UNIVERSITY

BY

BARIŞ EROĞLU

IN PARTIAL FULFILLMENT OF THE REQUIREMENTS
FOR
THE DEGREE OF MASTER OF SCIENCE
IN
MECHANICAL ENGINEERING

FEBRUARY 2009

Approval of the thesis:

INNER RING FATIGUE ANALYSIS OF ROLLING ELEMENT BEARINGS

submitted by **BARIŞ EROĞLU** in partial fulfillment of the requirements for the degree of **Master of Science in Mechanical Engineering, Middle East Technical University** by,

Prof. Dr. Canan Özgen
Dean, Graduate School of **Natural and Applied Sciences** _____

Prof. Dr. Süha Oral
Head of Department, **Mechanical Engineering** _____

Prof. Dr. Haluk Darendeliler
Supervisor, **Mechanical Engineering Dept., METU** _____

Examining Committee Members

Prof. Dr. Metin Akkök
Mechanical Engineering Dept., METU _____

Prof. Dr. Haluk Darendeliler
Mechanical Engineering Dept., METU _____

Prof. Dr. Mustafa İlhan Gökler
Mechanical Engineering Dept., METU _____

Prof. Dr. Suat Kadıoğlu
Mechanical Engineering Dept., METU _____

Prof. Dr. Can Çoğun
Mechanical Engineering Dept., Gazi University _____

Date: 09.02.2009

I hereby declare that all information in this document has been obtained and presented in accordance with academic rules and ethical conduct. I also declare that, as required by these rules and conduct, I have fully cited and referenced all material and results that are not original to this work.

Name, Last Name: Barış EROĞLU

Signature:

ABSTRACT

INNER RING FATIGUE ANALYSIS OF ROLLING ELEMENT BEARINGS

Eroğlu, Barış
M.S., Department of Mechanical Engineering
Supervisor: Prof. Dr. Haluk Darendeliler

February 2009, 108 pages

Rolling element bearings are the one of the most widely used machine elements in the industry. The most important criterion in bearing selection is the endurance life. The first attempts on the prediction of the endurance life of rolling elements bearings are done by Lundberg and Palmgren in 1950s (Harris, 1999). Their work adopted as an ANSI, ABMA and ISO standard which is widely used in industry today. The basic assumption of Lundberg-Palmgren formulation is that no matter how small the load applied on rolling element bearing, all material in the stressed volume is subject to fatigue failure.

In this study, four main life theories; Weibull, Lundberg-Palmgren, Ioannides-Harris, and Zaretsky on rolling element bearings have been investigated. Three-dimensional finite element models of a bearing's inner ring and rolling element have been prepared. The stress fields within the inner ring and the ball with respect to the applied load are obtained numerically. The fatigue life of the inner ring has been predicted by two methods that are widely used for fatigue analysis; Total Life Analysis (S-N method) and Crack Initiation Analysis (ε-N method). Obtained results are compared with ISO formulation.

As a result of the investigation, S-N and ε -N methods are determined to give more conservative results than ISO method for higher loads that cause stresses above the fatigue limit of the material. The used methods for bearing life prediction recognize the existence of the fatigue limit stress. Hence as the stresses within an operating bearing do not exceed the limit stress, the bearing can achieve infinite life. It is also observed that load variation has a direct influence on the bearing life. When the load significantly changes from the levels which create stress above the fatigue limit to the levels that result stress is below the fatigue limit, the bearing would have higher endurance life than predicted by ISO method.

Keywords: Rolling Element Bearing, Fatigue Life, Finite Element Method

ÖZ

RULMAN İÇ BİLEZİĞİNİN YORULMA ÖMRÜ ANALİZİ

Eroğlu, Barış
Yüksek Lisans, Makina Mühendisliği Bölümü
Tez Yöneticisi: Prof. Dr. Haluk Darendeliler

Şubat 2009, 108 sayfa

Rulman endüstride en çok kullanılan makine elemanlarından biridir. Rulman seçiminde göz önünde tutulması gereken en önemli kıstas rulmanın yorulma ömrüdür. Rulman ömrünün öngörülebilmesi için ilk çalışmalar 1950'lerde Lundberg ve Palmgren tarafından yapılmıştır (Harris, 1999). Bu çalışmaların sonuçları ANSI, ABMA ve ISO standartlarına geçmiş ve günümüzde sanayide yaygın olarak kullanılmaktadır. Lundberg-Palmgren formülasyonu, rulmana etki eden kuvvet ne kadar küçük olursa olsun, gerilim altındaki hacmin yorulmaya maruz kalacağını kabul eder.

Bu çalışmada, rulmanların yorulma ömrü için geliştirilmiş olan dört temel metot olan; Weibull, Lundberg-Palmgren, Ioannides-Harris, Zaretsky metodları incelenmiştir. Rulman iç bileziği ve bilyenin sonlu elemanlar modeli oluşturulmuş, iç bilezik ve bilya içindeki gerilim değerleri değişken rulman yüklerine göre sayısal olarak tespit edilmiştir. İç bilezik yorulma hesapları Tüm Ömür Analizi (S-N metodu) ve Çatlak Oluşumu Analizi (ε-N metodu) kullanılarak yapılmıştır. Elde edilen sonuçlar ISO formülasyonu ile karşılaştırılmıştır.

Çalışmanın sonunda, S-N ve ε-N metotları ile gerçekleştirilen ömür hesaplarının ISO metoduna göre malzemenin yorulma sınırından daha yüksek gerilmeye neden olan yüksek yükler için daha muhafazakar sonuçlar verdiği tespit edilmiştir. Kullanılan

yöntemler malzemenin yorulma sınırını göz önünde bulundurmaktadır. Bundan dolayı rulman içindeki gerilmelerin sınır gerilmeden daha büyük olmadığı durumlarda rulman ömrü sınırsız olmaktadır. Buna ek olarak rulman üzerindeki değişken yüklerin rulman ömrüne doğrudan etki ettiği tespit edilmiştir. Rulmana etkiyen kuvvetin yarattığı gerilimlerin malzemenin yorulma sınırının üzerindeki seviyelerden, uygulanan kuvvetlerin yarattığı gerilimlerin yorulma sınırı altında kalan seviyelere değişmesi durumunda rulman ömrünün ISO formülasyonu ile öngörülenden daha fazla olacağı tespit edilmiştir.

Anahta Kelimeler: Rulman , Yorulma Ömrü, Sonlu Elemanlar Metodu

To My Family and M. K. ATATÜRK

ACKNOWLEDGEMENTS

The author would like to express his appreciation and thankfulness to Prof. Dr. Haluk Darendeliler for his encouragements, advice, guidance, and support that created this study.

The author also wishes to thank ORS Bearings and Turkish Aerospace Industry where he always gets support and learn engineering practice in his early professional life.

Finally, author would like to thank his wife Aylin Konez Eroğlu for her support and endless patience throughout this study.

TABLE OF CONTENTS

LIST OF TABLES

LIST OF FIGURES

FIGURES

LIST OF SYMBOLS

Symbol	Symbol Name	Unit
a	Semimajor axis of the projected elliptical area of contact	mm
a*	Dimensionless semimajor axis of contact ellipse	-
a_1	Reliability factor	-
a_2	Material factor	-
a_3	Lubricant factor	-
A	Material-life factor	-
A_m	Material factor for ball bearings	-
A_R	Amplitude ratio	-
b	Semiminor axis of the projected elliptical area of contact	mm
b*	Dimensionless semiminor axis of contact ellipse	-
c	Empirical shear stress exponent	-
C	Dynamic load capacity of the bearing	N
C_0	Static load rating	N
d	Diameter of the stress track	mm
d_m	Pitch diameter of the bearing	mm
d_i	Inner ring raceway contact diameter	mm
d_{ir}	Inner ring diameter	mm
d_{or}	Outer ring diameter	mm
D_b	Ball diameter	mm
D_i	Damage fraction	1/cycle
e	Weibull slope	-
e_a	Nominal strain amplitude	-
E	Modulus of elasticity	MPa-GPa
f_0	Factor based on bearing raceway material and geometry	-
f_{cm}	Factor based on bearing raceway material and geometry	-
F	Probability of rupture	-
F_r	Radial load	N
g	Fatigue ductility exponent	-
$G(\rho)$	Curvature difference	-

h	Empirical exponent	-
H	Minimum lubricant film thickness	mm
i	Number of rows	-
$J_r(\kappa)$	Load distribution integral	-
K	Ratio of Young's modulus of inclusion and matrix	-
K′	Cyclic strength coefficient	-
K_t	Stress concentration factor	-
K_σ	True stress concentration factor	-
K_ε	True strain concentration factor	-
L	Life of the bearing	million cycles
L_{10}	Fatigue life that 90% of the bearing population will endure	million cycles
L_{50}	Median life that 50% of the bearing population will endure	million cycles
L_{na}	Modified life for special material properties and operating conditions	million cycles
L_{rw}	Fatigue life of the raceway	million cycles
L_{rwi}	Fatigue life of the inner ring	million cycles
L_{rwo}	Fatigue life of the outer ring	million cycles
L_n	Life in revolutions corresponding to reliability level n	million cycles
m	Load deflection exponent	-
M	Empirical constant for cumulative damage calculation	-
n	Stress-life exponent	-
n′	Cyclic strain hardening exponent	-
n_i	Total number of applied cycles	
N	Number of stress cycles endured	-
N_f	Number of load reversals to failure	-
N_t	Transition life	-
p	Empirical load-life exponent	-
P	Equivalent load on bearings	N
P_u	Limit load for fatigue	N
Q	Contact normal load	N
Q_c	Dynamic capacity of the raceway	N
Q_{ci}	Dynamic capacity of the inner ring	N

Q_{co}	Dynamic capacity of the outer ring	N
Q_e	Cubic mean load	N
$Q_{e\mu}$	Cubic mean load for rotating ring for fatigue life calculation	N
$Q_{e\upsilon}$	Cubic mean load for non-rotating ring for fatigue life calculation	N
Q_j	Loading on rolling element in position j	N
Q_{max}	Maximum ball load	N
Q_ψ	Rolling element load depends the angle ψ	N
r	Radius of curvature	mm
r_i	Raceway groove radius of the inner ring	mm
r_o	Raceway groove radius of the outer ring	mm
R	Stress ratio	-
S	Nominal stress	MPa-GPa
S_a	Alternating or variable stress amplitude	MPa-GPa
S_e, S_6	Endurance or fatigue limit stress	MPa-GPa
S'_f	Fatigue strength coefficient	MPa-GPa
S_H	Maximum Hertz stress	MPa-GPa
S_i	Stress amplitude	MPa-GPa
S_x, S_y, S_z	Principal stresses	MPa-GPa
S_m	Mean stress	MPa-GPa
S_{max}	Maximum stress	MPa-GPa
S_{min}	Minimum stress	MPa-GPa
S_r	Stress range	MPa-GPa
S_u	Ultimate tensile strength	MPa-GPa
S_y	Yield stress	MPa-GPa
ΔS	Nominal stress range	MPa-GPa
t	Fatigue strength exponent	-
U	Probability of survival	-
V	Stressed volume	m^3-mm^3
υ	Poisson's ratio	-
z	Depth from the surface	mm
z_{cr}	Depth of critically stresses volume	mm
Z	Number of rolling elements per row	-

σ	Stress	MPa-GPa
$\overline{\sigma}$	Maximum von Mises Stress	MPa-GPa
σ_a	True cyclic stress amplitude	MPa-GPa
σ_{max}	Maximum contact stress	MPa-GPa
σ_θ	Tangential normal stress	MPa-GPa
$\Delta\sigma$	Local stress range	MPa-GPa
τ	Critical shear stress	MPa-GPa
τ_0	Maximum value of subsurface orthogonal shear stress	MPa-GPa
τ_1	Endurance limit of shear stress	MPa-GPa
τ_{oct}	Octahedral shear stress	MPa-GPa
τ_{max}	Maximum shear stress	MPa-GPa
ρ	Radius of curvature	mm^{-1}
δ	Deformation at the center of contact	mm
$\delta*$	Dimensionless contact deformation	-
κ	Load distribution factor	-
ψ	Angle from the azimuth	rad-degree
α	Nominal contact angle	rad-degree
β	Composite rms roughness of the contacting surfaces	-
ε_a	Strain amplitude	-
ε_e	Elastic strain amplitude	-
ε_f'	Fatigue ductility coefficient	-
ε_p	Plastic strain amplitude	-
ε_t	Total strain	-
Δe	Nominal strain range	-
$\Delta\varepsilon$	Local strain range	-
$\Delta\varepsilon_e$	Elastic strain range	-
$\Delta\varepsilon_p$	Plastic strain range	-
$\Delta\varepsilon_t$	Total strain range	-

CHAPTER 1

INTRODUCTION

In this chapter, a brief summary of bearing classification and bearing parts are given. Bearing materials, lubrication, definitions of characteristic life requirements, and failure modes of the rolling element bearings are discussed.

The purpose of a rolling element bearing is to transmit a load between two structures while providing rotational freedom. Rolling element bearings are desirable when to compared other bearings, such as fluid film bearings, when low starting torque and low friction is required, and combined radial and thrust loads are present (Stella, 2006).

1.1 A GENERAL CLASSIFICATION OF ROLLING BEARINGS

Rolling bearings are one of the most commonly used machine elements in many fields of industry and generally, are constructed by inner and outer rings, rolling elements that are running in the raceways. Standard shapes of rolling elements include the ball, cylindrical roller, needle roller, tapered roller, symmetrical and unsymmetrical barrel roller (Figure 1.1).

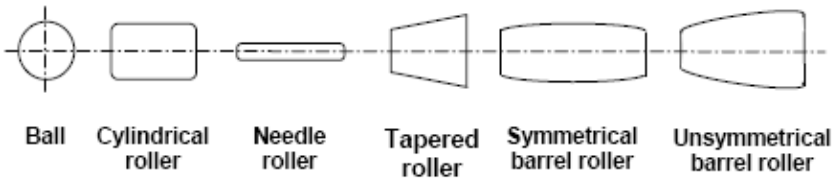

Figure 1.1 Rolling elements for roller and ball bearings

The main parts of a rolling bearing are given in Figure 1.2. Generally the rolling elements are guided in a cage that ensures uniform spaces and prevents the contact between rolling elements. The cage of a separable bearing has the additional function of holding together the rolling element set and therefore facilitates the bearing mounting. Rolling elements together with the cage are circled by the inner and the outer rings. The protection of inner region of the bearing, i.e., rolling elements and their paths, is achieved by rubber seals or metal shields.

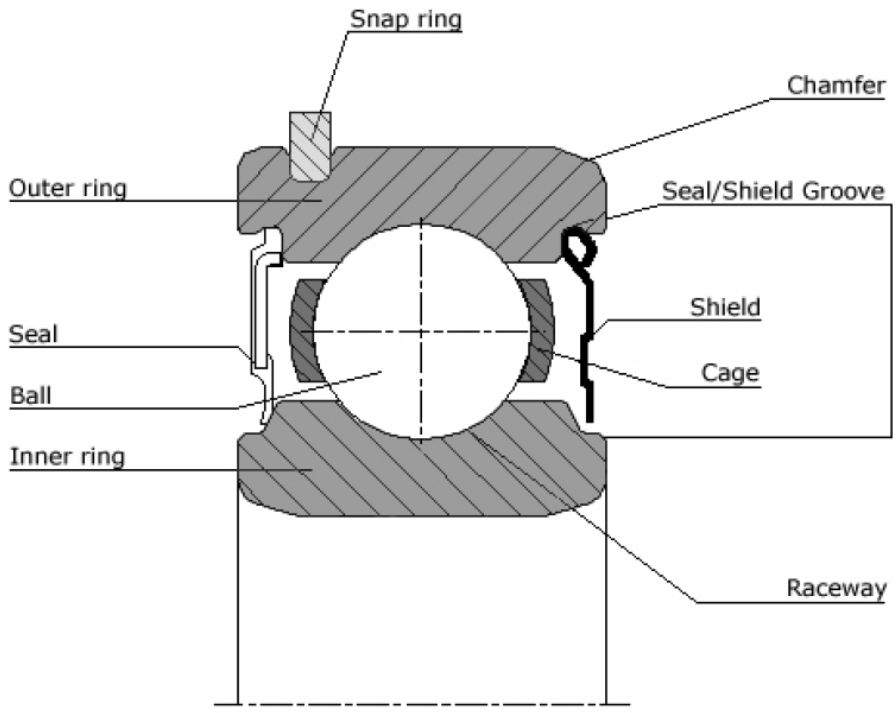

Figure 1.2 Designation of a radial ball bearing (ORS Bearings, 2005)

The radial and axial loading capacity with ball and roller elements forms 4 main branches on classification of bearings which is given in Figure 1.3. Further classification is done according to features like row number, roller shape, contact type etc.

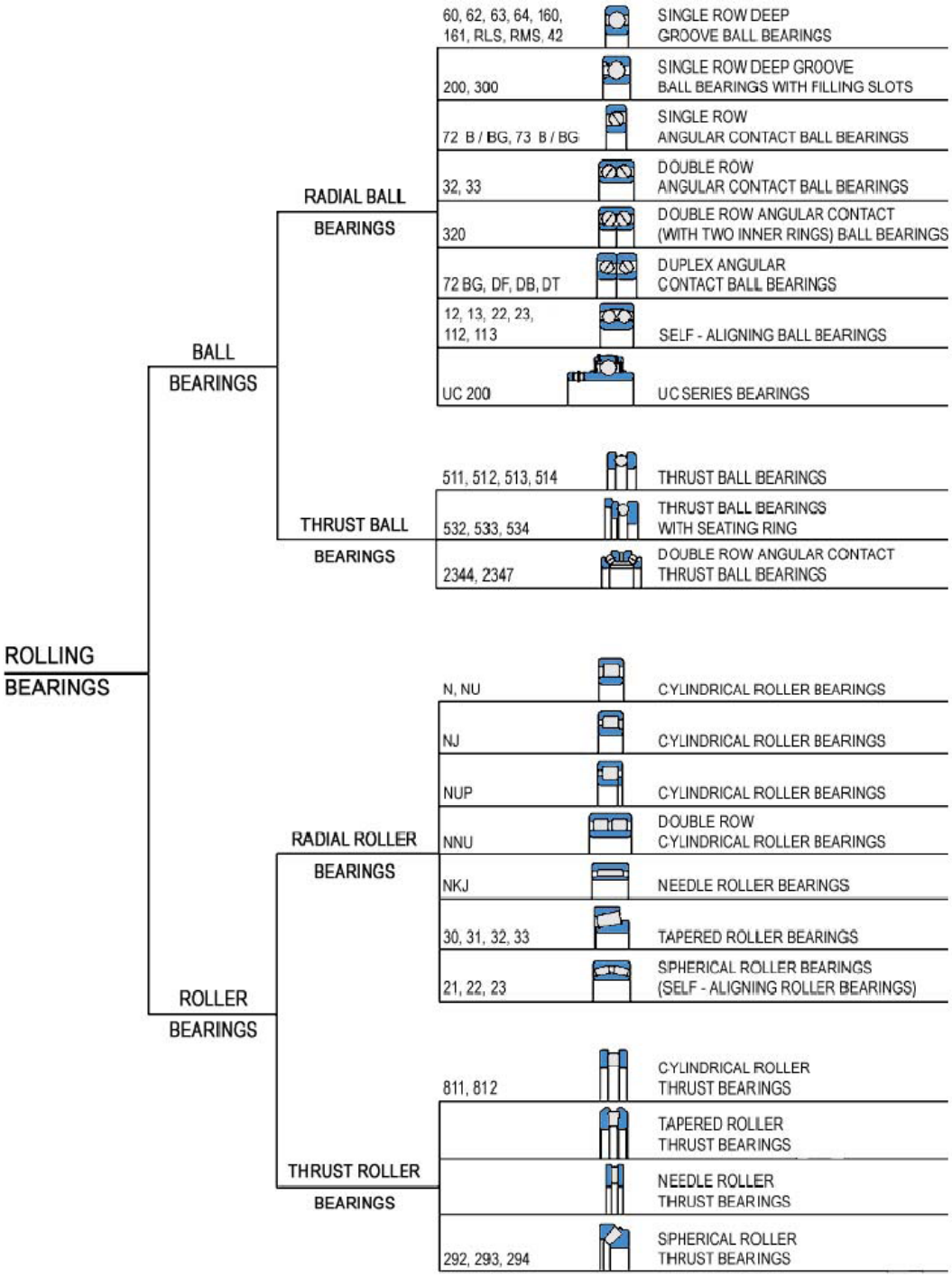

Figure 1.3 Classification of rolling bearings (ORS Bearings, 2005)

1.2 STANDARDS AND TOLERANCES FOR ROLLING ELEMENT BEARINGS

For standardization of rolling element bearings two ways are used. Firstly, the maximum or nominal dimensions are selected from the standard series which differ dimensionally by steps. Secondly, tolerances are assigned to the nominal dimensions. The tables of standards are issued by both the Antifriction Bearing Manufacturers Association (AFBMA) and the American Standards Association (ASA).

Tolerances on bore, outside diameter, and width have also been specified by the related technical committees of AFBMA. The standards mentioned for the rolling element bearing do not specify the internal design of the bearing but includes tolerances on internal looseness in the bearing, race to bore eccentricity, race to face runout, etc.

1.3 BEARING MATERIALS

The rolling element bearing operation conditions require the use of materials that can withstand high compressive stresses over millions of cycles. To have this capability the material must be relatively free of foreign matter and such as non-metallic inclusions (Dambaugh, 2006).

Both through-hardening and casehardening steels are used as bearing material. Of the through-hardening steels, AISI-E52100 (100Cr6) steel is the most widely used bearing steel in the industry (Harris, 2001). With carefully controlled furnace melt practices, foreign inclusions are held to a minimum. To improve the endurance of bearings much higher degree of cleanliness is obtained by vacuum melting techniques. The high carbon content, with chromium-alloy additions, ensures the development of uniform, high hardness with resulting high load-carrying capacity.

The hardness of the 52100 steel for bearing applications are is set to be 60-65 Rockwell C. At working temperatures above 260°C the hardness of the 52100 steel is decreases to less than 50 Rockwell C. Since hardness and load carrying capacity are

directly related, such a hardness drop will affect the load carrying capacity of the bearing. Generally, 230 °C is the maximum temperature at which 52100 is used. Above this temperature, materials with greater hardness retention like high-speed tool steels M50, M2, T1, and T5 are used (Music, 2005). Hybrid bearings have also increased in popularity in recent years. A hybrid bearing is one that has different materials for balls and races. Most of tests and calculation performed were done using a hot-pressed silicon nitride. In some tests hybrid bearings have exhibited longer fatigue lives than all steel bearings (Stella, 2006).

For special environmental conditions various materials can be used. For bearings operating in corrosive media 440 C stainless steel is often used. This grade stainless steel is hardenable to Rockwell C 60 and will retain useful hardness to temperatures of 450 °C (Brändlein et. al., 1999).

The cage parts are either stamped from sheet metal or machined from tube or cast. Stamped cages made from St4 sheet steel is used widely and for special applications brass is used. Plastic cages are cast. The rivets for fixing the cages together are made from USt 36-2 steel. The shield is made from St4 steel, and the seal made from FKM (Viton), NBR (Nitrile Butadiene Rubber) or ACM (Acrylic). The bearing materials are tabulated in Table 1.1.

Table 1.1 Bearing materials

PART	MATERIAL	RELATED STANDARDS
Inner and Outer Rings	100 Cr6 (SAE 52100, DIN 1.3505)	TS 6269
		ASTM A295-94
		DIN 17230
		TS 5823
		JIS 4805
Balls	100 Cr6 (SAE 52100, DIN 1.3505)	TS 6269
		DIN 5401
		ISO 3290
		JIS B 1501
Cage	St4 (DIN 1.0338)	DIN 1624
		DIN 1623
	Polyamide 6.6	TS 3813
Seal	St4 (DIN 1.0338)	TS 868
	NBR (Nitrile Butadiene Rubber)	
	ACM (Acrylic)	
	FKM (Viton)	
Rivet	USt 36-2	DIN 17111

1.4 BEARING LUBRICATION

The lubrication is a vital parameter for bearing life, the primary function of a lubricant is to lubricate the rolling and sliding contacts of a bearing to enhance its performance though the prevention of wear. Without appropriate lubrication in the contact areas on rolling elements and raceways where sliding and rolling occurs damage such as pitting, incipient welding, scuffing, development of oxide films can happen. Also the lack of adequate lubrication shortens the bearing life since the lubrication has the influence on fatigue development in the bearing life.

In the load-carrying areas of the rolling elements and raceways where very high Hertzian contact pressures occur, a load supporting lubricant film may be formed. The formation of a load-supporting lubricant film is directly influenced by the properties of the lubricant.

Additionally, the lubricants minimize the frictional power loss of the bearing. It acts as a heat transfer medium to remove heat from the bearing. It can redistribute the heat energy within the bearing to minimize geometrical effects due to differential and thermal expansions. Lubricants can protect the precision surfaces of the bearing components from corrosion. It can remove wear debris from the roller contact paths. It can minimize the amount of extraneous dirt entering the roller contact paths, and it can provide a damping medium for separator dynamic motions (Harris, 2001).

Both oils and greases are widely used for all types of rolling element bearings over a wide range of speeds and operating temperatures. Since grease lubrication does not require special supply systems and permits very simple sealing, most bearings are grease-lubricated. Oil lubrication can also be preferred because it has advantage over grease in its ability to provide more positive lubrication to the bearing surfaces, to flush away contaminants such as water and dirt, and particularly to transfer heat from heavily loaded bearings. It is also advantageous to lubricate bearings from a central oil system used for other machine parts.

1.5 LOAD CARRYING CAPACITY AND SERVICE LIFE

When deciding on the appropriate bearing for a certain application, the load must be related to the carrying capacity of the bearing. A certain degree of safety must exist to prevent excessive plastic deformation and premature material fatigue of the raceways and rolling elements. In an excessively stressed rotating bearing, material fatigue causes rolling surfaces to flake.

When necessary, wear must also to be taken into account. Unfavorable conditions such as dirt and lack of lubricant may increase wear, and therefore the clearance, to such an extent that the bearing ceases to fulfill its proper function.

1.5.1 Static Stressing

In rolling bearing engineering the term static stressing refers to bearings carrying a load when stationary or when subjected to small oscillating motions; the load may be constant or variable. The term static therefore relates to the operation of the bearing, not to the type of load.

Experience shows that rolling bearings under static load can be stressed to such a degree that minor plastic deformations occur in the rolling surfaces. These indentations and flattened areas, however, should not be of such an extent that they impair the rotation of the bearing.

In rolling bearing engineering the definition of admissible static rolling element loading is that the total plastic deformation of rolling element and raceway does not exceed 0.01% of the rolling element diameter D_b. For a ball of 10 mm diameter this corresponds to a plastic deformation of the two bodies of 1 μm. Experience has shown that such minor deformations neither impair the quiet running of a bearing at normal loading, nor shorten its fatigue life (Brändlein et al., 1999).

1.5.2 Dynamic Stressing

The term dynamic stressing refers to the loading of a rotating bearing. The load may be steady or varying as stated for static stressing, and here the term dynamic refers to the operation of the bearing, not to the action of the external load on the bearing.

After longer running times, depending on the load, fatigue phenomena occur on the operating surfaces of rotating rolling bearings. As a rule these initiate from micro-cracks below the surface. With further operation the cracks enlarge, and material pitting and flaking develop. Finally, the flaking extends over large areas of the operating surfaces. The first cracks emanate from weak points in the material or from inhomogeneities, which may be microscopically small non-metallic inclusions, non-uniform distributions of alloying elements, etc. The inhomogeneities are randomly distributed in the material and of varying size. The concentration and consistency of

these weak points therefore vary and thus pitting may form accordingly at an earlier or later time. The stress in the individual bearing components also varies due to differing manufacturing tolerances (Brändlein et al., 1999).

1.6 ROLLING ELEMENT BEARING DAMAGE

Rolling element bearing damage is generally detected by unusual operational behavior of the bearing arrangement. Uneven running, uncommon running noise and unexpected temperature changes in the system usually indicate damaged rolling surfaces or an alteration of the radial clearance due to wear. High friction, hence resistance to smooth running, can indicate damaged rolling contact surfaces, detrimental preload or damage caused by unsatisfactory lubrication. The important types and causes of bearing damage are; fatigue, wear or plastic deformation.

A bearing subjected to nominal loading fails due to material fatigue after certain running time. A detrimentally preloaded, overstressed bearing will also fail due to material fatigue, but after shorter running time. This also applies to abrasive wear. While a small amount of wear is natural and unavoidable in most bearing arrangements, severe wear due to heavy contamination and inadequate sealing must be considered as avoidable sources of damage (Eschmann et al., 1985).

1.6.1 Plastic Deformation

A rolling bearing subjected to excessive loading while stationary or performing small oscillating movements, becomes unserviceable due to plastic deformation at the contact surfaces. For this reason the static capacity of the bearing should be taken into account during the bearing selection phase.

1.6.2 Fatigue

The rolling bearing approaches the end of its life when the rolling surfaces of its rings and rolling elements are damaged by material fatigue. Fatigue is by definition, the failure of material caused by repeated cycles well bellow the yield stress. In bearings, fatigue is seen in the area of contact between balls and raceways.

Fatigue damage begins with the formation of minute cracks below the surface. This failure is physically manifested in bearings by the phenomenon spall (Figure 1.4). Spall is the propagation of cycle dependent loading cracks that occurs in the region of maximum stress (Stella, 2006).

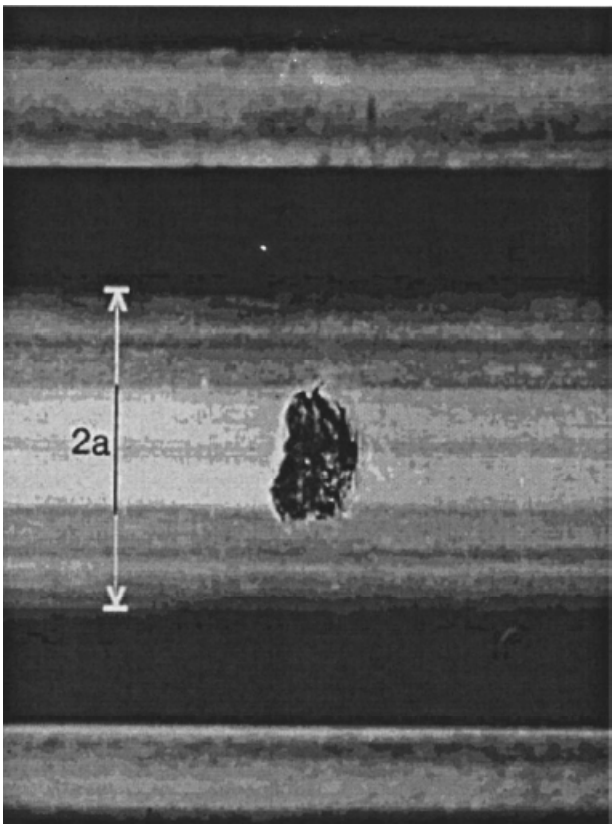

Figure 1.4 Ball bearing raceway with fatigue spall (Kotzalas, et. al., 2001)

1.6.3 Wear

The forces transmitted in a bearing give rise to stresses of varying magnitudes between surfaces in both rolling and sliding motion. As a result of repeated loads in concentrated contacts, changes occur in the contact surfaces and in the regions bellow surfaces. These changes cause surface deterioration or wear (Figure 1.5). Wear is the loss or displacement of material from surface. Material displacement may occur by local plastic deformation or the transfer of material from one location to another by adhesion. When wear has progressed to the degree that it threatens the essential function of the bearing, the bearing is considered to have failed (Harris, 2001).

Wear occurs mainly due to dirt and foreign particles entering the bearing though inadequate sealing. Wear damage is often due to contaminated lubricant. Where rolling bearings, gears and other machine components are lubricated in a common system, abraded metallic particles may be conveyed between rolling elements and raceways. Abrasive foreign particles such as dust, sand, and grit roughen the contact surfaces and giving them a dull appearance (Eschmann, et al., 1985).

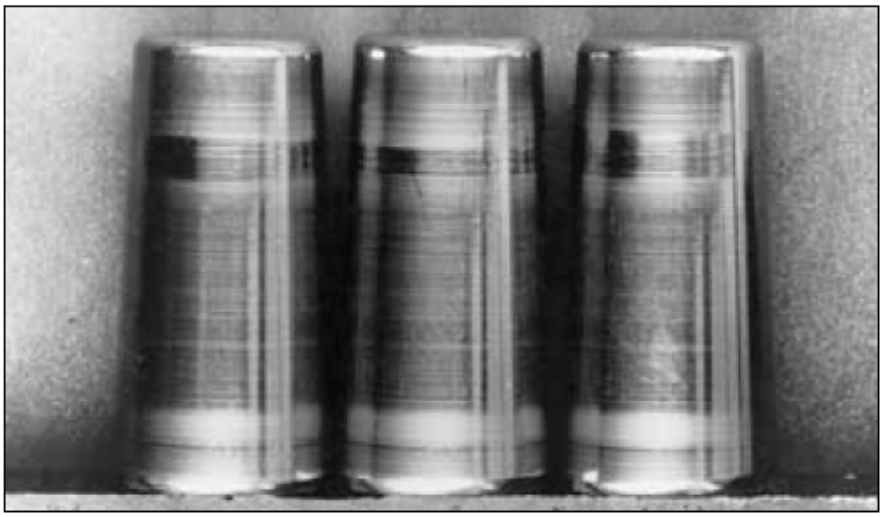

Figure 1.5 Worn surfaces of rollers (FAG, 2003)

1.6.4 Corrosion Damage

The result of severe rust on the running surfaces is uneven and noisy operation. The rust particles worn off by the rolling elements have an abrasive effect and generate wear (Figure 1.6). The rust pits are the starting points for subsequent flaking. Rust forms not only when water, acids, etc. penetrate the bearing, but also promoted by acidic lubricants. Another cause of corrosion is condensation, resulting mainly from sudden cooling of the bearing from operating temperature in very humid air.

Figure 1.6 Corrosion of the outer ring of a deep groove ball bearing (FAG, 2003)

1.6.5 Brinelling

The raceways of correctly hardened rolling bearings occasionally show indentations regularly distributed over their entire circumference, corresponding approximately, in their shape, to the Hertzian contact area. As a result the bearing becomes noisy and uneven in operation. This damage is known as Brinelling and may have three

possible causes. The indentations may result from static overloading which leads to perceptible plastic deformation of the raceway. Similar damage may occur when a stationary rolling bearing is exposed to vibration and shock loads. The indents on inner and outer rings of a deep groove ball bearing are shown in Figure 1.7.

Figure 1.7 Ball indentations in the shoulders of a deep groove ball bearing (FAG, 2003)

Vibrations have also been the cause of the indentations on the (Figure 1.8). Investigations have shown that such indentations are caused by fretting corrosion or false brinelling (Eschmann et al., 1985).

Figure 1.8 False brinelling on a ball bearing (FAG, 2003)

CHAPTER 2

LITERATURE SURVEY

Historically, rolling bearing theory postulated that no rotating rolling element bearing can give unlimited service, because of the probability of the fatigue at the surfaces in rolling contact. Rolling contact fatigue is manifested as a flaking off of metallic particles from the surface of the raceways and/or rolling elements. For well lubricated, properly manufactured bearings, this flaking off usually commences as a crack below the surface and is propagated to the surface, eventually forming a pit or spall in the load carrying surface (Figure 2.1).

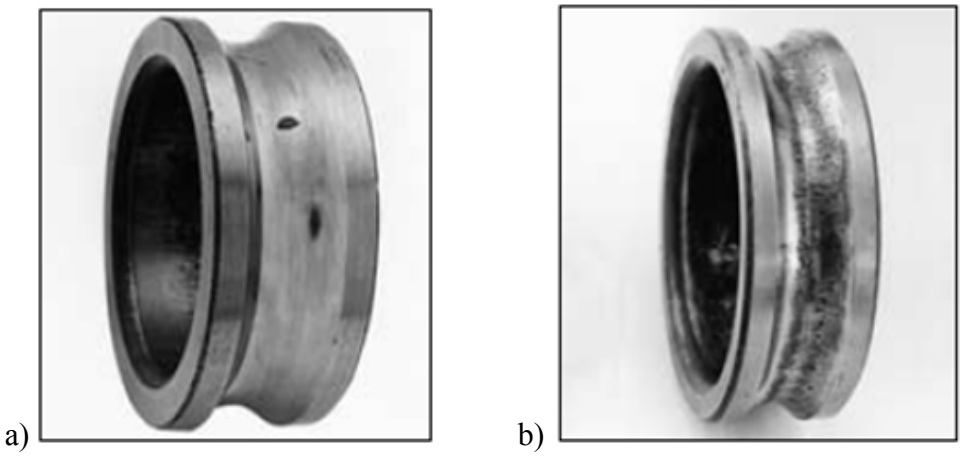

Figure 2.1 Fatigue damage on inner rings of deep groove ball bearings
a) Pit formation, b) Spall formation (FAG, 2003)

There are four major life theories that attempt to predict the life of a ball bearing assembly. The first was Weibull distribution that derived by W. Weibull in 1930s. He stated that the ultimate strength of the material can not be expressed by a single numerical value and that a statistical distribution was required for this purpose.

Weibull's principal contribution is the determination of structural failure is a function of the volume under stress. The theory is based on the assumption that the initial crack leads to a break. For the fatigue failure of rolling bearings, it is investigated by experiments that many cracks initiate at bellow the surface and do not propagate to the surface (Harris, 2001). Thus Weibull Theory is not directly applicable to rolling bearings. In 1950s Lundberg and Palmgren extending the work of Weibull to rolling element bearings relating the shear stress, cycles and maximum critical shear stress depth to fatigue life (Zaretsky, 1995). Their combined work formed the standards for the load ratings and life of ball bearings of American Bearing Manufacturers Association (ABMA), International Organization for Standardization (ISO) and American National Standards Institute (ANSI). In 1985 Ioannides and Harris (1985) came up with the theory which proposed that the bearing steel had a fatigue limit or loading where the specimen life is infinite. The most recent work has been done by NASA and Zaretsky and others (2000) proposed a Weibull-based life theory that more accurately accounts for the exponents in the equations for critical shear stress.

Other researchers have proposed modifications of the Lundberg theory; Lamagnere et.al. (1998) proposed a method for calculating load rating of rolling bearing for an infinite life. Their method based on the comparison between the local elastic shear stress built up around inhomogeneities present in bearing steels and microyield stress of martensitic matrix. Tallian (1992) has developed a mathematical model which also based on Lundberg-Palmgren model considering the tractive surface stress distributions, crack propagation, defect severity within the material and contamination.

Wangquan and Cheng (1997) in their work inspect the needle roller bearings, at the end of the endurance tests they conduct, they find out that surface cracks did not lead the fatigue failure and the dominant fatigue mechanism was subsurface crack initiation and propagation. They claim the fatigue life of a needle roller bearing can be predicted by simply knowing the maximum contact pressure.

2.1 ROLLING BEARING FATIGUE MECHANICS

Although several failure mechanisms can occur in bearing rolling element surfaces, the fatigue cracking typically develops at or beneath the surface of the loaded bearing elements as shown in Figure 2.2.

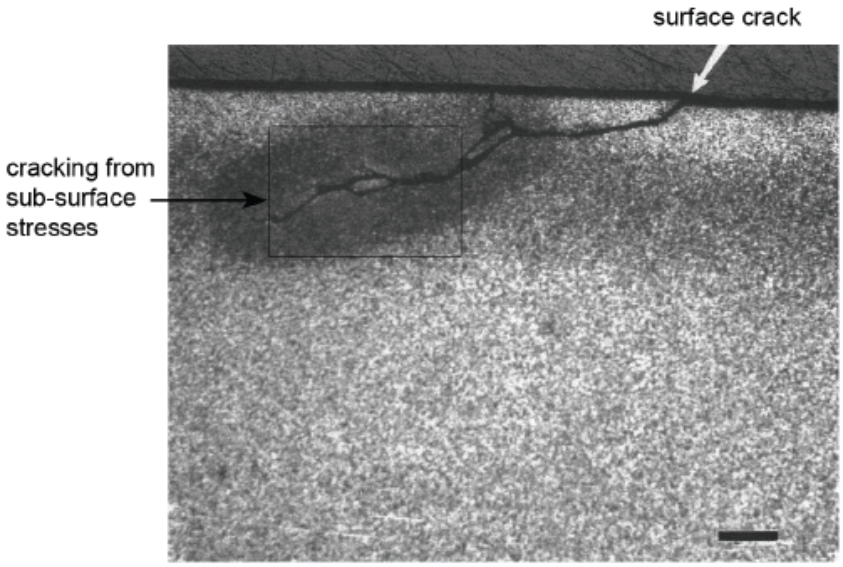

Figure 2.2 Sub-surface fatigue cracking (Dambaugh, 2008)

Contact pressure, which is defined as the normal stress in the surface at the point contact, is developed between the curved surfaces according to theories of Hertz. It has been so widely adopted in structural metal fatigue concepts that fatigue is generated in an area of a mechanical member that sees plasticity, or development of slip-bands under cyclic loading, typically occurring in small areas of a structure such as a stress riser or discontinuity (Pook, 2007). Hence the sub-surface stress important for rolling element bearing fatigue analyses, since the shear and von Mises stress have the maximum values below the surface.

2.2 SCATTER IN ROLLING BEARING FATIGUE LIFE RESULTS

Weibull reliability analysis (Harris, 2001, Eschmann, 1985) is widely used in fatigue testing and is a primary means of evaluating bearing fatigue results. For rolling bearings reliability is a very important discussion of how much service life can be expected from a bearing design due to a very wide scatter of fatigue results can be found from tests.

In Figure 2.3 from Eschmann, 1985 an example scatter plot from a test of thirty 6309 ball bearings run until failure. Although the tested bearings are all identical and were run under identical conditions, it is seen that the shortest run time was about 15.e6 cycles while the longest run time was 300e6 cycles, a 20:1 range. Due to wide scatter, it is clear that predicting a service life for a single bearing is not possible, and that statements on fatigue life can only be made in terms of expected reliability.

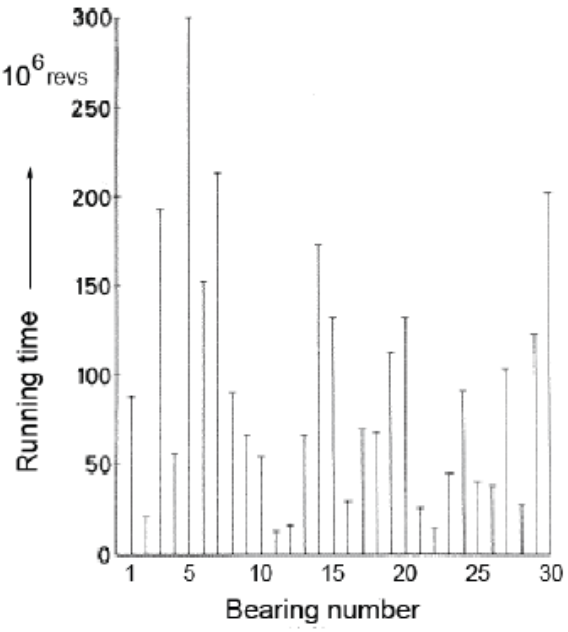

Figure 2.3 Scatter plot of 6309 bearing fatigue test results (Eschmann, 1985)

The explanation of the wide scatter is that few "weak" points exist in the manufactured surfaces and in the base material. The weak points which are formed because of the non metallic inclusions (Harris 2001, Eschmann, 1985) distributed randomly within the material. If the highly stressed portion of the bearing consists inclusions that bearing gives lower fatigue life and if not higher fatigue live is observed.

2.3 FATIGUE LIFE DISPERSION

If a population of apparently identical rolling bearings is subjected to identical load, speed, lubrication, and environmental conditions, all the bearings does not exhibit the same life in fatigue. Since such a life dispersion exists, bearing manufacturers have chosen to use L_{10} and L_{50} values, where;

L_{10} : The fatigue life that 90% of the bearing population will endure

L_{50} : The median life, the life that 50% of the bearing population will endure

2.4 LIFE THEORIES

2.4.1 Weibull Equation

The Weibull Equation was the first step into predicting the life of mechanical samples. The statistical analysis is used to determine the properties of solids. Weibull claimed that the material properties or strength of a control group of test specimens could be expressed by the following equation;

$$\ln(1-F) = \int_V n(\sigma)dV \qquad (2.1)$$

The above equation describes the probability of rupture F due to a given stress distribution σ over volume V in which n(σ) is a material characteristic. Harris (2001) gives the Weibull distribution of rolling bearing fatigue life as;

$$\ln \ln\left(\frac{1}{U}\right) = e \ln L + \ln A_m \tag{2.2}$$

where U is the probability of survival, L is the life, A_m is the material factor for ball bearings, and e is called Weibull slope. Weibull also stated that the probability of survival S can be expressed as (Zaretsky et al., 1995);

$$\ln\left(\frac{1}{U}\right) \sim \tau_{cr}{}^{c} N^{e} V \tag{2.3}$$

where

V : the stressed volume,

c : empirical shear stress exponent,

N : the number of stress cycles endured with probability of survival U.

τ_{cr} : critical shear stress

From the Equation (2.2) it can be seen lnln(1/U) vs. ln(L) plots a straight line. Figure 2.4 shows a Weibull plot of bearing testing data. The Weibull slope e is a measure of bearing fatigue life dispersion (Harris, 2001). Weibull slope for a test group is given by;

$$e = \frac{\ln \dfrac{\ln(1/U_1)}{\ln(1/U_2)}}{\ln \dfrac{L_1}{L_2}} \tag{2.4}$$

in which (L_1, U_1) and (L_2, U_2) are any two points on the best straight line passing through the test data. The e value for ball bearings is accepted to be e = 10/9, and for roller bearings e = 27/20 (Eschmann et al., 1985).

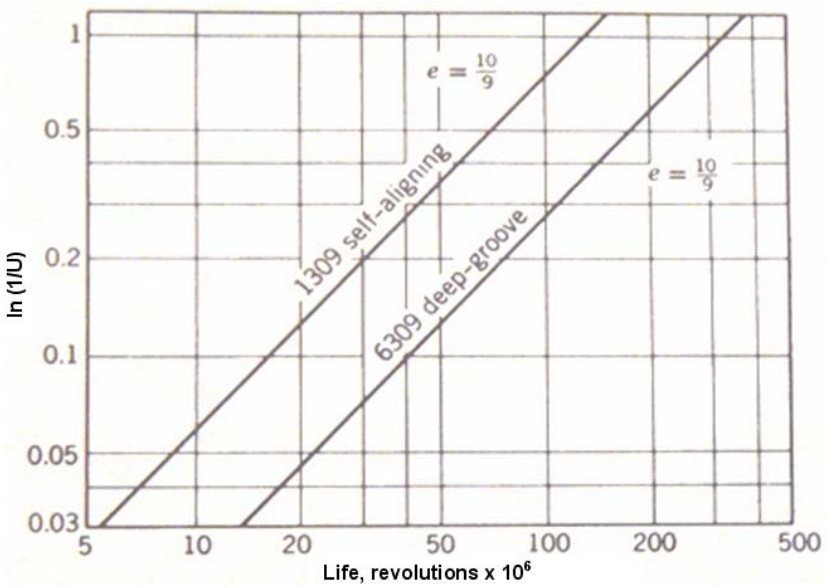

Figure 2.4 Typical Weibull plot for ball bearings (Harris, 2001)

2.4.2 Lundberg-Palmgren Equation

As mentioned before**,** Weibull's theory is based on the assumption that the initial crack at subsurface leads to failure on surface of the raceway. In the fatigue of rolling bearings experiments it is observed that many cracks initiate at below the surface and do not propagate to the surface (Harris, 2001). Thus Weibull Theory is not directly applicable to rolling bearings. In 1950s Lundberg and Palmgren theorized that consideration ought to be given to the fact that the probability of the occurrence of a fatigue break should be a function of the depth z_0 below the load carrying surface at which the most severe shear stress occurs. The basic Lundberg-Palmgren equation relating the probability of survival, stress cycles to failure, fatigue stress and the depth at which that stress occurs is given as (Ioannides et al., 1990);

$$\ln\frac{1}{U} \sim \frac{N^e \tau_o^c V}{z_{cr}^h} \tag{2.5}$$

where

τ_o : the maximum value of subsurface orthogonal shear stress (the stress orthogonal to the surface)

z_{cr} : the depth of critically stressed volume,

h : empirical exponent

During the examination of the failed bearings on the tests, Lundberg and Palmgren concluded that the maximum shear stress was representative of failure causing stress. They further considered that the stressed volume could be represented by the proportionality (Ioannides et al., 1990);

$$V \propto 2az_0\pi d \tag{2.6}$$

where 2a is the semi-major axis of the Hertz contact ellipse, and d is the diameter of the stressed track. According to the Lundberg-Palmgren theory, life prediction of a rolling bearing raceway can be found by the following equation;

$$L = \left(\frac{Q_c}{Q}\right)^{(c-h+2)/3e} \tag{2.7}$$

or

$$L = \left(\frac{Q_c}{Q}\right)^{p} \tag{2.8}$$

where

L : life in millions of revolutions,

Q : contact normal load (N),

Q_c : basic dynamic capacity of the contact (N),

p : empirical load-life exponent.

The dynamic capacity is defined as the equivalent load that 90% of the bearings can endure for one million revolutions of the inner ring. Endurance test of ball bearings have shown the load-life exponent to be very close to 3 (Harris, 2001). Lundberg-Palmgren approach formed the standards for the load rating and life of ball bearings in ABMA, ISO, and ANSI. Figure 2.5 is a typical plot of fatigue life vs. load for ball bearing and endurance life ISO formula is given in the equation bellow.

$$L_n = a_1 a_2 a_3 \left(\frac{C}{P}\right)^p \tag{2.9}$$

where

C : basic dynamic capacity of the bearing,

P : equivalent load on bearing,

p : empirical load-life exponent (3 for ball bearings and 10/3 for roller bearings),

L_n : fatigue life in millions of revolutions corresponding to reliability level (100 - n)

a_1 : reliability factor (a_1 = 1 for n = 90 percent)

a_2 : material factor (a_2 = 1 for precision bearings manufactured from good quality bearing steel hardened to 58 R_c minimum)

a_3 : lubrication factor (a_3 is based upon the degree of separation of the surfaces in rolling contact effected by the lubricant; a_3 = 1 for adequate separation)

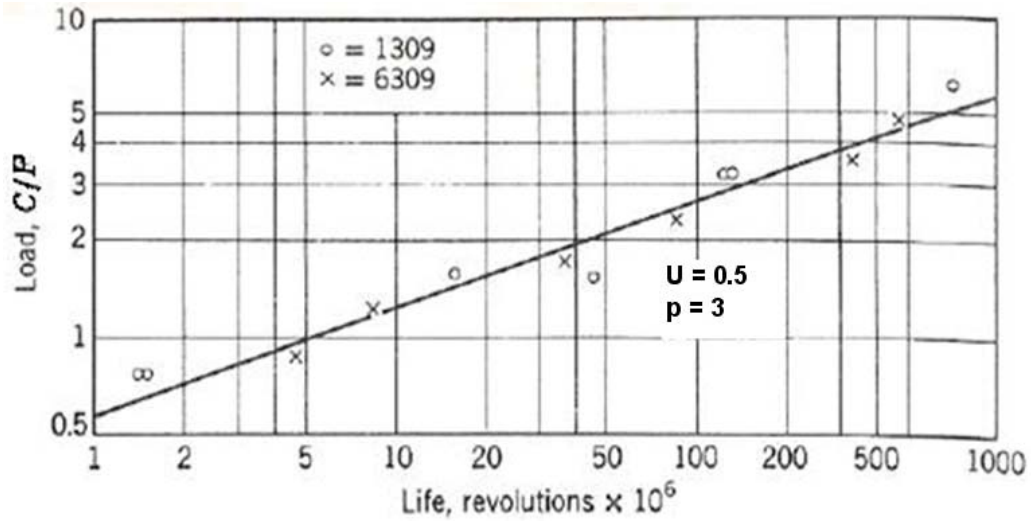

Figure 2.5 Load vs. life for ball bearings with 50% survivability (Harris, 2001)

Limitations of the Lundberg-Palmgren equation in structural fatigue point of view: Lundberg-Palmgren formulas represented a significant development in rolling bearing technology; however, it was not possible to correlate the fatigue of bearing surfaces in rolling contact so calculated to structural fatigue. It is widely known that materials tested for structural fatigue have typically exhibited a fatigue limit.

According to the tests done on the bearing steel (100Cr6), for cyclic loading less than the fatigue limit, fatigue does not occur (Dambaugh, 2008). On the contrary, a basic assumption in the formulation of Lundberg-Palmgren is that no matter how small the load applied to a rolling bearing, all the material in the stressed volume V is subject to fatigue failure (Harris and McCool, 1996). This phenomenon is illustrated schematically by Figure 2.6.

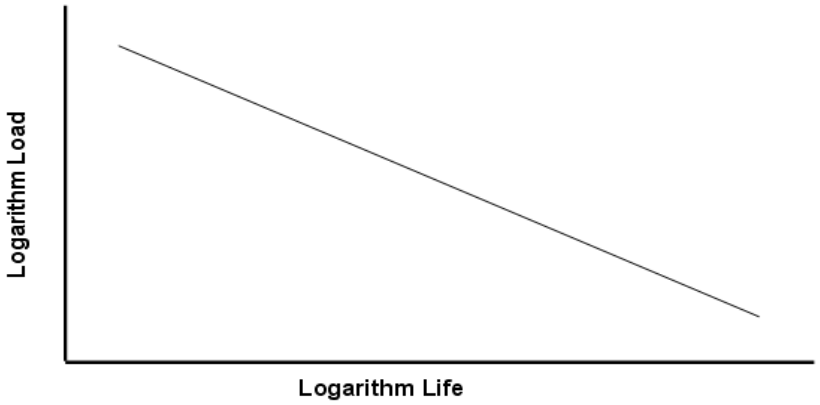

Figure 2.6 Load versus life for Lundberg-Palmgren Theory

Ioannides and Harris (1985) during their researches on endurance characteristics of bearings observed that bearings manufactured from very clean steel, lubricated to achieve separation of rolling elements and raceways and kept free of contaminants may not experience fatigue failure.

Also Lundberg-Palmgren states that the critical stressed volume for fatigue failure is, as given in Equation (2.5), proportional to the product of the major axis of the contact ellipse, the depth to maximum shear stress, and the circumference of the raceway contact (Figure 2.7). On contrary Harris and Yu (1999) in their work prove that the effectively stressed volume in bearing substantially less than that of Lundberg-Palmgren assumed.

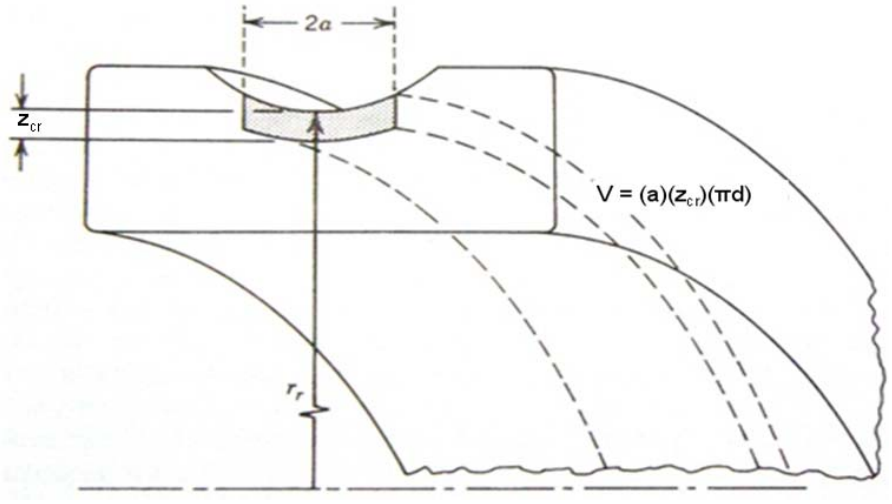

Figure 2.7 Volume at risk to fatigue in rolling contact according to Lundberg-Palmgren Equation (Harris, 2001)

2.4.3 Ioannides-Harris Equation

Ioannides and Harris worked from both Weibull and Lundberg-Palmgren, adding in the fatigue-limiting stress term, τ_1, and published following equation (Ioannides and Harris, 1985);

$$\ln\frac{1}{\Delta U} \sim \frac{N^e(\tau_o - \tau_1)^c \Delta V}{z_{cr}^h} \tag{2.10}$$

In Equation (2.10), z is the depth at which stress occurs and τ_1 is an endurance limit shear stress. If $\tau_o < \tau_1$ in any incremental volume, that volume will not experience fatigue failure. Only the volumes where $\tau_o > \tau_1$ can fail in fatigue, not the entire volume V (Figure 2.8). Thus for sufficiently low loads, bearings will not fail in fatigue. Ioannides and Harris are used the orthogonal shear stress for the formula to be consistent with Lundberg-Palmgren equation but they also claimed another stress criterion such as von Mises or maximum shear stress can be used (Harris, 2001).

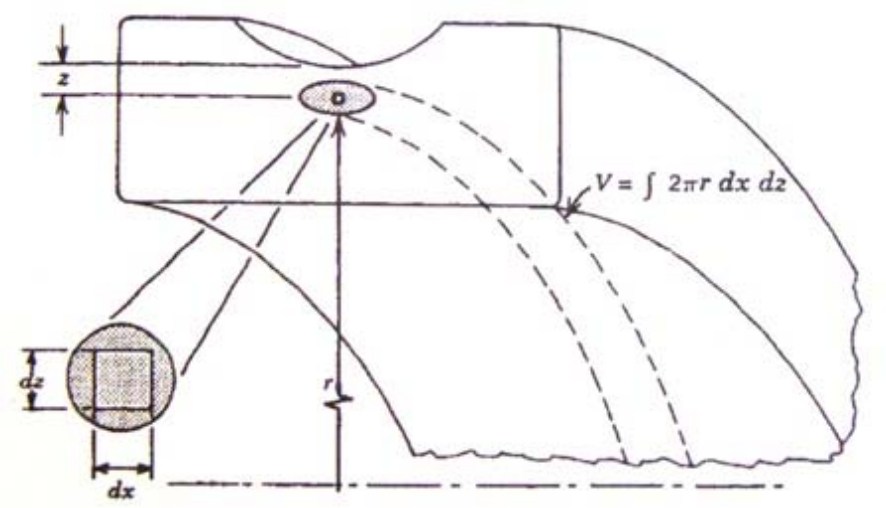

Figure 2.8 Volume at Risk for Ioannides-Harris Equation (Harris, 2001)

Since it is recognized that from the tests the crack propagation time is orders of magnitude shorter than time for crack initiation, the exact reason for use of z^{-h} remains undefined. Ioannides and Harris continue the Lundberg-Palmgren model concept with the use of z^{-h} (Ioannides and Harris, 1985).

Using Equation (2.10) in conjunction with Equation (2.5), the life prediction equation can assume a form as following equation (Ioannides and Harris, 1985);

$$L_n = a_1 \left(\frac{C}{P - P_u} \right)^p \quad P \geq P_u \tag{2.11}$$

where P_u is the limit load for fatigue. The effect of the Equation (2.11), shown as a potential standard-like format for common bearing applications, is illustrated by Figure 2.9, which also show a comparison with the load vs. life curve given in Figure 2.6.

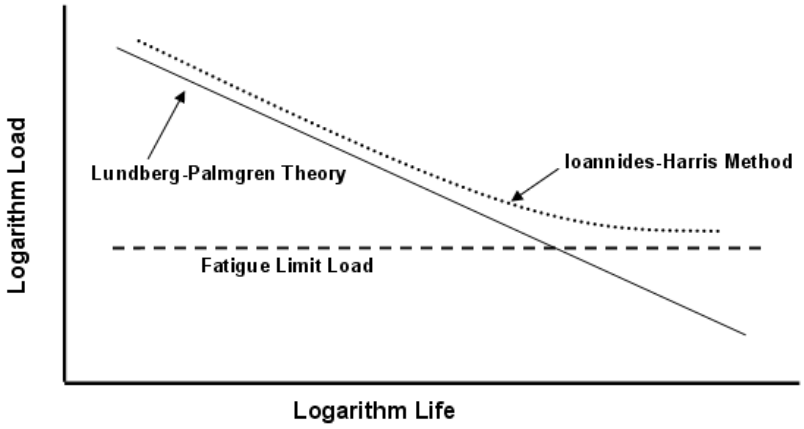

Figure 2.9 Load versus life, Ioannides-Harris model compared to Lundberg-Palmgren model

2.4.4 Zaretsky Equation

Zaretsky in his research suggest that bearing life dispersions are dependent on the critical shear stress-life exponent. He found that for a wide ranging set of conditions, most stress-life exponents vary between 6 and 12. The Zaretsky formula is given in following equation (Zaretsky et al., 2000).

$$L = A\left(\frac{1}{V}\right)^{\left(\frac{1}{e}\right)}\left(\frac{1}{\tau}\right)^{c} \sim \frac{1}{S_H^n} \tag{2.12}$$

where

A : material-life factor

S_H : maximum Hertz stress

n : stress-life exponent

Parker and Zaretsky (1972) conduct endurance tests on bearing balls made from 100Cr6 steel and suggest that for air melt processed steels the stress-life exponent n is approximately 9. However, for cleaner and vacuum-processed steels, n =12.

Zaretsky claimed that since the Lundberg-Palmgren equation considers the depth of critically stressed volume their equation was propagation time dependent and crack propagation time was included to equation. However according to Zaretsky crack propagation was an extremely small time fraction for the total life or running time of the bearing. To decouple the dependence of bearing life and crack propagation rate, Zaretsky et al. (1995) dispensed with the Lundberg-Palmgren relation with the depth of critically stresses volume, z.

2.4.5 Comparison of Life Theories

Since the formulations for the endurance life of the bearings differs, it is necessary to compare the theories and outcomes of these theories. It can be seen from the Equations (2.3), (2.5), and (2.6) the formulations provide ratios between the life and stress values. The appropriate constants for the materials from the experiments should be added to the relations to calculate the life for bearings. Zaretsky et al. (1995) redefine the Weibull, Lundberg Palmgren, and Ioannides Harris formulations with the material factor A to compare the outcomes with the Zaretsky formulation. The redefined equations are as follows;

Weibull Equation:

$$L_{10} = A\left(\frac{1}{V}\right)^{\frac{1}{e}}\left(\frac{1}{\tau}\right)^{\frac{c}{e}} \tag{2.13}$$

Lundberg-Palmgren Equation:

$$L_{10} = A\left(\frac{1}{V}\right)^{\frac{1}{e}}\left(\frac{1}{\tau_o}\right)^{\frac{c}{e}}\left(z_{cr}\right)^{\frac{h}{e}} \tag{2.14}$$

Ioannides-Harris Equation:

$$L_{10} = A\left(\frac{1}{\Delta V}\right)^{\frac{1}{e}}\left(\frac{1}{\tau_o - \tau_1}\right)^{\frac{c}{e}}\left(z_{cr}\right)^{\frac{h}{e}} \tag{2.15}$$

Zaretsky et al. (1995) use the appropriate material constants in the formulations and relates the life of the inner ring for different stress criterion by normalizing life values as L_{10} life of 1 million at maximum value of selected stress criterion. Zaretsky (1995) calculates the stress values for 3 different loads as given in Table 2.1 and propose the stress-life exponents, n, for the formulations by which the fatigue life of an inner ring can be relatively found from the maximum stress values within the ring by using the Equation (2.16). Comparison of relative life and stress-life exponents from four life equations is tabulated in Table 2.2.

$$L \sim \frac{1}{S_{\max}^{n}} \tag{2.16}$$

Table 2.1 The ball loads and stress values (Zaretsky, 1995)

Parameter	Normal Load on Ball [N]		
	623	1617	3333
Max. Hertz stress, S_{max} [GPa]	1.4	1.9	2.4
Max. Orthogonal shear stress, τ_o [GPa]	0.343	0.472	0.601
Max. Shear stress, τ_{max} [Gpa]	0.459	0.644	0.814
Max. von Mises stress, $\overline{\sigma}$ [Gpa]	0.821	1.154	1.465

Table 2.2 Comparison of relative life for four life equations (Zaretsky, 1995)

Normal Load on Ball [N]	Relative Theoretical Lives [million cycles]					
	Weibull Eq. (Based on τ_{max})	Lundberg-Palmgren Eq. (Based on τ_o)	Ioannides-Harris Eq.		Zaretsky Eq.	
			Based on τ_{max}	Based on $\overline{\sigma}$	Based on τ_{max}	Based on $\overline{\sigma}$
623	423.9	154.7	12112.0	4643.0	431.4	495.6
1617	13.6	7.1	149.7	85.2	11.7	12.9
3333	1.0	1.0	1.0	1.0	1.0	1.0
n	10.8	9.0	16.8	15.1	10.8	11.1

Zaretsky, et al. (2000) conduct the calculations with the Lundberg-Palmgren, Ioannides-Harris and Zaretsky life theories and compare the results of the methods with the ISO formulation (Figure 2.10.).

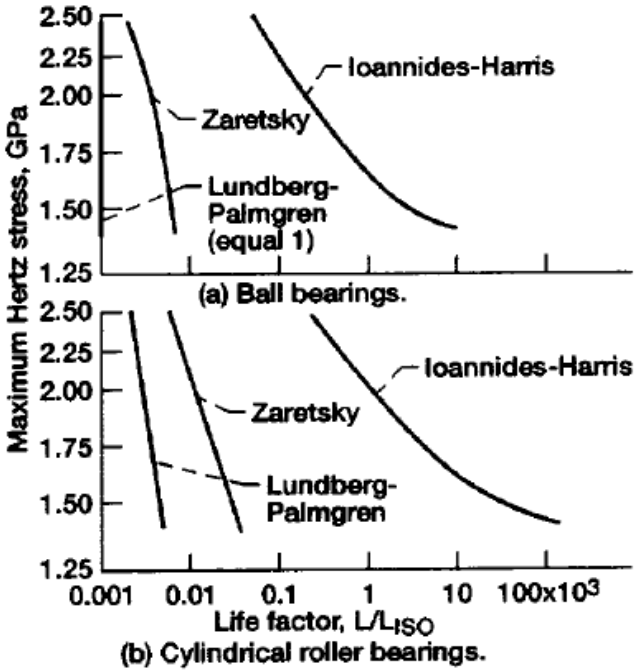

Figure 2.10 Comparison of three methods on rolling element bearing life (Zaretsky, et al. 2000)

As seen in Figure 2.10 and Table 2.2 the results of the theories have significant differences. Of the three theories the most conservative one is Lundberg-Palmgren and the maximum difference in results of the theories are between 0.1% and 10% for ball bearings.

2.5 THE AIM AND SCOPE OF THIS THESIS

The increasing competition in the industry and the huge cost pressure on companies, require decreasing the budget for testing activities, while having the obligation to

offer good quality and reliable products. From that point of view, for a designer it is important to estimate the fatigue life of the rolling element bearing used in a system for predictive maintenance applications. From the stock expenses and stock planning point of view the necessary quantity of bearings that should be ready in the stock is another important issue.

The main scope of this thesis is to use a numerical method for rolling element inner ring fatigue life prediction. The hypothesis of this thesis can be explained that since the fatigue limit stress and the effects of variable loading are put into consideration by structural fatigue analysis methods, these methods are applicable for the rolling element bearing life prediction purposes and give more realistic results than that of the ISO formulation.

This work is intended to use a numerical method to calculate fatigue lives of bearings under different loading conditions. Organization of this thesis can be summarized as following steps. Firstly, classification, material properties, and bearing damage modes of rolling bearings are summarized in Chapter 1. Secondly, literature survey of the four main fatigue life methods for rolling element bearings are investigated and compared in Chapter 2. In this thesis, contact stress and load distribution for rolling element bearings are represented in Chapter 3.

Fatigue theory is evaluated and the theory used for structural fatigue analysis is given in Chapter 4. Chapter 5 describes the details of the bearing fatigue and formulations used for fatigue prediction. In Chapter 6 a case study is for a selected bearing inner ring is given. The stress field evaluation within the inner ring and fatigue life calculations with structural fatigue methods, comparison of results with the published formulations are given in Chapter 6. Finally, in Chapter 7 summarizes the work done, also recommendations for further work are given in Chapter 7.

CHAPTER 3

CONTACT STRESS AND LOAD DISTRIBUTION FOR ROLLING ELEMENT BEARINGS

Loads acting between the rolling elements and raceways in rolling bearings develop only small areas of contact between the mating members. Consequently, although the elemental loading may only be moderate, stresses induced on the surfaces of the rolling elements and raceways are usually large which causes contact deformations. In this chapter, focus is placed on the contact stresses and load distribution within the bearing.

3.1 DEFORMATION OF TWO BODIES CONTACTING AT A SINGLE POINT

The classical solution for the local stress and deformation of two elastic bodies apparently contacting at a single point was established by Hertz in 1881. Today, contact stresses are frequently called Hertzian or Hertz stresses in recognition of this accomplishment.

Two bodies of revolution having different radii of curvature in a pair of principal planes through the contact between the bodies may contact each other at a single point under the condition of no applied load. Such a condition is called point contact.

To determine the deformation of two contacting bodies at a single point, denote the upper body by I and the lower body by II as shown in Figure 3.1. The principal planes are denoted by 1 and 2. Therefore, the radius of curvature of body I in plane 2 is denoted by r_{I2}. Since r denotes radius of curvature, curvature is defined as;

$$\rho_i = \frac{1}{r_i} \tag{3.1}$$

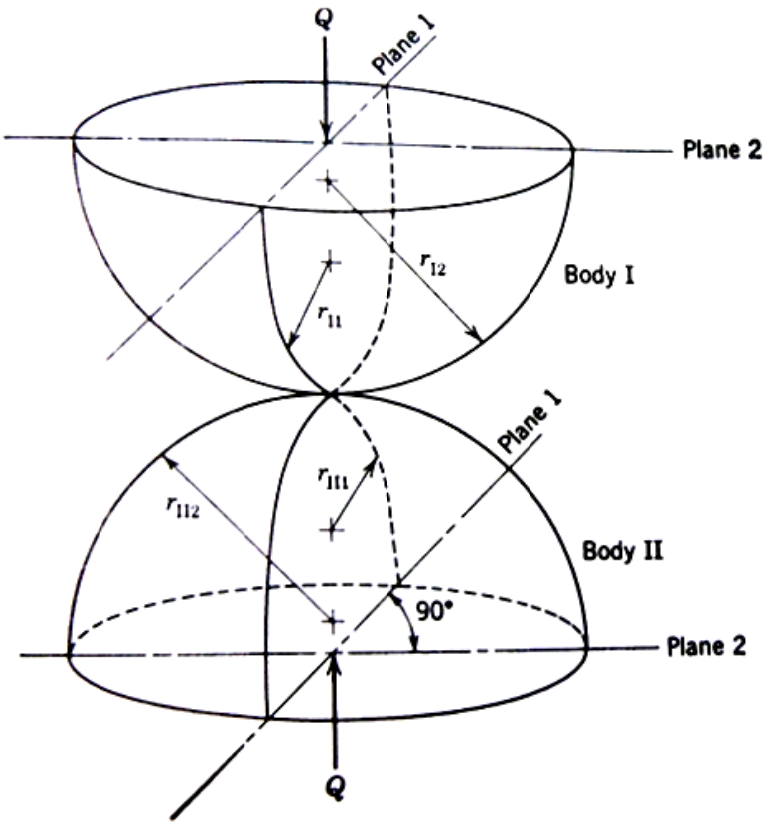

Figure 3.1 Contact surface pairs (Harris, 2001)

The curvature sum is given by;

$$\sum \rho = \frac{1}{r_{I1}} + \frac{1}{r_{I2}} + \frac{1}{r_{III}} + \frac{1}{r_{II2}} \tag{3.2}$$

where

r_{I1} : the radius of curvature of body I in plane 1,

r_{I2} : the radius of curvature of body I in plane 2,

r_{III} : the radius of curvature of body II in plane 1,

r_{II2} : the radius of curvature of body II in plane 2.

The curvature difference is given as;

$$G(\rho) = \frac{(\rho_{II} - \rho_{I2}) + (\rho_{III} - \rho_{II2})}{\sum \rho} \tag{3.3}$$

For an elliptical contact area, the maximum compressive stress occurs at the geometrical center. The magnitude of this stress is;

$$\sigma_{max} = \frac{3Q}{2\pi ab} \tag{3.4}$$

where Q is normal force between rolling element and raceway, a and b are the semimajor and the semiminor axes of the projected elliptical area of contact and given as;

$$a = a^* \left[\frac{3Q}{2\sum \rho} \left(\frac{1-\upsilon_I^2}{E_I} + \frac{1-\upsilon_{II}^2}{E_{II}} \right) \right]^{1/3} \tag{3.5}$$

$$b = b^* \left[\frac{3Q}{2\sum \rho} \left(\frac{1-\upsilon_I^2}{E_I} + \frac{1-\upsilon_{II}^2}{E_{II}} \right) \right]^{1/3} \tag{3.6}$$

where

a* : dimensionless semimajor axis of contact ellipse,

b* : dimensionless semiminor axis of contact ellipse,

υ_1, υ_2 : Poisson's ratio for body I and body II respectively,

E_I, E_{II} : modulus of elasticity for body I and body II respectively.

The normal stress at other points within the contact area is given by the following equation in accordance with Figure 3.2;

$$\sigma = \frac{3Q}{2\pi ab} \left[1 - \left(\frac{x}{a} \right)^2 - \left(\frac{y}{b} \right)^2 \right]^{\frac{1}{2}} \tag{3.7}$$

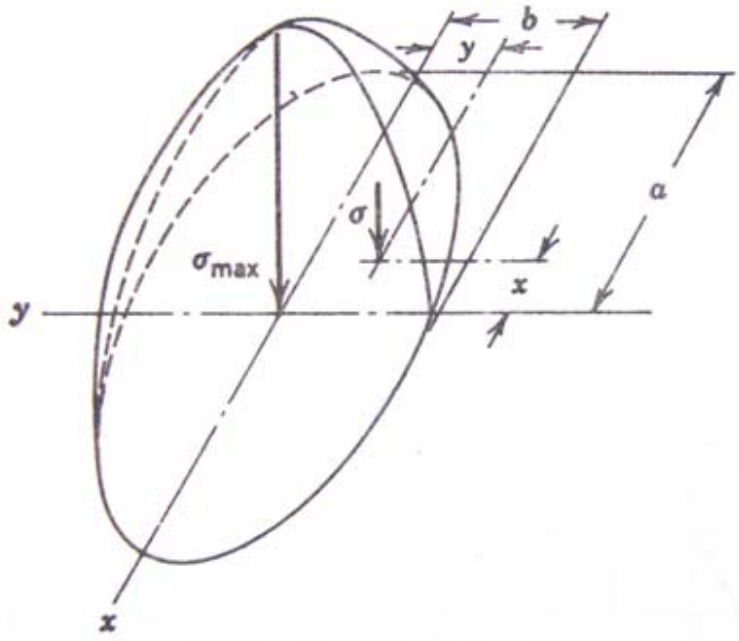

Figure 3.2 Hertz stress distribution over a ball-raceway contact surface (ASME, 2003)

Deformation at the center of the contact is given by the following formula;

$$\delta = \delta^* \left[\frac{3Q}{2\sum\rho} \left(\frac{(1-\upsilon_I^2)}{E_I} + \frac{(1-\upsilon_{II}^2)}{E_{II}} \right) \right]^{2/3} \frac{\sum\rho}{2} \tag{3.8}$$

In the above equation δ* is dimensionless contact deformation value. The a*, b* and δ* values which are the functions of G(ρ) and can be found from the Table 3.1

Table 3.1 Dimensionless contact parameters (Harris, 2001)

G(ρ)	a*	b*	δ*
0	1	1	1
0.1075	1.076	0.9318	0.9974
0.3204	1.2623	0.8114	0.9761
0.4795	1.4556	0.7278	0.9429
0.5916	1.644	0.6687	0.9077
0.6716	1.8258	0.6245	0.8733
0.7332	2.011	0.5881	0.8394
0.7948	2.265	0.548	0.7961
0.83495	2.494	0.5186	0.7602
0.87366	2.8	0.4863	0.7169
0.90999	3.233	0.4499	0.6636
0.93657	3.738	0.4166	0.6112
0.95738	4.395	0.3830	0.5551
0.9729	5.267	0.3490	0.496
0.98379	6.448	0.3150	0.4352
0.990902	8.062	0.2814	0.3745
0.995112	10.222	0.2497	0.3176
0.9973	12.789	0.2232	0.2705
0.998185	14.839	0.2072	0.2427
0.998916	17.974	0.18822	0.2106
0.999479	23.55	0.16442	0.17167
0.999853	37.38	0.1302	0.11995
1	∞	0	0

3.2 SUBSURFACE STRESSES

Investigations indicate that the contact fatigue of a rolling bearing is a process of the initiation and the propagation of fatigue cracks. They initiate either from a point below contact surfaces of from a point at the surfaces. Besides defects at or below the surfaces, the initiation and propagation are mainly effected by the stress distribution below the surfaces, especially the shear stress distribution (Changsen, 1991).

Some early attempts to apply the fracture mechanics to the study of pit formation mechanism assume that the crack is initiated on the surface due to significant friction forces. Under cyclic contact loading the crack then propagates at a shallow angle to

the core by the combined action of shear forces. In 1950's Lundberg Palmgren observe that in the case of high precision mechanical components and fine surface finish and good lubrication the fatigue crack is usually initiated under the contacting surface in the area of the largest stresses (Harris, 1996, ASME, 2003).

The corresponding axis system for principal stresses (S_x, S_y, S_z) and shear stresses (τ_{xz}, τ_{zy}, τ_{xy}) is sketched in Figure 3.3. τ_{xz} is the one of the critical stress that causes the fatigue failure for some of the researchers and is called orthogonal shear stress. The subsurface stresses are derived by Harris (2001) and the results are given in plots which are illustrated in Figure 3.4 through Figure 3.6.

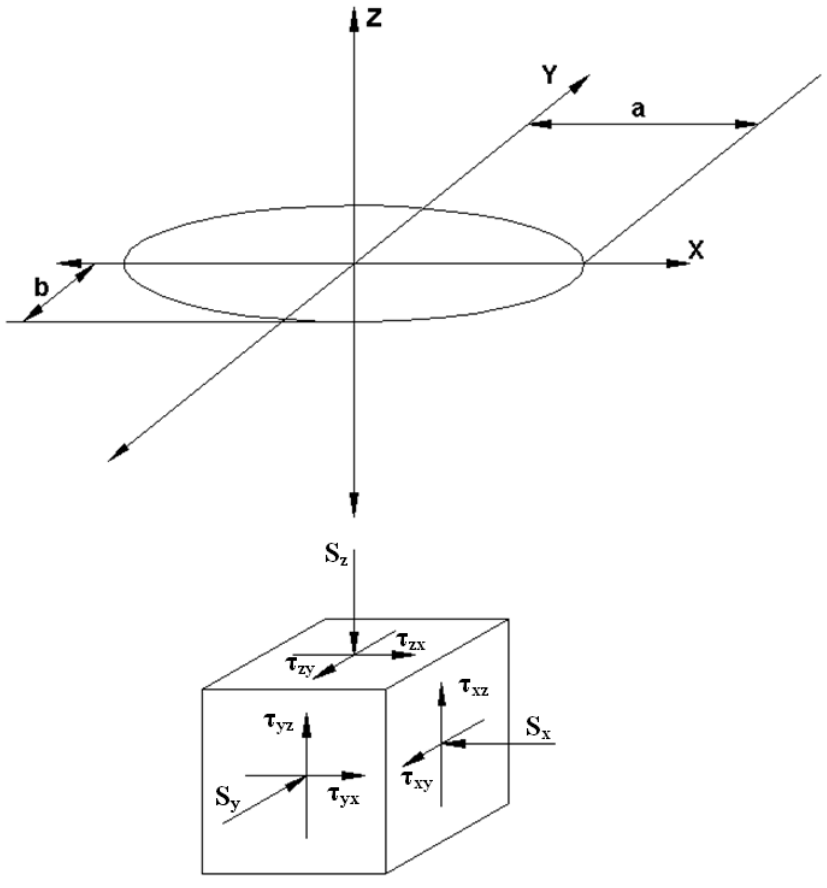

Figure 3.3 Principal stresses occurring on element on Z axis below contact surface

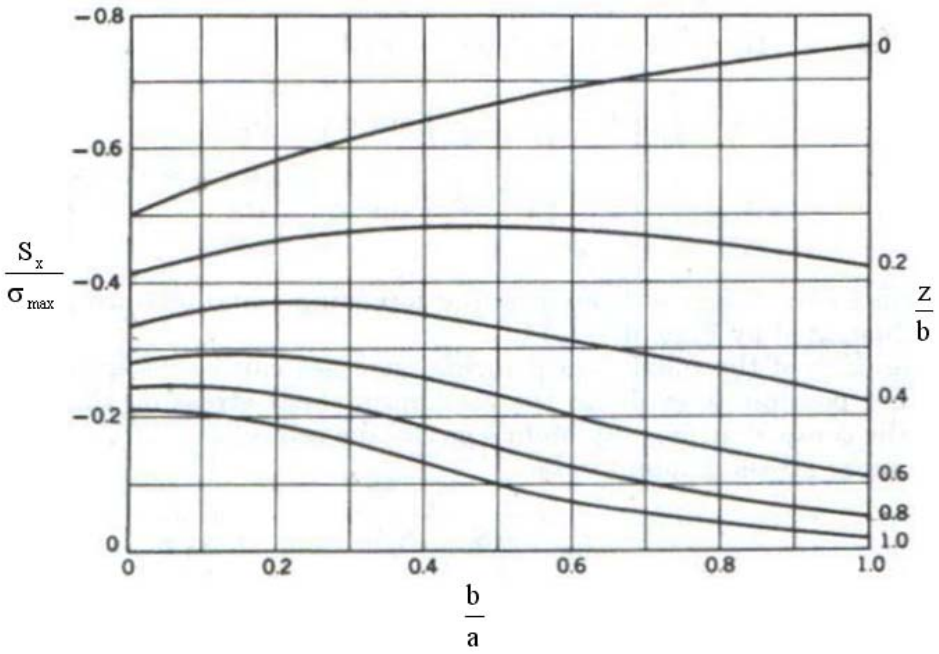

Figure 3.4 S_x/σ_{max} vs. b/a and z/b (Harris, 2001)

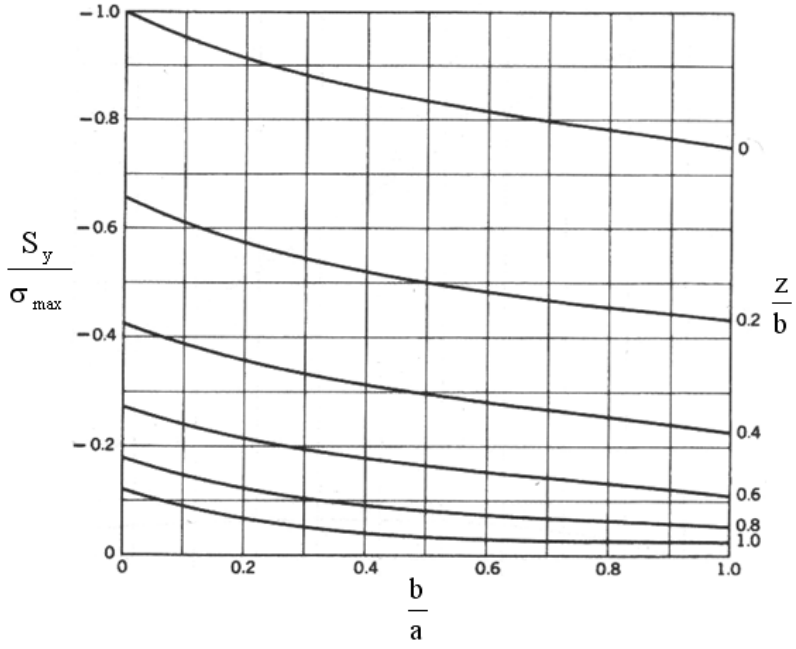

Figure 3.5 S_y/σ_{max} vs. b/a and z/b (Harris, 2001)

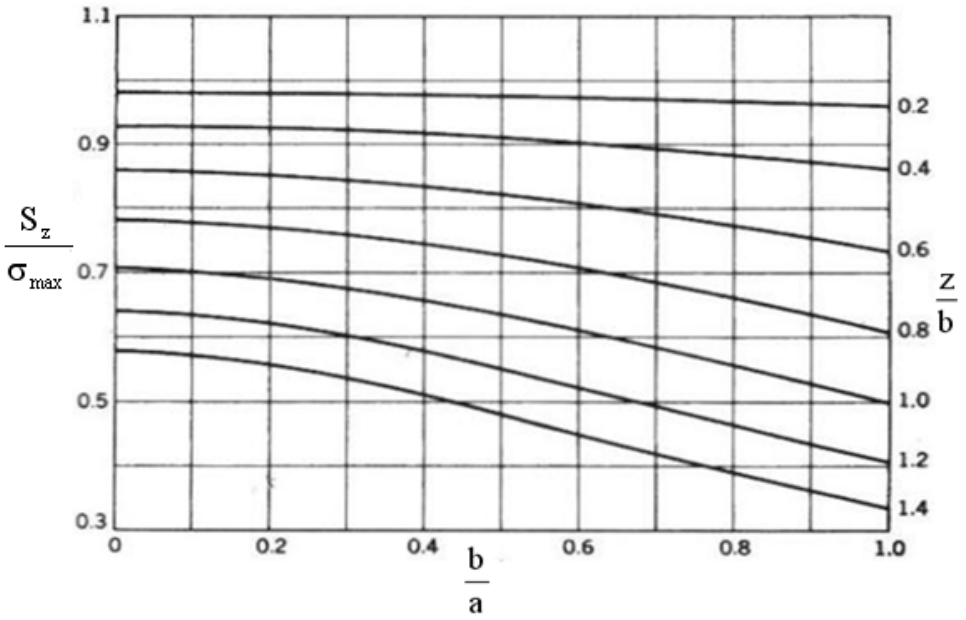

Figure 3.6 S_z/σ_{max} vs. b/a and z/b (Harris, 2001)

Lundberg and Palmgren assumed the maximum orthogonal shear stress which is formed below the contact surfaces to be significant in causing fatigue failure of the surfaces in rolling contact. However many researchers considers the Mises-Hencky distortion energy theory and scalar von Mises stresses a better criterion for rolling contact fatigue (Harris, 2001, ASME, 2003). von Misses stress is given by;

$$\bar{\sigma} = \frac{1}{\sqrt{2}}\left[(\sigma_x - \sigma_y)^2 + (\sigma_y - \sigma_z)^2 + (\sigma_z - \sigma_x)^2 + 6(\tau_{xy}^2 + \tau_{yz}^2 + \tau_{zx}^2)\right]^{1/2} \qquad (3.9)$$

Octahedral shear stress, a vector quantity favored by some researchers, is directly proportional to $\bar{\sigma}$ by the Equation (3.10)

$$\tau_{oct} = \frac{\sqrt{2}}{3}\bar{\sigma} \qquad (3.10)$$

3.3 INTERNAL LOAD DISTRIBUTION OF BALL BEARINGS

To be able to go in detail in stress analyses, the distribution of an external load within the bearing shall be put into consideration. An applied load on a rolling element bearing is distributed over the outer ring of the bearing as shown in the following figure.

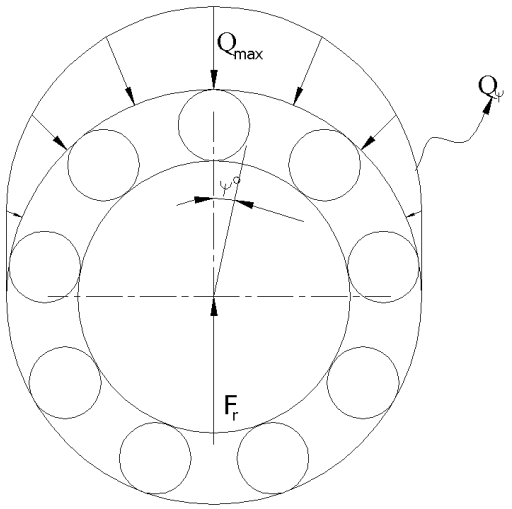

Figure 3.7 Schematic illustration of load distribution on a rolling element bearing

The loading variation for different ball locations considered by utilizing the following equation (Harris, 2001);

$$Q_{\psi} = Q_{max}[1 - \frac{1}{2\kappa}(1 - \cos\psi)]^{m} \quad (3.11)$$

where

Q_{max} : maximum loaded rolling element load (N)

Q_{ψ} : rolling element load depends the angle ψ from the azimuth (N)

κ : load distribution factor, 0.5 for 0 clearance

ψ : angle from the azimuth (rad, °)

m : load deflection exponent, 1.5 for ball bearings

For static equilibrium the applied radial load must equal the sum of the vertical components of the rolling element loads, so;

$$F_r = \sum_{\psi=0}^{\psi=\pm\psi_I} Q_\psi \cos\psi \tag{3.12}$$

$$F_r = Q_{max} \sum_{\psi=0}^{\psi=\pm\psi_I} [1 - \frac{1}{2\kappa}(1-\cos\psi)]^m \cos\psi \tag{3.13}$$

Equation (3.13) can also be written in integral form;

$$F_r = ZQ_{max} \frac{1}{2\pi} \int_{-\psi_I}^{+\psi_I} [1 - \frac{1}{2\kappa}(1-\cos\psi)]^m \cos\psi \quad d\psi \tag{3.14}$$

or,

$$F_r = ZQ_{max} J_r(\kappa) \tag{3.15}$$

in which,

$$J_r(\kappa) = \frac{1}{2\pi} \int_{-\psi_I}^{+\psi_I} [1 - \frac{1}{2\kappa}(1-\cos\psi)]^m \cos\psi \cdot d\psi \tag{3.16}$$

The radial integral, $J_r(\kappa)$, has been evaluated by Changsen (Changsen, 1991) and given for various values of κ in Table 3.2.

For ball bearings under pure radial load and zero clearance the maximum loaded ball load is found from the Stribeck's equation (Harris, 2001);

$$Q_{max} = \frac{4.37F_r}{iZCos\alpha} \tag{3.17}$$

Table 3.2 Load distribution integral $J_r(\kappa)$ for point contact rolling element bearings (Changsen, 1991)

κ	$J_r(\kappa)$
0	1/Z
0.1	0.1156
0.2	0.159
0.3	0.1892
0.8	0.2559
1.25	0.2289
2.5	0.1339
5.0	0.0711

or, it can also be given by the equation (ASME, 2003);

$$Q_{max} = \frac{5F_r}{iZ\cos\alpha} \tag{3.18}$$

where

Fr : radial load (N)

α : contact angle (rad, °)

Z : number of rolling elements per row

i : number of rows

For a ball bearing with 0 clearance, Equation (3.11) becomes;

$$Q_{\psi} = Q_{max}[1 - 1(1 - Cos\psi)]^{1.5} \tag{3.19}$$

The contact angle for a rolling element bearing is defined as the angle of the rolling element–raceway contact from the azimuth of the bearing. The contact angle is schematically illustrated in the following figure.

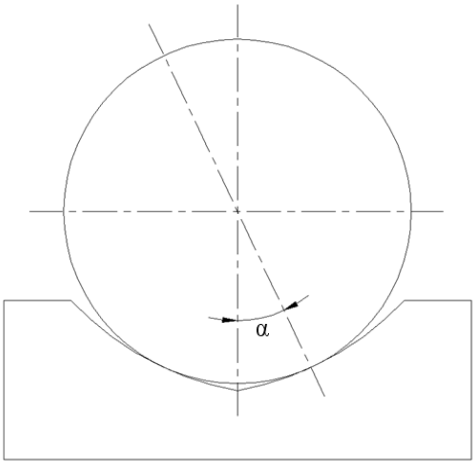

Figure 3.8 Schematic illustration of contact angle

3.4 STATIC LOAD RATING OF BALL BEARING

Rolling Bearings which are stationary, rotate at very low speeds, or make slow oscillating movements should not be selected by fatigue of the bearings but by the permanent deformation at the contact between rolling elements and raceways.

Experience shows that rolling bearings under static load can be stressed to such a degree that minor plastic deformations occur in the rolling surfaces. These indentations and flattened areas, however, should not be of such an extent that they impair the rotation of the bearing. Admissible static rolling element loading, therefore, means that the total plastic deformation of rolling element and raceway does not exceed 0.01% of the rolling element diameter d_w. On the basis of the international standard ISO 76, the static load rating is given a magnitude such that approximately this deformation occurs when the static equivalent load is equal to the load rating (Brändlein et al., 1999).

Static load rating for i-row deep groove ball bearings is given as:

$$C_0 = f_0 i Z D_b^2 \cos\alpha \tag{3.20}$$

where

C_0: static load rating (N)

f_o : factor based on bearing raceway material and raceway geometry

i : number of rows

Z : number of rolling elements per row

D_b: ball diameter (mm)

α : contact angle

Although f_0 is depends on type, material and internal geometry of the bearing in international standard ISO76, f_0 is specified to depend only on bearing types. For deep groove bearings the value of f_0 is given as 12.26 (Changsen, 1987).

In the latest revision of the ISO standard, it is stated that contact stresses at the center of contact at the maximum loaded rolling elements yield permanent deformations of 0.0001D for the bearing types indicated as shown in the Table 3.3 (Changsen, 1991).

Table 3.3 Contact stresses that causes 0.0001D permanent deformation (Changsen, 1991)

Bearing Type	Contact Stress (N/mm^2)
Self-aligning ball bearing	4600
Other ball bearings	4200
Roller bearings	4000

For most radial ball bearing and roller bearing applications the force on the maximum loaded rolling element is approximated by the Equation (3.18). To relate this approximation with the static load rating of the bearing with setting $F_r = C_0$ yields,

$$C_0 = 0.2iZQ_{max}\cos\alpha \qquad (3.21)$$

CHAPTER 4

FATIGUE THEORY

Fatigue is failure under a repeated or otherwise varying load which never reaches a level sufficient to cause failure in a single application. It can also be thought as the initiation and growth of a crack, or growth from a preexisting defect, until it reaches a critical size, such as separation into two or more parts.

Fatigue analysis itself usually refers to one of two methodologies: the stress life or "S-N method", commonly referred to as total life since it makes no distinction between initiating or growing a crack, and the local strain or strain-life (ε-N) method, commonly referred to as the "crack initiation method" which concerns only the initiation of a crack.

4.1 TOTAL LIFE (S-N) ANALYSIS

A metal subjected to a repeated or fluctuating load will fail at a stress level lower than that required to cause fracture on a single application of the load. The nominal stress (S-N) method was the first approach developed to try to understand this failure process and is still widely used in applications where the applied stress is nominally within the elastic range of the material and the number of cycles to failure is large. From this point of view, the nominal stress approach is best suited to that area of the fatigue process known as high-cycle fatigue (HCF). For relatively large cyclic loads that cause significant plastic deformations in the material is inspected by low-cycle fatigue (LCF) methodology. The transition from low-cycle fatigue to high- cycle fatigue generally occurs in the range 10^4 to10^5 cycles.

4.1.1 Stress Cycles

Figure 4.1 details some typical fatigue stress cycles. In the Figure 4.1-(a) illustrates a fully-reversed stress cycle with a sinusoidal form. This is an idealized loading condition typical of that found in rotating shafts operating at constant speed without overloads. For this kind of stress cycle, the maximum and minimum stresses are of equal magnitude but opposite sign. Figure 4.1-(b) illustrates the more general situation where the maximum and minimum stresses are not equal. In this case they are both tensile and defining an offset for the cyclic loading. Figure 4.1-(c) illustrates a more complex, random loading pattern which is more representative of the cyclic stresses found in real structures.

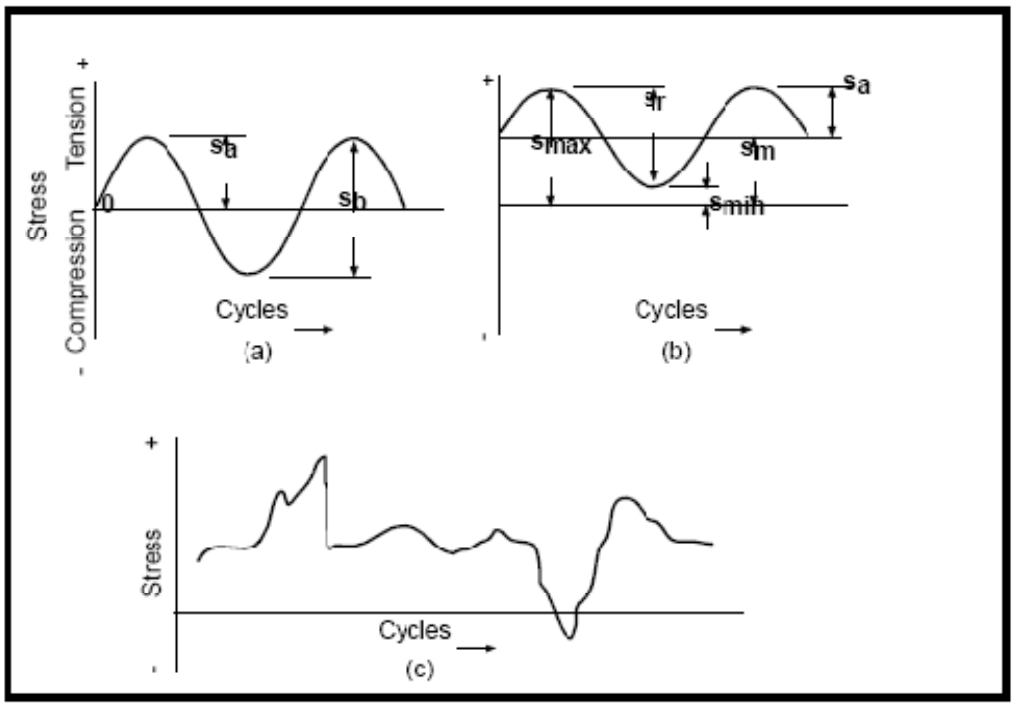

Figure 4.1 Typical fatigue stress cycles,
a) Fully Reversed, b) Offset, c) Random (MSC. Software, 2005)

A fluctuating stress cycle can be considered to be made up of two components, a static or steady mean stress S_m, and alternating or variable stress amplitude, S_a. It is also often necessary to consider the stress range, S_r, which is the algebraic difference between the maximum and minimum stress in a cycle.

$$S_r = S_{max} - S_{min} \tag{4.1}$$

The stress amplitude, S_a , then is one half the stress range.

$$S_a = \frac{S_r}{2} = \left(\frac{S_{max} - S_{min}}{2} \right) \tag{4.2}$$

The mean stress is the algebraic mean of the maximum and minimum stress in the cycle.

$$S_m = \left(\frac{S_{max} + S_{min}}{2} \right) \tag{4.3}$$

Two ratios are often defined for the representation of mean stress, the stress or R ratio, and the amplitude ratio A_R.

$$R = \frac{S_{min}}{S_{max}} \tag{4.4}$$

and

$$A_R = \frac{S_a}{S_m} = \frac{(1-R)}{(1+R)} \tag{4.5}$$

The S-N, or Wohler, diagram shown in Figure 4.2 is the standard way to characterize the behavior of materials under completely reversed loading.

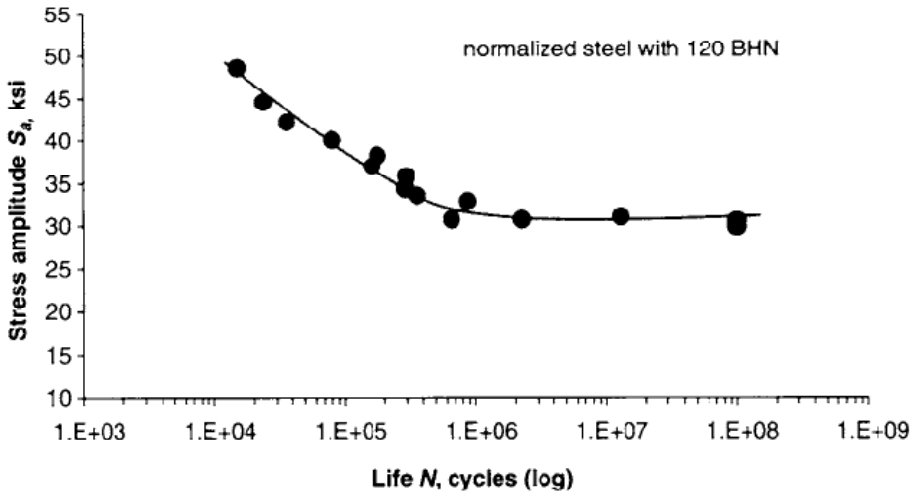

Figure 4.2 Typical S-N curve plotted on semilog coordinates (Lee, 2005)

S-N data are nearly always presented in the form of semilog or log-log plot of alternating stress, amplitude S_a or range S_r, versus cycles to failure, with the actual Wohler line representing the mean of the data. Certain materials, steels for example, display a fatigue limit (also called endurance limit), S_e, which is defined as the maximum value of stress amplitude at zero mean stress which can be repeated an infinite number of times on a test specimen without causing a failure. For most engineering purposes, infinite life is taken to be 1 million cycles. S-N curves do not separate crack initiation from propagation, and only the total life to fracture is given (Fuchs et. al, 1980).

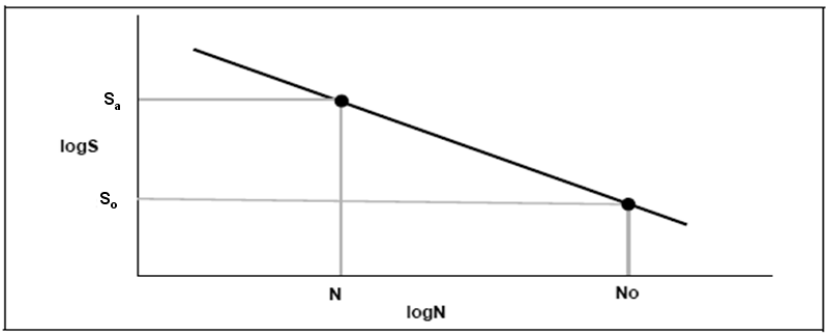

Figure 4.3 Idealized form of the S-N curve

When plotted on log-log scales, the relationship between alternating stress, S, and number of cycles to failure, N can be described by a straight line in Figure 4.3. The slope of the line, t, can be derived from the following:

$$t = \frac{-\left(\log S_a - \log S_0\right)}{\left(\log N_0 - \log N\right)} \tag{4.6}$$

$$N = N_0 \left(\frac{S_a}{S_0}\right)^{\frac{1}{t}} \tag{4.7}$$

Sometimes, for convenience, the term 1/t is replaced by the letter k,

$$N = N_0 \left(\frac{S_a}{S_0}\right)^{k} \tag{4.8}$$

With the use of above equation any other coordinate pair (N-S), for a given stress amplitude S, the number of cycles can be calculated directly. Typically, N_o is taken to be 10^6 cycles and the corresponding stress amplitude is taken to be an endurance limit, usually denoted as S_e or S_6, so that the above equation may be rewritten as:

$$N = 10^6 \left(\frac{S_a}{Se}\right)^{k} \tag{4.9}$$

4.1.2 Combined Mean and Alternating Stress

Mean stress component has significant effect on failure. When a tensile mean component of stress is added to the alternating component the material fails at lower alternating stresses than it does under fully reversed loading (Norton, 2006).

Fatigue data collected from a series of tests designed to investigate different combinations of stress amplitude and mean stress are characterized in Figure 4.4 for a given number of cycles to failure. The diagram plots the mean stress, both tensile

and compressive, along the x-axis and the alternating constant stress amplitude along the y-axis. This kind of representation was first proposed by Haigh and is therefore commonly referred to as the Haigh diagram.

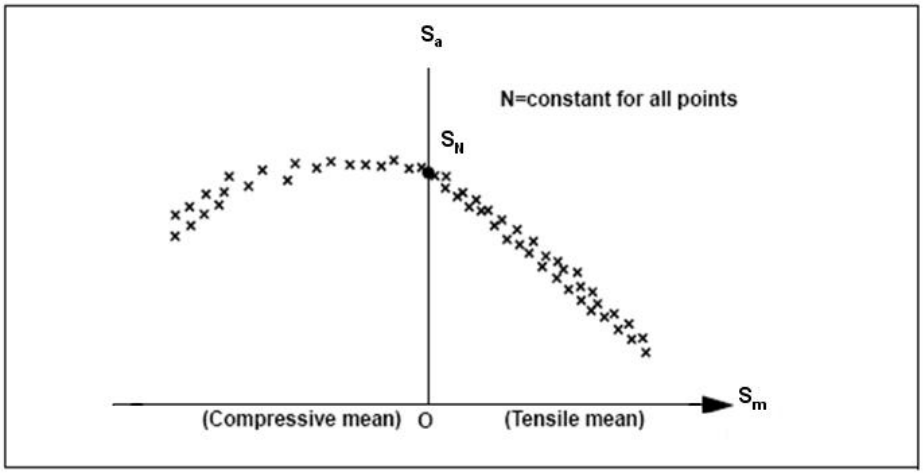

Figure 4.4 High-cycle fatigue data showing the influence of mean stress (Norton, 2006)

As seen in the figure the effect of mean stress is different for compressive and tensile values. Failure appears to be more sensitive to tensile mean stress, than compressive mean stress.

Empirical relationships that relate alternating stress amplitude to mean stress have been developed. These relationships characterize a material with its ultimate tensile strength, S_u. For infinite life design strategies, the methods use various curves to connect the endurance limit, S_e, on the alternating stress axis to either the yield stress, S_y, ultimate strength, S_u, or true fracture stress, S_f, on the mean stress axis. Of all the proposed relationships, Goodman and Gerber lines have been most widely used.

The fatigue strength or endurance limit of the material is effectively increased by the introduction of a compressive mean stress, whether applied or residual. The fact provides an opportunity to decrease the effects of alternating tensile stresses by the

intentionally introduced mean compressive stresses. One way to this is to create residual compressive stress in the material in regions where large alternating components are expected (Norton, 2006).

Typical dimensionless plots are shown in Figure 4.5, where S_a/S_f versus S_m/S_u is plotted. S_f is fully reserved fatigue strength and S_u is the ultimate tensile strength. It can be seen that many of the data is between the straight and curved lines. The straight line is the Goodman line and the curved is Gerber parabola.

a)

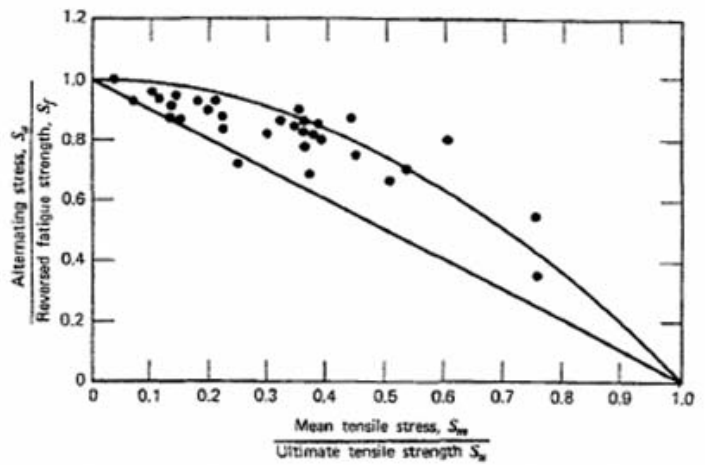

b)

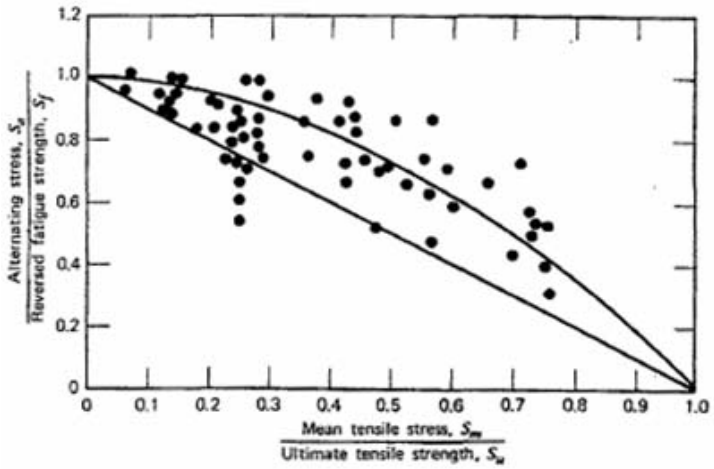

Figure 4.5 Effect of mean stress on alternating fatigue strength at long life. a) Steels based on ~10E7 cycles, b) Aluminum alloys based on ~5x10E7 cycles (Forrest, 1962)

The modified Goodman and Gerber formulae are given in following equations;

Modified Goodman Equation:

$$\frac{S_a}{S_f} + \frac{S_m}{S_u} = 1 \tag{4.10}$$

Gerber Equation:

$$\frac{S_a}{S_f} + \left(\frac{S_m}{S_u}\right)^2 = 1 \tag{4.11}$$

4.2 CUMULATIVE DAMAGE

To predict life expectancy in parts with spectrum loading is one of the difficult problems concerned with limited fatigue life. The fatigue life in spectrum loading is a function of gathered effects on the part, at various stress levels, throughout its performance.

Palmgren-Miner Rule: The Palmgren-Miner rule is based on an assumption of linear concept that the changing of the sequence of the loading cycles did not affect the fatigue life. The rule is a combined result, introduced first by Palmgren in analysis of ball bearings and adapted by Miner for aircraft structures (Zahavi, 1996).

Life estimates made by employing Palmgren-Miner rule along with a cycle counting procedure. Target is to estimate how many of the blocks can be applied before failure occurs. This theory may be described using the S-N plot.

In Figure 4.6, a spectrum of amplitudes of stress cycles is described as a sequence of constant amplitude blocks, each block having stress amplitude S_i and the total number of applied cycles n_i. The constant amplitude S-N curve, in log scale is also shown by Figure 4.7.

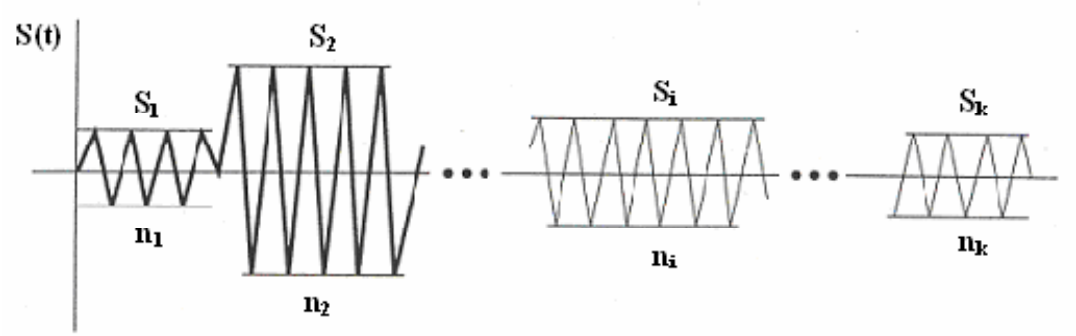

Figure 4.6 Spectrum of amplitudes of stress cycles (Arıduru, 2003)

By using the S-N data, number of cycles of S_1 is found as N_1 which would cause failure. Operation at stress amplitude S_1 for a number of cycles n_1 smaller than N_1 produces a smaller fraction of damage which can be termed as D_1 and called as the damage fraction.

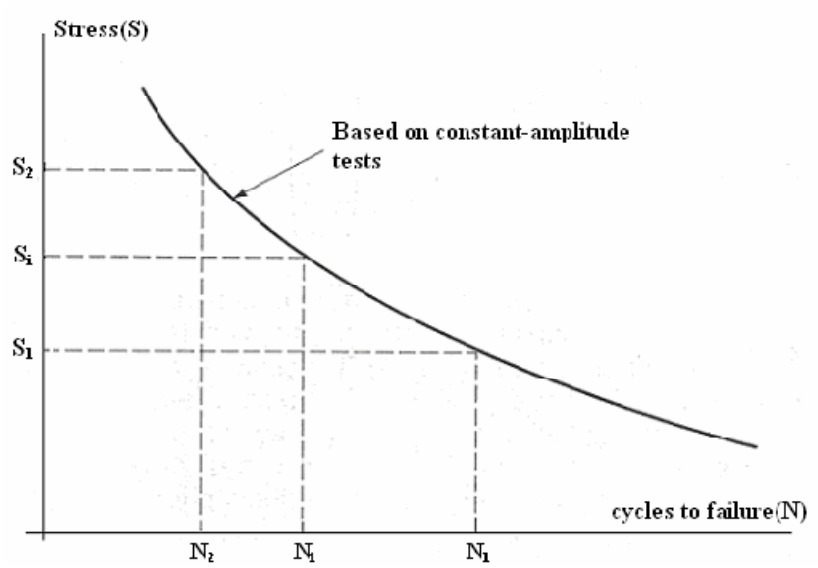

Figure 4.7 Constant amplitude S-N curve

At each load level the theoretical life expectancy is N_i number of cycles. The damaging effect of a single cycle at this level is assumed to be;

$$D_i = \frac{1}{N_i} \tag{4.12}$$

The damage after n_i cycles at this level is;

$$n_i D_i = \frac{n_i}{N_i} \tag{4.13}$$

The accumulated damage from the entire loading can be given by;

$$\sum n_i D_i = \sum \frac{n_i}{N_i} = \frac{n_1}{N_1} + \frac{n_2}{N_2} + \frac{n_3}{N_3} + \ldots \tag{4.14}$$

For practical application, the Miner equation can be revised as;

$$\sum n_i D_i = M \tag{4.15}$$

Where M is an empirical constant which usually varies within the range (Zahavi, 1996)**;**

$$0.7 \leq M \leq 2.2 \tag{4.16}$$

4.3 CRACK INITIATION/STRAIN LIFE (ε-N) ANALYSIS

In a notched component or specimen subjected to cyclic external loads, the behavior of material at the root of the notch is best considered in terms of strain. As long as there is elastic constraint surrounding a local plastic zone at the notch the strains can be calculated more easily than the stress (Shigley, 1989). This concept has motivated a finite fatigue life design philosophy based on relating the fatigue of notched parts to the life of small unnotched specimens that are cycled to the same strains as the material at the notch root. This is called strain control. Reasonable expected fatigue life, based on the initiation or formation of small macro cracks can be determined

knowing the local-time history at a notch in a component and the unnotched strain-life fatigue properties of the material and assuming a reasonable damage theory (Fuchs et. al, 1980). Sraml et al. (2003) claims that although strain-life method is recommended for low cycle fatigue considerations it is claimed that the method can be used as advantage over the S-N method even in high cycle application, due to its less scatter-prone materials data.

In performing smooth specimen tests which characterize fatigue performance, it must be recognized that fundamental material properties are being measured which are independent of component geometry.

Strain-life fatigue curves plotted on log-log scale are shown in Figure 4.8, N or 2N is the number of cycles or reversals to failure, respectively. Failure criteria for strain-life curves have not been consistently defined in that failure may be the life to a small detectable crack, life to a certain percentage decrease in load amplitude, or life to fracture. Differences in fatigue life depending on these three criteria may be small or appreciable (Shigley, 1989).

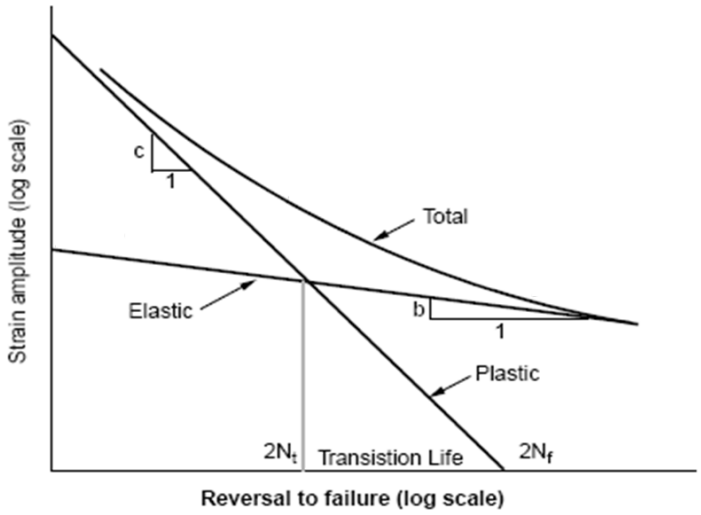

Figure 4.8 Strain curves showing the total elastic and plastic strain components

4.3.1 Cyclic Stress-Strain Curve

The cyclic response of a material describes the process of change in the resistance of a material to deformation due to cyclic loading. If a material is repeatedly cycled under fully reversed strain-controlled loading, the material respond in one of the following ways: cyclic hardening, cyclic softening, remaining stable, or some combination of these responses.

If a specimen of a material is loaded in tension to beyond the yield stress to a maximum stress of σ_{max}, point B in Figure 4.9 and at this point the loading reversed and the specimen is unloaded from point B through the zero stress level than loaded into compression to a stress level equal to - σ_{max} and if the loading process started is continued, the loading direction is again reversed and the specimen is loaded back up to σ_{max}, then a complete loop will be defined. The stress-strain loop illustrated in Figure 4.10 is called a hysteresis loop and defines, in stress-strain space, a single fatigue cycle. During the initial loading, the stress-strain response is according to the curve O-A-B where yielding starts at σ_a. On unloading, yielding begins in compression at point C where yielding starts at σ_c and $|\sigma_a|>|\sigma_c|$. This behavior is called Bauschinger Effect.

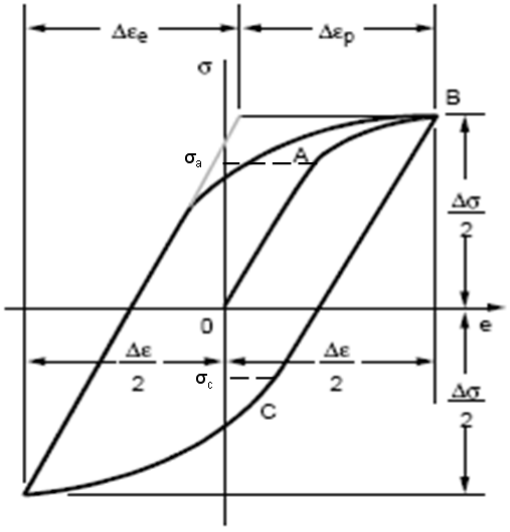

Figure 4.9 A complete stress-strain cycle, a hysteresis loop.

The dimensions of the hysteresis loop are described by its total width, the total strain range $\Delta\varepsilon$, and its height, the total stress range $\Delta\sigma$. The total strain range is the sum of its elastic and plastic components:

$$\Delta\varepsilon_t = \Delta\varepsilon_e + \Delta\varepsilon_p \tag{4.17}$$

where

$\Delta\varepsilon_e$: elastic strain range

$\Delta\varepsilon_p$: plastic strain range

$\Delta\varepsilon_t$: total strain range

The softening or hardening response of the material is believed to have relation with stability of the dislocation substructure within the metal crystal lattice of the material. In general, soft materials such as aluminum alloys with low dislocation densities tend to harden and hard materials such as steels tend to soften. A rule of thumb is that the material will harden if Su/Sy>1.4 and the material will soften is Su/Sy<1.2 (Lee, 2005). For ratios between 1.2 and 1.4, the material can exhibit hardening, softening or both. These behaviors of materials indicate that use of monotonic material properties for fatigue life predictions can sometimes lead to inaccurate results.

Figure 4.10 shows the cyclic softening and hardening effects for two different materials where the first two hysteresis loops are plotted. In both cases, the specimen is between fixed-strain limits and the load is allowed to find its own level. In case of hardening, the maximum stress reached in each successive strain cycle increases with number of cycles and in the case of softening the maximum stress decreased with imposed cycles. These processes do not continue for both cases. The stress will have a constant level and remain stable at that level until the first fatigue crack.

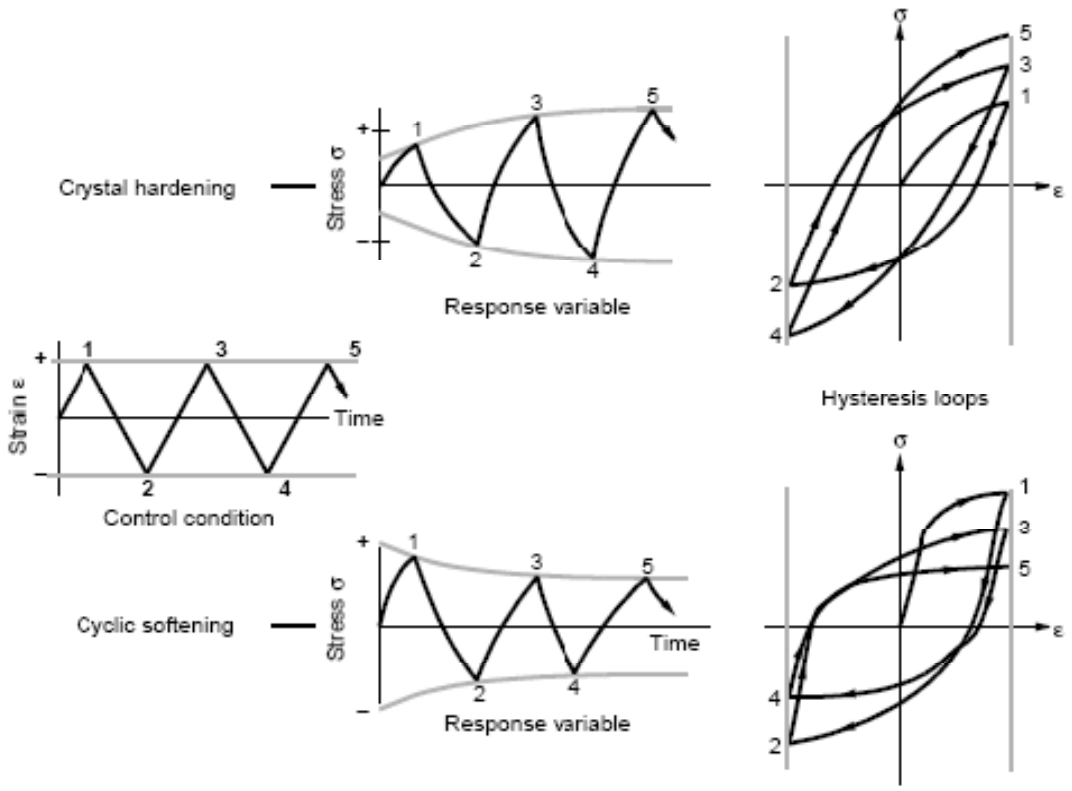

Figure 4.10 Cyclic hardening and softening under strain control
(MSC Software, 2005)

4.3.1.1 Determination of the cyclic stress-strain curve

As mentioned before the stress-strain response of most materials changes with applied cyclic strains. However after small number of cycles the hysteresis loops stabilizes so the stress amplitude remains constant over the remaining portion of fatigue life. As shown in Figure 4.11, if the stress-strain coordinates of the tips from a number of stable hysteresis loops are plotted in stress-strain space, then the locus of these points defines the cyclic stress-strain curve.

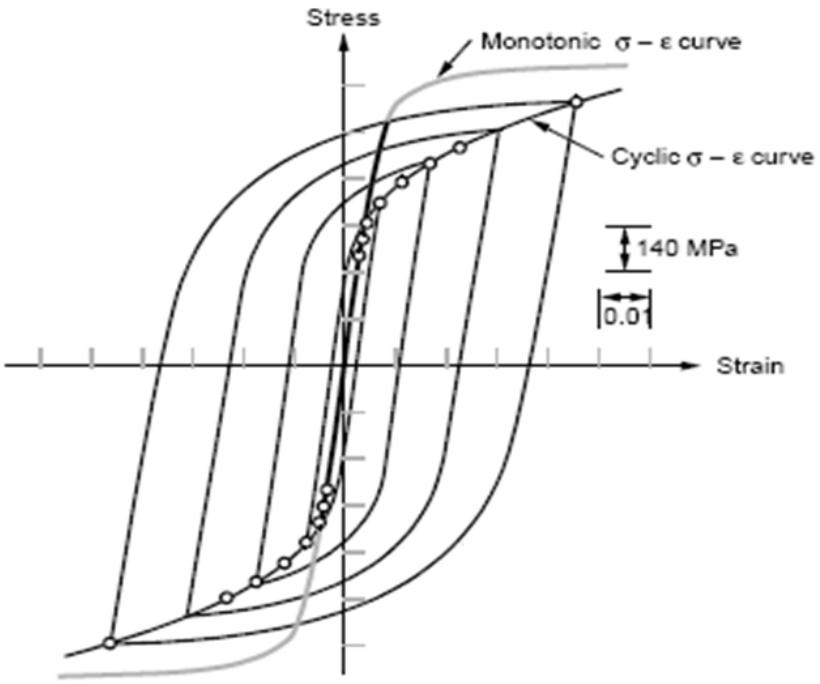

Figure 4.11 Definition of the stable cyclic stress-strain curve
(MSC Software, 2005)

The cyclic stress-strain curve defines the relationship between stress and strain under cyclic loading conditions. The cyclic stress-strain curve can be compared directly with the monotonic stress-strain curve to quantitatively asses the cyclically induced changes in material behavior.

In the plastic domain beyond the yield point the true stress-strain relationship can be expressed by Hollomon correlation (Zahavi, 1996);

$$\sigma = K'\varepsilon^{n'} \tag{4.18}$$

where

K’ : cyclic strength coefficient

n’ : cyclic strength exponent

The cyclic stress-strain curve is defined by;

$$\varepsilon_t = \frac{S}{E} + \left(\frac{S}{K'}\right)^{\frac{1}{n'}} \tag{4.19}$$

The elastic and plastic components are defined as follows. The elastic strain is given with the equation;

$$\varepsilon_e = \frac{S}{E} \tag{4.20}$$

and the plastic part of the strain is given by;

$$\varepsilon_p = \left(\frac{S}{K'}\right)^{\frac{1}{n'}} \tag{4.21}$$

Since the many homogenous materials have symmetric behavior in tension and compression, Equation (4.19) can be rewritten in terms of strain range and stress range;

$$\Delta\varepsilon_t = \frac{\Delta S}{E} + 2\left(\frac{\Delta S}{2K'}\right)^{\frac{1}{n'}} \tag{4.22}$$

Equation (4.22) may be simplified with the help of data from cyclic tests, for the stress and strain that cause a specimen's fracture at the first reversal of cyclic loading, the stress is referred as fatigue strength coefficient, and is denoted by σ'_f, and the strain, referred as fatigue ductility coefficient, is denoted by ε'_f (Figure 4.12). The cyclic strength coefficient K' can be expressed in terms of σ'_f and ε'_f as;

$$K' = \frac{\sigma'_f}{(\varepsilon'_f)^{n'}} \tag{4.23}$$

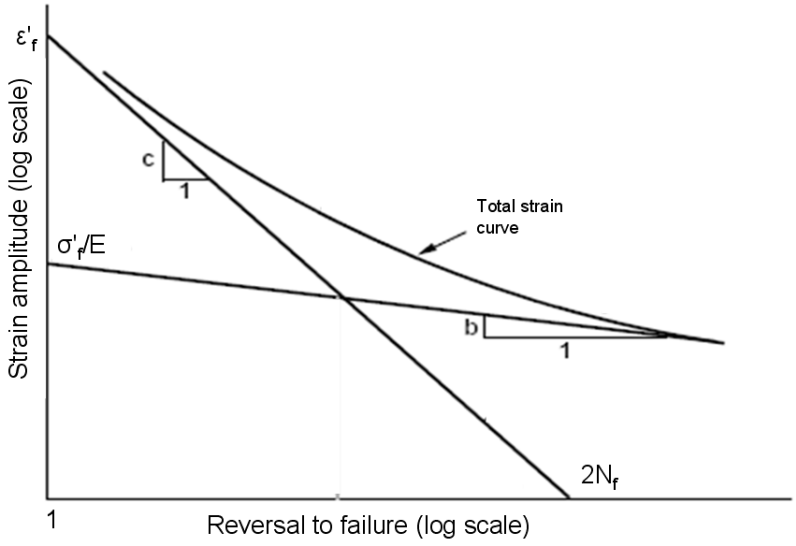

Figure 4.12 Illustration of fatigue strength and fatigue ductility coefficients on strain-life plot

4.3.1.2 The Strain-Life Curve

The method of fatigue life prediction is dependent on stress based method. It began with Basquin equation which is depended on empirical formula (Zahavi, 1996). Stress-life data can be represented by a straight line relationship when plotted using log scales. The relationship can be expressed in terms of true stress as:

$$S_a = S'_f (2N_f)^t \tag{4.24}$$

where

S_a : true cyclic stress amplitude

$2N_f$: number of load reversals to failure

t : fatigue strength exponent

Equation (4.24) can be written in terms of elastic strain amplitude as;

$$\varepsilon_e = \frac{\sigma_a}{E} = \frac{\sigma'_f}{E}(2N_f)^t \tag{4.25}$$

where

ε_e : the elastic strain amplitude

E : the modulus of elasticity

Plastic strain component of a fatigue cycle may be related to life by;

$$\varepsilon_p = \varepsilon'_f (2N_f)^g \tag{4.26}$$

where

ε_p : the plastic strain amplitude

ε'_f : the regression intercept called fatigue ductility coefficient

$2N_f$: number of reversals, to failure

g : fatigue ductility exponent

The total strain is the sum of elastic and plastic components as;

$$\varepsilon_t = \varepsilon_e + \varepsilon_p \tag{4.27}$$

Utilizing the Equations (4.25), (4.26) and (4.27) gives:

$$\varepsilon_t = \frac{S'_f}{E}(2N_f)^t + \varepsilon'_f (2N_f)^g \tag{4.28}$$

which is the Manson-Coffin relationship between fatigue life and total strain (Lee, 2005).

If the formulae given in Equations (4.25) and (4.26) plotted on log-log scales, both curves become straight lines and the sum of them gives the strain-life curve of the material, (Figure 4.13). The cross point, between the elastic and plastic lines, divides the total strain range. This cross point occurs at transition life, $2N_t$ and it shows a transition from a plastic domain into elastic one. To the left of transition life $2N_t$, the deformation is mainly plastic with only minor elastic strain. To the right, the

deformation is mainly elastic with insignificant plastic strain. At transition point elastic and plastic strains become equal;

$$\varepsilon_e = \varepsilon_p \tag{4.29}$$

or, can be written as;

$$\frac{S'_f}{E}(2N_f)^t = \varepsilon'_f\,(2N_f)g \tag{4.30}$$

and transition life can be determined by;

$$2N_t = \left(\frac{\varepsilon'_f\,E}{S'_f}\right)^{\frac{1}{(t-g)}} \tag{4.31}$$

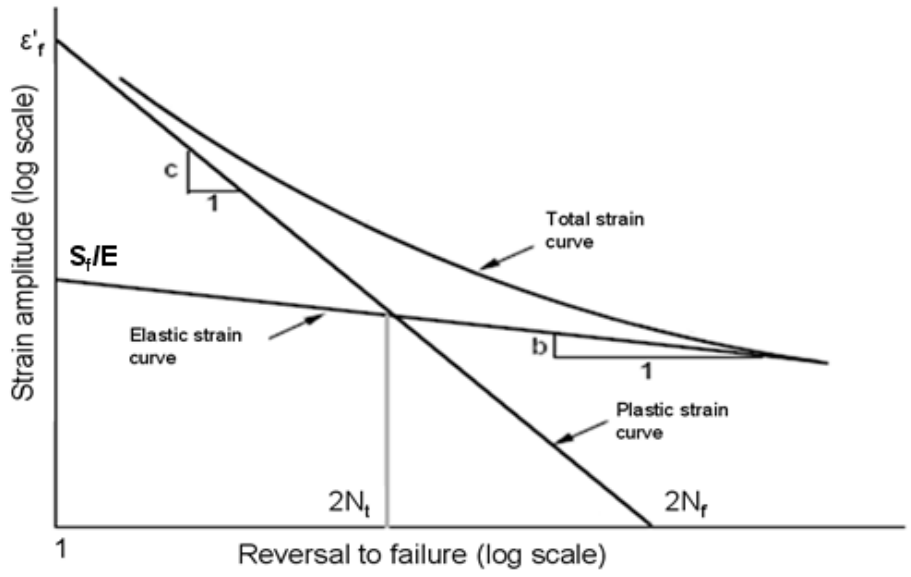

Figure 4.13 Schematic of total strain-life curve

4.3.2 Effect of Mean Stress and Correction Approaches

Most basic fatigue data are collected with testing procedures which employs fully reversed loading. However the products generally service under nonzero mean stresses. Therefore the influence of the mean stress shall be put into consideration during fatigue calculations.

In Figure 4.14 the effect of mean stress on the strain-life curve is shown schematically. It can be observed from the figure that with compressive means the life is extended and for tensional means reducing the life of the material. Generally following modified approaches of the strain-life method are most often used for fatigue calculations: Morrow's method, Smith-Watson-Topper (SWT) method (Lee, 2005).

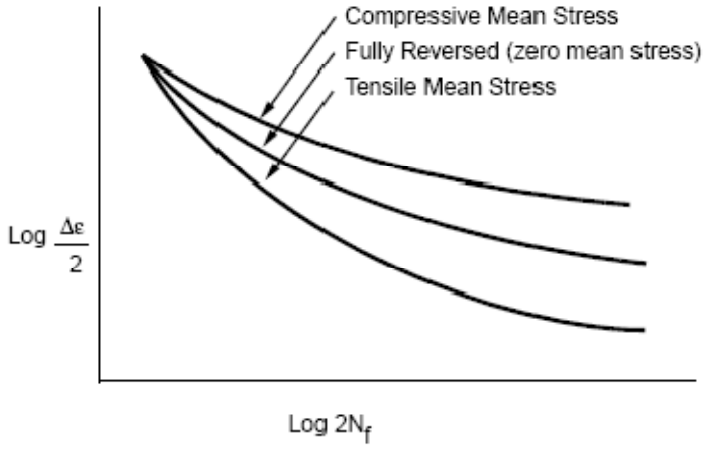

Figure 4.14 Effect of mean stress on the strain-life curve (MSC Software, 2005).

4.3.2.1 The Morrow Mean Stress Correction

According to Morrow Correction the effect of mean stress can be taken into account by modifying the elastic part of the strain curve by mean stress, S_m (Suresh, 1991):

$$\varepsilon_e = \frac{S_f^{'} - S_m}{E}(2N_f)^t \tag{4.32}$$

So, the total strain can be found from the formula,

$$\varepsilon_t = \frac{S'_f - S_m}{E}(2N_f)^t + \varepsilon'_f (2N_f)^g \tag{4.33}$$

The Morrow mean stress correction is illustrated graphically by Lee and Taylor (2005) and given by Figure 4.15.

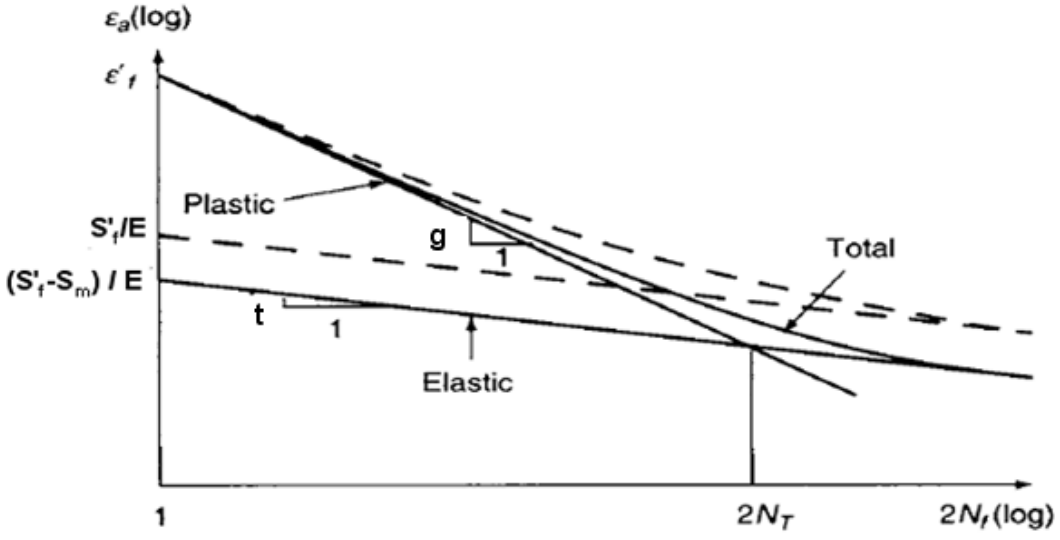

Figure 4.15 Morrow mean stress correction model (Lee, 2005)

As illustrated in Figure 4.15, the formulation indicates that a tensile mean stress would reduce the fatigue strength, S'_f, and a compressive mean stress would increase the fatigue strength coefficient.

4.3.2.2 The Smith-Watson-Topper Mean Stress Correction

This approach considers the maximum stress present in any cycle for taking the mean stress into account. In this case, the damage parameter is taken to be the product of the maximum stress, σ_{max}, and the strain amplitude, ε_a of a cycle.

For fully reversed loading, the maximum stress is given by

$$S_{max} = S'_f (2N_f)^t \tag{4.34}$$

and by multiplying the strain-life equation by this term gives,

$$S_{max}\varepsilon_a = \frac{S'_f}{E}(2N_f)^t + S'_f \varepsilon'_f (2N_f)^{t+g} \tag{4.35}$$

The Smith-Watson-Topper approach predicts that no fatigue damage can occur when the maximum stress becomes zero or negative, which is not applicable for rolling element bearing fatigue.

4.3.3 Neuber's Rule

Notch analysis is used to relate the nominal stress or strain changes in a component to the local stress response at a notch. This can be used to predict the crack initiation life of notched components by using fatigue life data from smooth laboratory specimens (Lee, 2005).

Neuber is the first to analyze a grooved shaft subjected to monotonic torsional loading and derived a rule for nonlinear material behavior at the notched root. Once the elastic stress and strain distribution are determined for the fatigue calculations, in order to use ε-N method for fatigue life Neuber method is used to determine the purely elastic stress and strains in elasto-plastic stresses and strains. With the use of Neuber method the elastic stresses and strains are looked up on the elastic line and corrected to fall onto the cyclic stress-strain curve to determine the elastic-plastic

stresses and strains. This elastic-plastic strain is used to determine the damage on the strain-life damage curve. As seen in the Figure 4.16, Neuber's elastic-plastic correction is based on the simple principle that the product of the elastic stress and strain should be equal to the product of the elastic-plastic stress and strain from the cyclic stress-strain curve (Sraml et al., 2003).

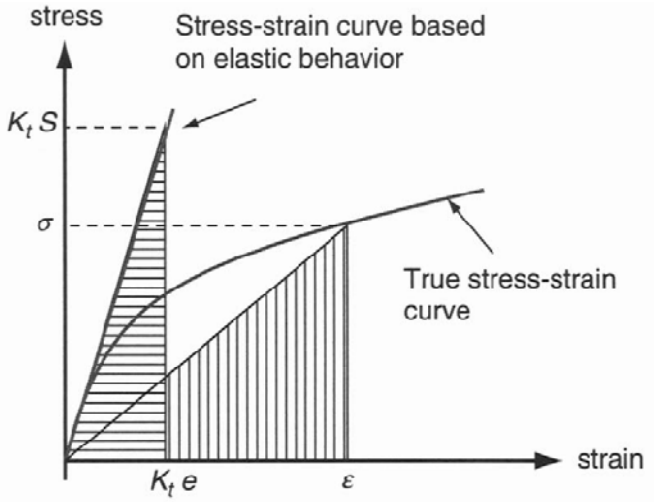

Figure 4.16 Interpretation of the Neuber model (Lee, 2005)

The Neuber's rule is given by the following equation;

$$\Delta\sigma\Delta\varepsilon = K_t^2 \Delta S \Delta e \tag{4.36}$$

where

$\Delta\sigma$: local stress range,

$\Delta\varepsilon$: local strain range,

ΔS : nominal stress range,

Δe : nominal strain range,

K_t : Stress concentration factor.

Neuber hypothesized that the stress concentration factor (K_t) is the geometric mean of the true stress and strain concentration factors, i.e.,

$$K_t = \sqrt{K_\sigma K_\varepsilon} \tag{4.37}$$

and

$$K_\sigma = \frac{\sigma_a}{S} \tag{4.38}$$

$$K_\varepsilon = \frac{\varepsilon_a}{e_a} \tag{4.39}$$

where, K_σ is the true stress concentration factor and K_ε is the true strain concentration factor, S and e_a are the nominal stress and strain amplitudes, respectively, and σ_a and ε_a are the local true stress and strain amplitudes respectively.

During the cyclic loading, it is assumed that the material follows the cyclic stress-strain curve for the initial loading and hysteresis stress-strain behavior for the subsequent loading reversals. Therefore, in terms of the initial cyclic stress-strain curve the modified Neuber equation can be reduced to following equation.

$$\sigma_1 \varepsilon_1 = K_t^2 S_1 e_1 \tag{4.40}$$

where σ_1 and ε_1 are true stress and strain for initial loading respectively and S_1 and e_1 are the nominal stress and strain for the initial loading, respectively. For hysteresis behavior Neuber equation can be written as;

$$\Delta\sigma\Delta\varepsilon = K_t^2 \Delta S \Delta e \tag{4.41}$$

where $\Delta\sigma$ and $\Delta\varepsilon$ are true stress and strain ranges, respectively and ΔS and Δe are the nominal stress and strain ranges, respectively.

Figure 4.17 shows the application of the modified Neuber model to a notched plate subjected to first loading reversal, where the nominal strain Δε and Kt are known based on the applied nominal stress ΔS and notch geometry. The Neuber constant C can be calculated and a hyperbola of the local stress and strain changes ($\Delta\sigma\Delta\varepsilon = C$) is generated. A hysteresis stress-strain curve for the material is needed to intersect the hyperbola for the solution of Δσ and Δε (Lee, 2005).

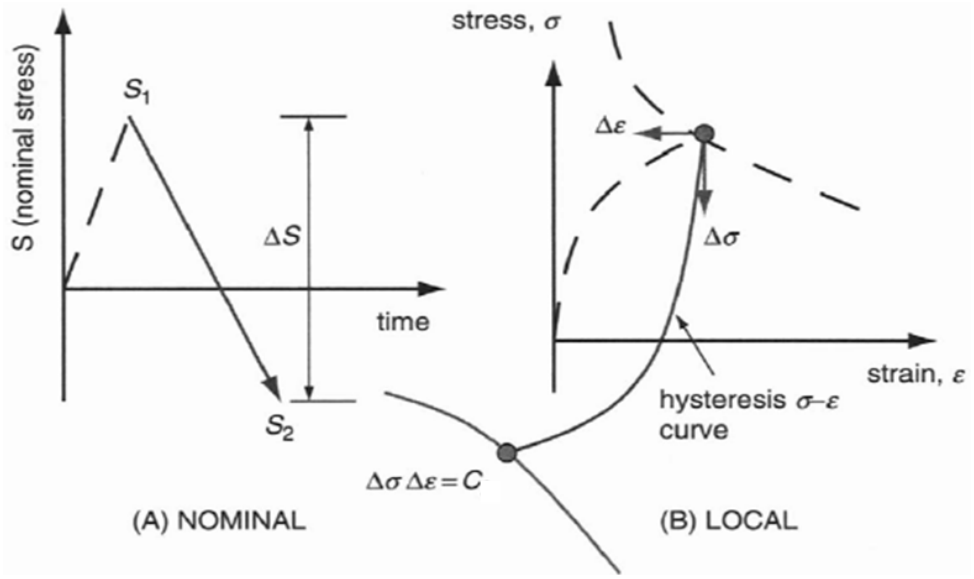

Figure 4.17 Nominal stress reversal loading with the Neuber rule (Lee, 2005)

Nominally Elastic Behavior

When a notched component behaves elastically and plasticity takes place locally at the notch root (i.e., nominally elastic condition), the following equations hold (Lee, 2005):

For the initial cyclic stress-strain curve:

$$e_1 = \frac{S_1}{E} \tag{4.42}$$

$$\varepsilon_1 = \frac{\sigma_1}{E} + \left(\frac{\sigma_1}{K'}\right)^{1/n'} \tag{4.43}$$

For the hysteresis stress-strain curve:

$$\Delta e = \frac{\Delta S}{E} \tag{4.44}$$

$$\Delta\varepsilon = \frac{\Delta\sigma}{E} + 2\left(\frac{\Delta\sigma}{2K'}\right)^{1/n'} \tag{4.45}$$

Substituting the elastic nominal stress-strain and the local cyclic stress-strain relations (Equations (4.42) and (4.45)) into the Neuber equations given by Equations (4.40) and (4.41) gives the following equations;

$$\frac{\sigma_1^2}{E} + \sigma_1\left(\frac{\sigma_1}{K'}\right)^{1/n'} = \frac{(K_t S_1)^2}{E} \tag{4.46}$$

and

$$\frac{(\Delta\sigma)^2}{E} + 2\Delta\sigma\left(\frac{\Delta\sigma}{K'}\right)^{1/n'} = \frac{(K_t \Delta S)^2}{E} \tag{4.47}$$

For given K_t and the nominal stress data, these equations for the local stress can be solved. Once the local stress is determined, Equation (4.43) or (4.45) is used to obtain the local strain value.

CHAPTER 5

BEARING FATIGUE

Every rolling bearing element has a definite fatigue life depending on the number of rolling cycles and the load. Fatigue damage begins with the formation of cracks bellow the surface. As loading continues, the cracks progress to the surface where they cause material to break (Eschmann et al., 1985).

5.1 DYNAMIC LOAD CAPACITY OF ROLLING ELEMENT BEARING

The dynamic load capacity (rating) C of a radial bearing corresponds to a purely radial constant load at which a large number of identical bearings each with rotating inner ring and fixed outer ring, reach a rating life of 1 million revolutions (Eschmann et al., 1985). Dynamic loading capacity for a radial bearing can be given by:

for bearings with ball diameter, $D_b \leq 25.4$ mm

$$C = f_{cm}(i\cos\alpha)^{0.7} Z^{2/3} D_b^{1.8} \tag{5.1}$$

for bearings with ball diameter, $D_b > 25.4$ mm

$$C = f_{cm}(i\cos\alpha)^{0.7} (3.647) Z^{2/3} D_b^{1.4} \tag{5.2}$$

where

C : dynamic load capacity of the bearing,

f_{cm} : factor based on bearing raceway material and raceway geometry,

i : number of rolling element rows in bearing

α : nominal contact angle between the ball-raceway,

Z : number of rolling elements in a row,

D_b : ball diameter

5.2 FATIGUE LIFE OF BEARINGS

Rolling bearing theory postulated that no rotating bearing can give unlimited service because of the probability of fatigue of the surfaces in rolling contact. Fatigue life of a radial bearing is given by the following equation which is also accepted by ISO and ANSI/ABMA standards;

$$L_{10} = L = \left(\frac{C}{P}\right)^3 [10^6 \text{ revolutions}] \tag{5.3}$$

where

L : rating life (10^6 revolutions)

P : applied load (N)

The subscript 10 for the life in ISO formulation postulated that 90% of the bearing population will endure.

5.3 EXTENDED BEARING LIFE CALCULATION

The rating life L_{10} is for bearings of conventional rolling bearing steel (good quality hardened steel) operating under most appropriate condition (correct mounting, lubrication, sealing, temperature etc).

To consider the effects mentioned, L_{na} life calculation is used with the help of adjustment factors a_1, a_2 and a_3, so that,

$$L_{na} = a_1 a_2 a_3 L_{10} [10^6 \text{ revolutions}] \tag{5.4}$$

where

a_1 : Life adjustment factor for a probability other than the 10% failure rate.

a_2 : Life adjustment factor special material properties

a_3 : Life adjustment factor for special operating conditions

- Life adjustment factor a_1:

The life calculation is generally based on a 10% failure rate. There are cases in which the calculation must be based on a smaller percentage. For such cases the factor a_1 can be determined from the failure distribution. Table 5.1 lists the respective values.

Table 5.1 Life adjustment factor, a_1 (Eschmann et al., 1985)

Failure probability, %	10	5	4	3	2	1
Life adjustment factor, a_1	1	0.62	0.53	0.44	0.33	0.21

- Life adjustment factor a_2:

The factor a_2 accounts for the properties of material and its heat treatment. The fatigue tests on which the conventional rating life calculation is based were carried out with bearings of high quality rolling bearing steel. For this case the value of a_2 is equal to 1.

- Life adjustment factor a_3:

The factor a_3 contains all operational conditions which have a positive or negative effect on the fatigue life. First of these is the lubrication. The highest life values are reached with the circumstances where there is no metal to metal contact exist between rolling element and raceways.

a_3 is further determined by the following equation (Harris, 1996);

$$\lambda = \frac{H}{\beta} \tag{5.5}$$

where, H is the minimum lubricant film thickness between the rolling elements and raceways and β is the composite rms roughness of the "contacting" surfaces. When $\lambda = 1$, $a_3 = 1$; $\lambda > 3$; $a_3 \geq 2$; and $\lambda < 1$, $a_3 < 1$.

Decreasing the lubricating film thickness and increasing metal to metal contact between rolling elements and the raceways and the contamination of the lubricant reduce the life.

5.4 VARIABLE LOAD CONSIDERATION

In many bearing arrangements, loads and rotary speed change either randomly or according to a work cycle. In these cases equivalent dynamic load must be calculated for the given load and speed values.

In rolling element bearing arrangements with variable load and constant speed conditions the load for fatigue life calculation is approximated by following equation

$$Q = \sqrt[3]{Q_1^3 \frac{q_1}{100} + Q_2^3 \frac{q_2}{100} + ...} \tag{5.6}$$

where, Q_1 is the load applied on bearing in q_1 percent of operating life, Q_2 is the load applied in q_2 percent of operating life etc.

5.5 FATIGUE LIFE CALCULATION FOR RACEWAYS

The loading for the parts of the rolling bearing varies during the operation. For instance, a point on the inner raceway of a bearing with inner ring rotation may experience a load cycle as shown in Figure 5.1.

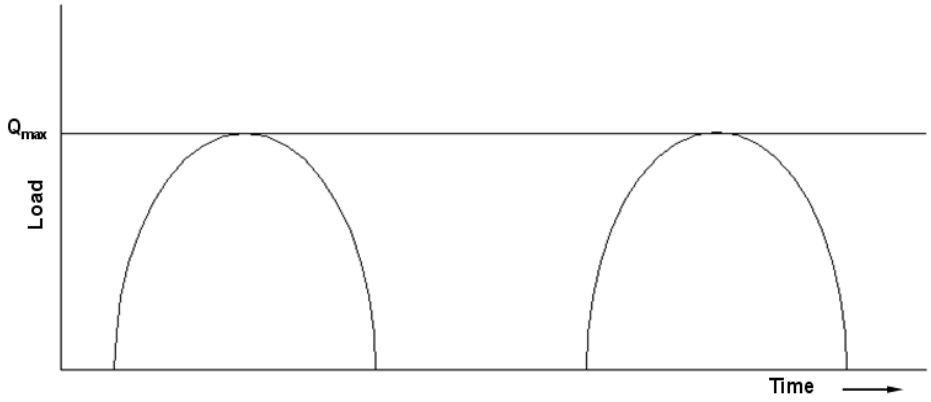

Figure 5.1 Load cycle for a point on inner raceway of a radial bearing (Harris, 2001)

Although the maximum load and maximum stress is significant in causing fatigue failure, the statistical nature of fatigue failure requires that the load history to be considered. Lundberg et al. determined empirically that cubic mean load fits the test data very well for point contact (Harris, 2001). The cubic mean load for a rotating raceway is given by the following equation;

$$Q_{e\mu} = \left(\frac{1}{Z} \sum_{j=1}^{j=z} Q_j^3 \right)^{0.3} \tag{5.7}$$

For a non-rotating ring the cubic mean load is given as;

$$Q_{e\upsilon} = \left(\frac{1}{Z} \sum_{j=1}^{j=z} Q_j^{10/3} \right)^{0.3} \tag{5.8}$$

where

$Q_{e\mu}$: cubic mean load for rotating ring for fatigue life calculation,

$Q_{e\upsilon}$: cubic mean load for non-rotating ring for fatigue life calculation,

Q_j : loading on rolling element in position j,

Z : number of rolling element in bearing.

The basic dynamic capacity can be found by the following equations for inner and outer raceway, respectively;

$$Q_{ci} = 98.1 \left(\frac{2f}{2f-1}\right)^{0.41} \frac{(1-\gamma)^{1.39}}{(1+\gamma)^{1/3}} \left(\frac{\gamma}{\cos\alpha}\right)^{0.3} D_b{}^{1.8} Z^{-1/3} \tag{5.9}$$

$$Q_{co} = 98.1 \left(\frac{2f}{2f-1}\right)^{0.41} \frac{(1+\gamma)^{1.39}}{(1-\gamma)^{1/3}} \left(\frac{\gamma}{\cos\alpha}\right)^{0.3} D_b{}^{1.8} Z^{-1/3} \tag{5.10}$$

The two geometrical parameter f and γ in Equation (5.9) and Equation (5.10) can be found for inner and outer ring by the equations given bellow;

$$f_i = \frac{r_i}{D_b} \tag{5.11}$$

$$f_o = \frac{r_o}{D_b} \tag{5.12}$$

$$\gamma = \frac{D_b \cos\alpha}{d_m} \tag{5.13}$$

where

Q_{co} : dynamic capacity of the outer ring,

Q_{ci} : dynamic capacity of the inner ring,

r_i : raceway groove radius of the inner ring,

r_o : raceway groove radius of the outer ring,

D_b : ball diameter,

d_m : pitch diameter of the bearing.

The fatigue life (L_{10}) of a raceway can be calculated with ISO formulation, as follows:

$$L_{rw} = \left(\frac{Q_c}{Q_e} \right)^3 \quad \text{[million cycles]} \tag{5.14}$$

where L_{rw} is the life of the raceway in million cycles, Q_c is the dynamic capacity of the raceway, and Q_e is the cubic mean load found by using Equation (5.9) or Equation (5.10).

The fatigue life (L_{10}) for entire bearing can be found from the following equation;

$$L = (L_{rwi}^{-1.11} + L_{rwo}^{-1.11})^{-0.9} \tag{5.15}$$

where
L : life of the bearing (million cycles)
L_{rwo} : life of the outer ring (million cycles),
L_{rwi} : life of the inner ring (million cycles).

Ball failure is not considered for endurance calculations because it is not frequently observed during tests. It was explained that, because a ball could change rotational axis, the entire ball surface is subjected to stress, spreading the stress cycles over greater volume consequently reducing the probability of ball fatigue prior to raceway fatigue failure (Harris, 2001).

5.6 INCLUSION EFFECT ON BEARING FATIGUE LIFE

As mentioned in Chapter 2.2 the explanation of the wide scatter in bearing fatigue lies in the random inhomogeneities in the microstructure. Some forms of inhomogeneities are pores and banding both of which are caused by improper solidification processes. More common sources of inhomogeneities are non-metallic inclusions. The content of these inclusions are controlled in bearing steels but the still exists with present technology but small in number (Dambaugh, 2006). In elastically stressed matrix beneath the surface of the raceway, any discontinuity will cause higher stresses, plastic deformation and hence crack initiation.

5.6.1 Stress Concentration

The stress at the edge of a hole or at a notch root has higher value than the remote stress. This phenomenon is called “stress concentration” and fatigue cracks mostly initiate at the stress concentration regions.

Figure 5.2 shows a circular hole in an infinite plate under a uniaxial remote tensile stress, σ_{x0}, in the x direction. The tangential normal stress, σ_θ, at points A and C is three times larger than σ_{x0}, that is $\sigma_\theta = 3\ \sigma_{x0,}$ and stress concentration factor, K_t =3. For the machine element fatigue calculations, lost of stress concentration factors for different types of holes and notches are given in books and handbooks in the literature, one of which most widely used is written by Peterson (1974).

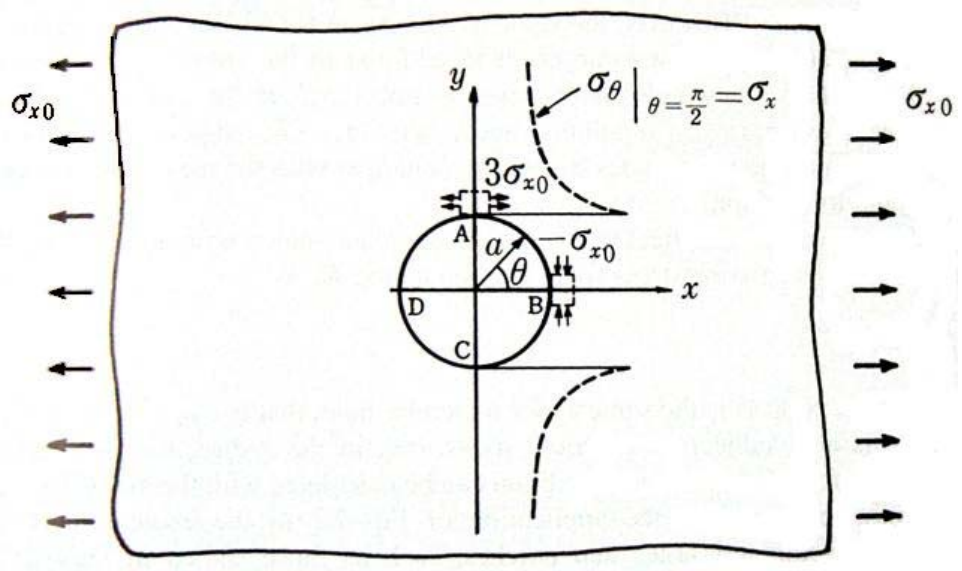

Figure 5.2 Stress concentration at a circular hole

5.6.2 Stress Concentration Factors for Inclusions

For the notch effect evaluation, stress concentration factors are applicable to notches which may be seen by the naked eye, which is a notch greater than approximately 1

mm. For such kind of notches, from the laboratory tests one can predict a value for maximum allowable stress at notch root for infinite life of a component. However, as notches become extremely small (like inclusions), the size of notches becomes of the same order as the size of fatigue damage domain at notch root. That causes propagation of the crack easier (Murakami, 2002).

Murakami (2002) claims that the stress concentration factor for inclusions are dependent on the position, shape and the Young's modulus of the material of the inclusion. The values dependent on tests for stress concentration factors for inclusion in steels (Table 5.2) for an elliptical inclusion which is illustrated in Figure 5.3.

It can be seen in Table 5.2 that the stress concentration factors can be less than unity for the inclusion materials which have greater elastic modulus than that of the surrounding matrix. Also the position of the inclusion with respect to the stress direction also has an effect on stress concentration factor.

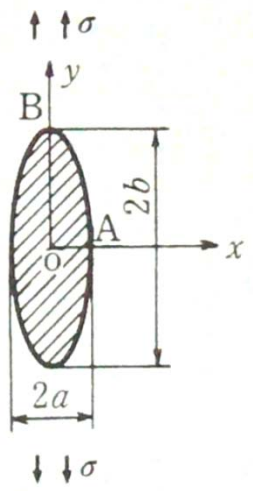

Figure 5.3 Elliptical inclusion under the effect of stress, σ (Murakami, 2002)

Table 5.2 Stress concentration factors for inclusions (Murakami, 2002)

Ratio of Young's modulus of inclusion and matrix, $K = E_I/E_M$	**Stress concentration factor, K_t**		**Aspect Ratio, a/b**		
			0.1	**0.5**	**1.0**
K = 0 (Hole)	**Equator A**	σ_x / σ	0.000	0.000	0.000
		σ_y / σ	1.200	2.000	3.000
	Pole B	σ_x / σ	-1.000	-1.000	-1.000
		σ_y / σ	0.000	0.000	0.000
K = 0.65 (MnS inclusion)	**Equator A**	σ_x / σ	-0.009	-0.014	0.000
		σ_y / σ	1.054	1.205	1.304
	Pole B	σ_x / σ	-0.137	-0.162	-0.152
		σ_y / σ	0.684	0.781	0.848
K = 0.94 (Cementite)	**Equator A**	σ_x / σ	-0.001	-0.002	0.000
		σ_y / σ	1.007	1.025	1.035
	Pole B	σ_x / σ	-0.018	-0.019	-0.017
		σ_y / σ	0.957	0.973	0.983
K = 1.82 (Al_2O_3 inclusion)	**Equator A**	σ_x / σ	0.018	0.024	0.000
		σ_y / σ	0.895	0.722	0.649
	Pole B	σ_x / σ	0.251	0.207	0.175
		σ_y / σ	1.615	1.301	1.175

CHAPTER 6

RESULTS AND DISCUSSION

In the case studies the ORS 624607 radial deep groove ball bearing is used to determine the contact stress and fatigue life of the inner ring. The dimensions of the bearing are given in Figure 6.1

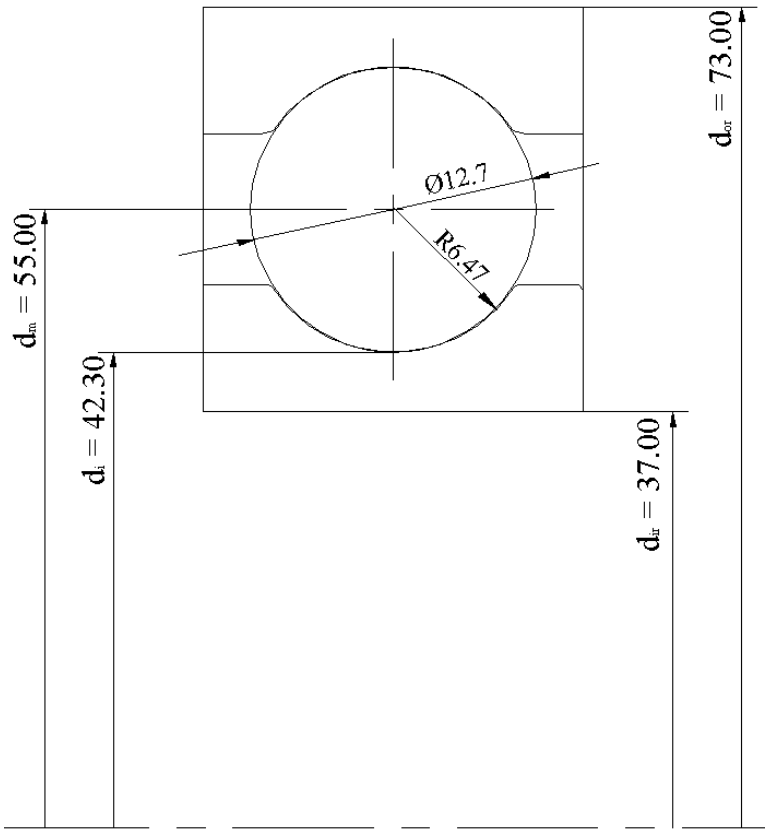

Figure 6.1 Main dimensions of the 624607 bearing

Ball diameter, D_b: 12.7 mm

Pitch diameter, d_m: 55 mm

Inner ring diameter, d_{ir}: 37 mm

Outer ring diameter, d_{or}: 73 mm

Inner ring raceway radius, r_i : 6.47 mm

Inner ring raceway contact diameter, d_i : 42.30 mm

Number of rolling elements, Z : 9

Number of rows : 1

Contact angle, α : 0°

Also, the Young's Modulus and Poisson's ratio for the 100Cr6 bearing steel are E= 210000 MPa and υ=0.3.

6.1 DETERMINATION OF FATIGUE LIFE OF THE INNER RING BY USING ISO FORMULATION

In this part the ISO formulation is used to determine the fatigue life of the inner ring with respect to applied bearing force.

6.1.1 Static Load Rating

Static load rating of the bearing can be found with the use of Equation (3.20);

$$C_0 = f_0 i Z D_b^2 \cos\alpha$$

$$C_0 = (12.26)(1)(9)(12.7)^2(\cos 0)$$

$$C_0 = 17796.73\text{N}$$

It is assumed that the bearing is operating under the load of 8898 N which is the half of the static load rating of the bearing.

6.1.2 Determination of Fatigue Life of the Inner Ring

For a radial ball bearing the force on the maximum loaded ball can be found from Equation (3.18). Hence,

$$Q_{\max} = \frac{5F_r}{iZ\cos\alpha}$$

$$Q_{\max} = \frac{(5)(8898)}{(1)(9)(\cos 0)}$$

$Q_{\max} = 4943.3N$ is the maximum ball load for the applied 8898 N force on bearing.

The loading variation for different ball locations is given by Equation (3.11). For the values κ=0.5 and m=1.5 the Equation (3.19) can be used;

$$Q_{\psi} = Q_{\max}[1 - 1(1 - Cos\psi)]^{1.5}$$

At the instant when the center of a ball coincides with the azimuth of the bearing, the positions of the 9 balls are given in Figure 6.2. Since for 0 clearance condition the rolling elements only loaded at the upper half of the bearing, only the loads for upper part is considered. Loading that effect the balls and the raceways for different ball locations are found by use of Equation (3.19). These values are given in Table 6.1.

Table 6.1 Loading for each ball location

ψ	Q_{ψ} (N)
± 0	4943.3
± 40	3314.3
± 80	357.7
± 120	0
± 160	0

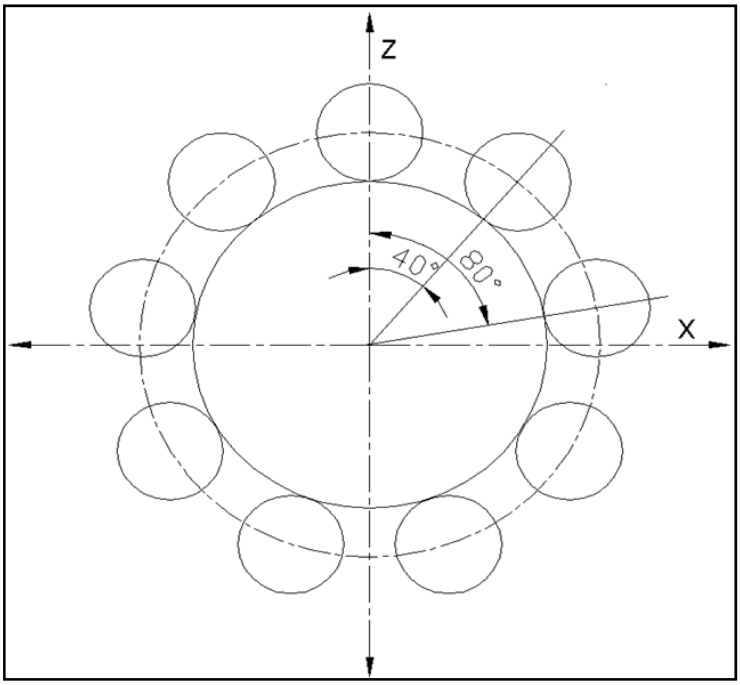

Figure 6.2 Location of the rolling elements

The inner ring fatigue life is calculated with the Equations (5.9) and (5.14), for a non-rotating ring the equivalent load given with the Equation (5.8);

$$Q_{e\upsilon} = \left(\frac{1}{Z} \sum_{j=1}^{j=z} Q_j^{10/3} \right)^{0.3}$$

$$Q_{e\upsilon} = \left(\frac{1}{9} \left[(4943.3)^{10/3} + 2(3314.3)^{10/3} + 2(357.7)^{10/3} + 0 + 0 \right] \right)^{0.3}$$

$$Q_{e\upsilon} = 2903.8\text{N}$$

The basic dynamic capacity of inner raceway can be found from the Equation (5.9);

$$Q_{ci} = 98.1 \left(\frac{2f}{2f-1} \right)^{0.41} \frac{(1-\gamma)^{1.39}}{(1+\gamma)^{1/3}} \left(\frac{\gamma}{\cos\alpha} \right)^{0.3} D_b^{1.8} Z^{-1/3}$$

$$Q_{ci} = 98.1 \left(\frac{(2)(0.51)}{(2)(0.51)-1} \right)^{0.41} \frac{(1-0.23)^{1.39}}{(1+0.23)^{1/3}} \left(\frac{0.23}{\cos 0} \right)^{0.3} (12.7)^{1.8} (9)^{-1/3}$$

$$Q_{ci} = 9579.71\text{N}$$

Where, the two geometrical parameter f and γ can be found for inner ring by the Equations (5.11) and (5.13), respectively;

$$f_i = \frac{r_i}{D_b} = \frac{6.47}{12.7} = 0.51$$

$$\gamma = \frac{D_b \cos\alpha}{d_m} = \frac{12.7(\cos 0)}{55} = 0.230$$

The fatigue life of a raceway can be calculated with the use of Equation (5.14):

$$L_{rw} = \left(\frac{Q_{ci}}{Q_{e\upsilon}} \right)^3 \text{ [million cycles]}$$

So, the fatigue life of a non-rotating inner ring raceway can be found by using the ISO formulation;

$$L_{rw} = \left(\frac{Q_{ci}}{Q_{e\upsilon}} \right)^3 = \left(\frac{9579.71\text{N}}{2903.8\text{N}} \right)^3 = 35.9 \text{ [million cycles]}$$

Further analytical calculations are done in similar way to obtain the results of the ISO for various loads on the inner ring and are illustrated in Figure 6.3.

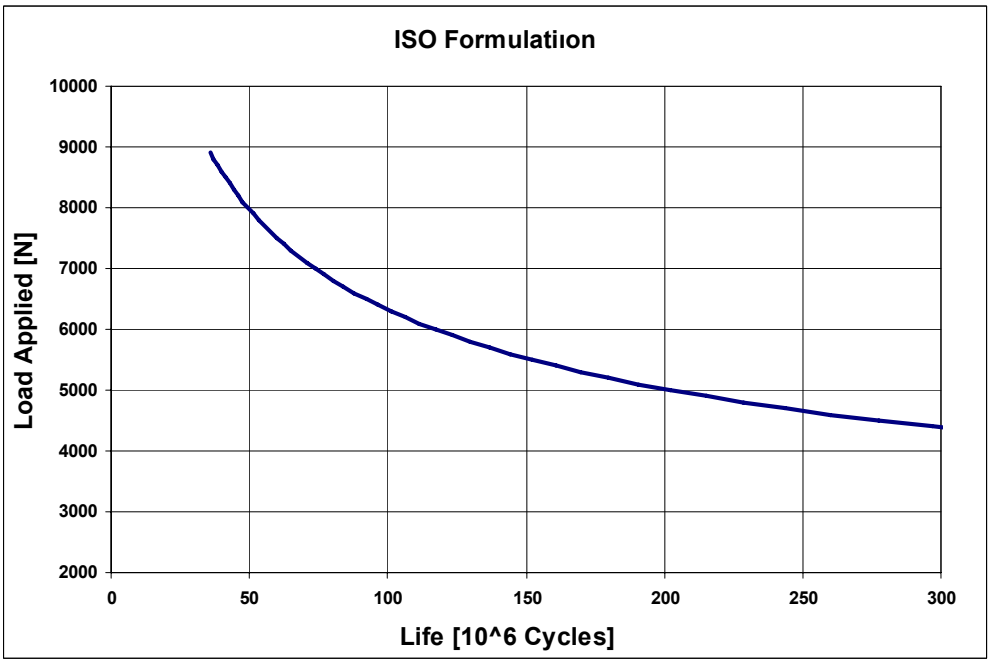

Figure 6.3 Inner ring life calculated with ISO formulation

6.2 DETERMINATION OF THE CONTACT STRESS

The curvature sum for ball and raceway can be found from the Equation (3.2),

$$\sum \rho = \frac{1}{6.35} + \frac{1}{6.35} + \frac{1}{21.15} - \frac{1}{6.47} = 0.2078$$

With the use of Equation (3.3), the curvature difference is found as;

$$G(\rho) = \frac{0.0472 + 0.1543}{0.2078} = 0.9696$$

a*, b* values are found from the Table 3.1 with interpolation as;

a* = 5.08158

b* = 0.35623

Hence, substituting the values into Equations (3.5) & (3.6) using the values E= 210000 MPa, υ=0.3 and the maximum ball load of 4943.3 N;

$$a = a^{*}\left[\frac{3Q}{2\sum\rho}\left(\frac{1-\upsilon_{I}^{2}}{E_{I}}+\frac{1-\upsilon_{II}^{2}}{E_{II}}\right)\right]^{1/3}$$

$$a = (5.0818)\left[\frac{(3)(4943.3)}{(2)(0.2078)}\left(\frac{1-(0.3)^{2}}{210000}+\frac{1-(0.3)^{2}}{210000}\right)\right]^{1/3}$$

$$a = 3.4376\text{mm}$$

$$b = b^{*}\left[\frac{3Q}{2\sum\rho}\left(\frac{1-\upsilon_{I}^{2}}{E_{I}}+\frac{1-\upsilon_{II}^{2}}{E_{II}}\right)\right]^{1/3}$$

$$b = (0.35623)\left[\frac{(3)(4943.3)}{(2)(0.2078)}\left(\frac{1-(0.3)^{2}}{210000}+\frac{1-(0.3)^{2}}{210000}\right)\right]^{1/3}$$

$$b = 0.2409\text{mm}$$

Substituting a and b values into Equation (3.4), the maximum contact stress is found as;

$$\sigma_{max} = \frac{3Q}{2\pi ab}$$

$$\sigma_{max} = \frac{(3)(4943.3)}{(2\pi)(3.4376)(0.2409)} = 2851.15\text{MPa}$$

6.3 NUMERICAL CALCULATIONS

To be able to conduct numerical endurance calculations and compare the results with the formulations in the literature a three-dimensional finite element ball-raceway model is created. The numerical stress analyses are conducted with the following assumptions;

- The inner ring is mounted on a nonflexible shaft,
- No significant surface shear stress occurs between ball-raceway contact,
- Asperity contact induced stresses are not undertaken,
- Hoop stresses because of press fitting operation to mount the bearing on shaft are neglected,
- Residual stresses within the material are neglected,
- Operational speed is sufficiently slow such that rolling element centrifugal loads are assumed to be insignificant,
- Internal clearance of the bearing is 0
- Lubrication effects are neglected
- Thermal effects are neglected.

6.3.1 Stress Analysis

6.3.1.1 Numerical Model

All the numerical simulations are done with the commercially available non-linear FE software, MSC. Marc Mentat (MSC. Software, 2005). To model the geometry of the ball bearing and inner ring, 16428 brick shape hexahedral elements are created. The contact areas are fine meshed and the areas far from the contact zone are meshed coarse to avoid time consuming numerical calculations. Since the geometry is symmetric, only one quarter of the ball and a segment of the inner ring are modeled as seen in Figure 6.4. To apply the necessary loading on the ball a node controlled “Loading Plane” is created and the load applied through this plane.

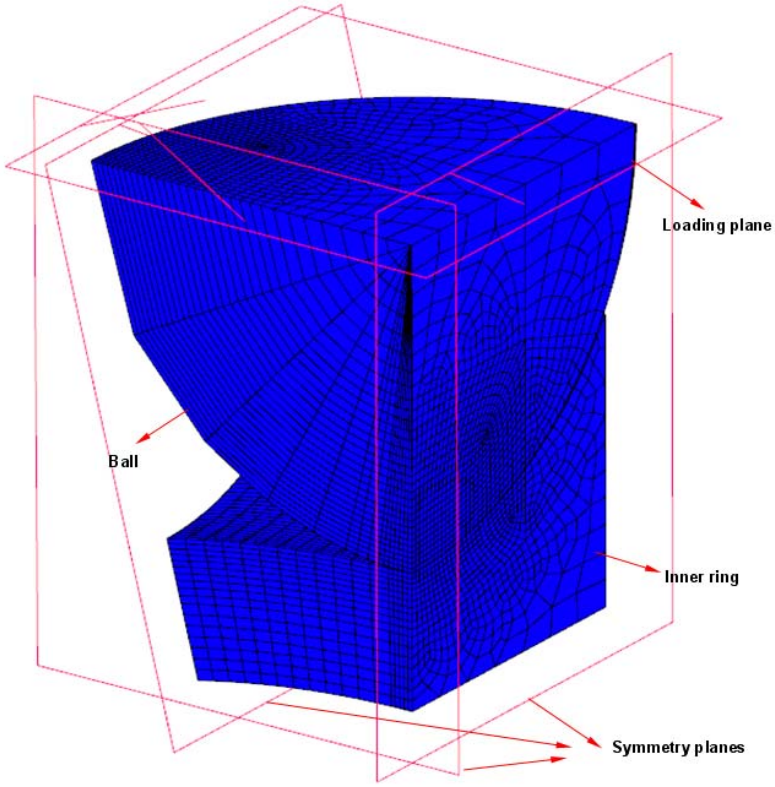

Figure 6.4 Numerical model of ball and raceway

6.3.1.2 Determination of Element Size at Contact

Topology of the finite element mesh will directly affect the results of the conducted analyses. Increasing the number of elements in the mesh will result in a more accurate representation of the stress in the geometry. However, the cost of increasing number of elements is the increase in computational time.

In this study, element edge length is determined with consecutive simulations. By putting the applied load remain constant a series of analyses are performed, with mesh being refined at each step, finally converging to the solution. For the Hertz contact process the mesh size (edge length) in the contact zone is decreased from 0.16 mm to 0.1 mm (Figure 6.5) and the stress values examined within the contact zone.

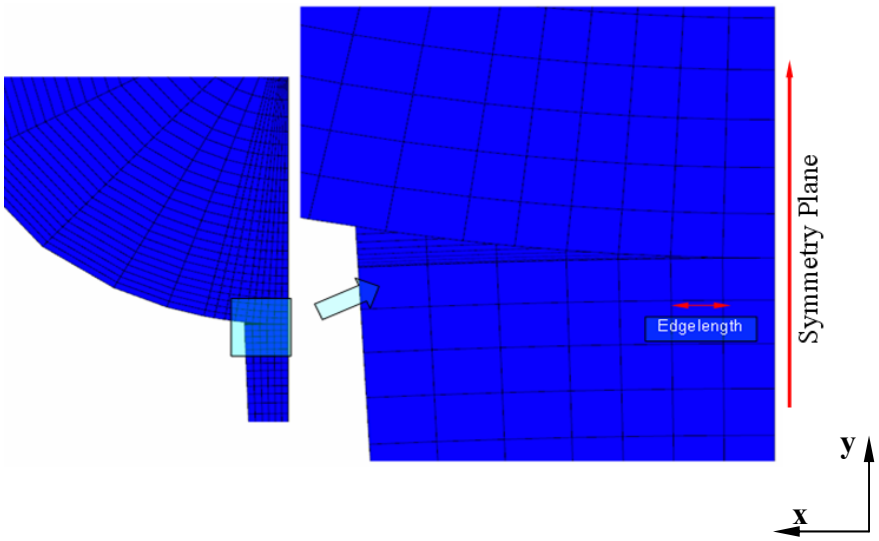

Figure 6.5 Edge length at contact zone

As seen in Figure 6.6 the stress values are changing with respect to the edge length of the elements significantly and converge to a certain value with the edge length of 0.1 mm. Hence the effect of further refinement does not give a significant effect on the solution. Thus it is decided to use of 0.1 mm edge length is satisfactory for the analyses.

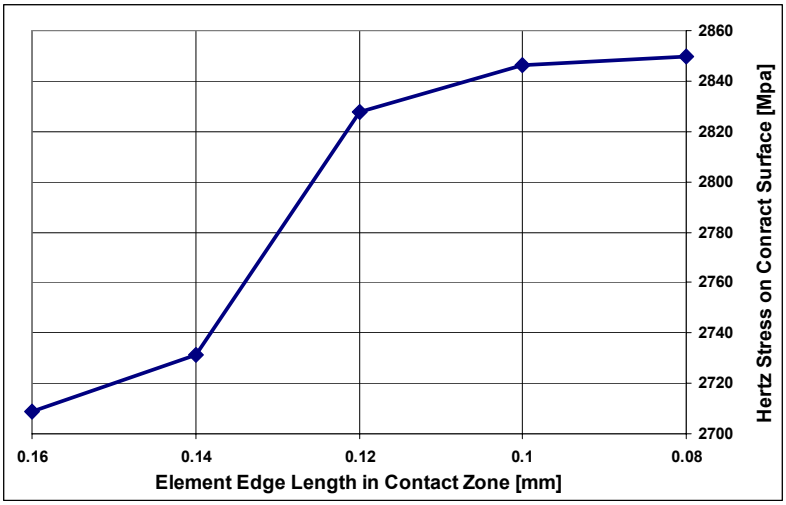

Figure 6.6 Maximum Hertz stress in contact zone for various element edge lengths

6.3.2 Results of Stress Analysis and Comparison with Analytical Calculations

The calculated stress values with FEA are compared by analytical results for 8898 N radial bearing load in Table 6.2. The Hertz stresses obtained both numerically and analytically for various bearing loads are given in Figure 6.7.

Table 6.2 Analytical and numerical calculation results

	Hertz Stress in Contact Area [MPa]
Analytical Calculations	2851.15
Numerical Calculations	2846.2
% Difference	0.17

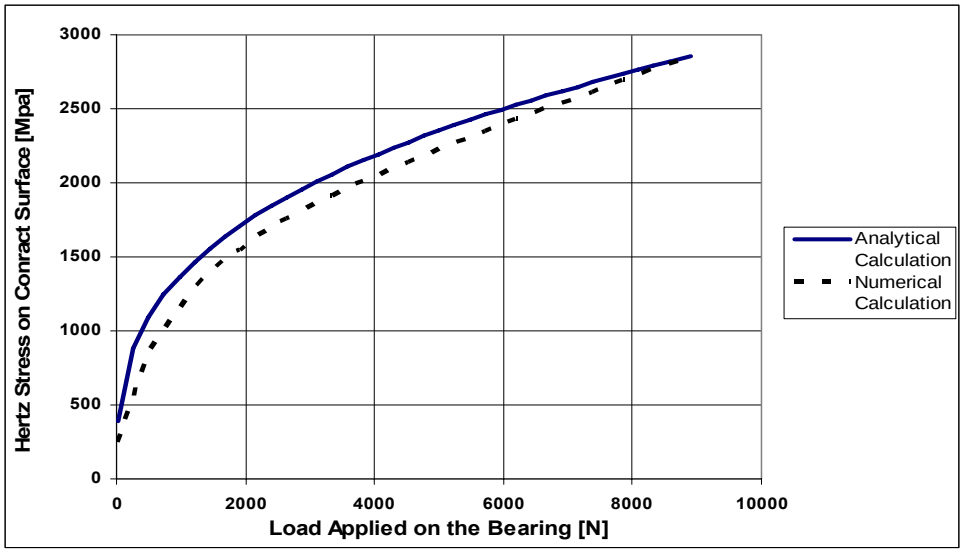

Figure 6.7 Hertz stress at the surface of the raceway vs. applied load

As mentioned in previous chapters the maximum stress is expected to be formed below the surface which also causes the crack initiation. It is proposed by several sources (Harris, 2001, ASME, 2003) the von Mises stress below the surface is a good criterion for rolling contact fatigue calculations. The von Mises stress variation from

the surface to 0.5 mm depth is given in Figure 6.8 and the distribution of the von Mises stress within the inner ring is illustrated in Figure 6.9.

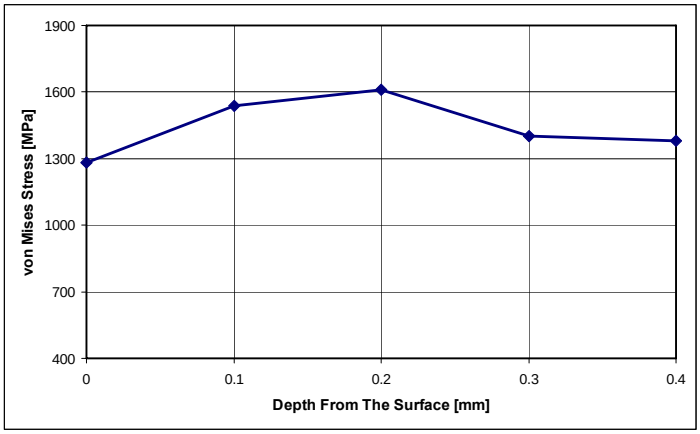

Figure 6.8 Equivalent von Mises stress distribution below the surface

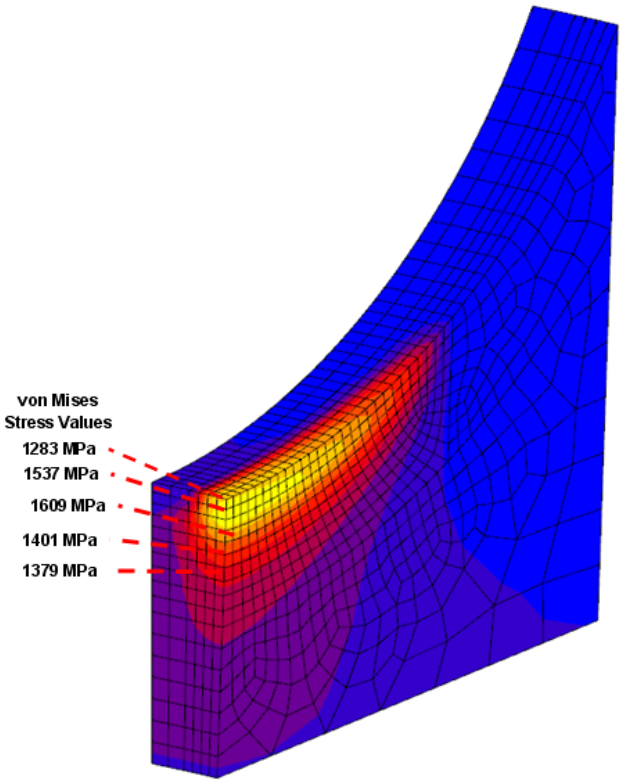

Figure 6.9 von Mises stress distribution on inner ring

6.3.3 Stresses That Act on Observed Zone During Rolling

To determine the stress variation and the loading history on the bearing inner ring during the ball rolling over the observed zone, successive numerical analyses conducted for different ball locations. For each location of the ball, the stress values at the point on azimuth of the inner ring are determined numerically under the bearing load of 8898 N (Figure 6.10).

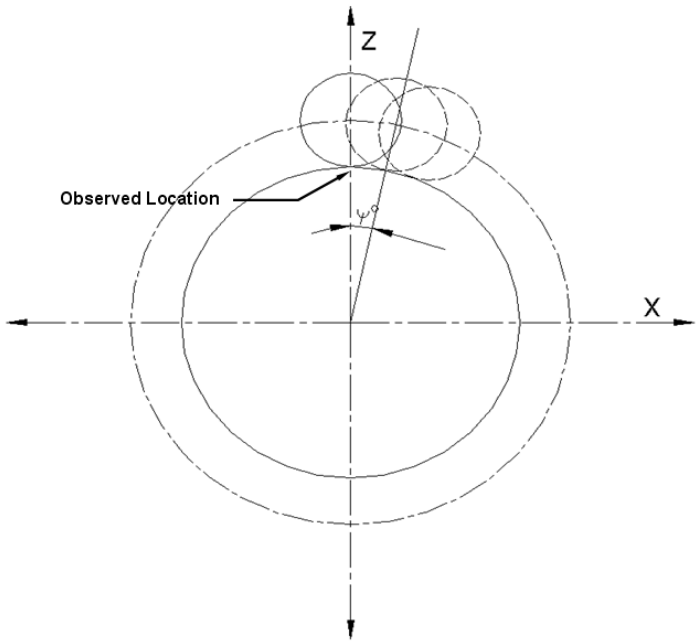

Figure 6.10 Schematic representation of ball position

The loading variation for different ball locations considered by utilizing the Equation (3.19), calculated stress values of the point on azimuth for different ball locations are given in Table 6.3. It can be seen from the Table 6.3 that the maximum stress values are observed at 0.2 mm bellow the contact surface. Since this region also will be critical for fatigue calculations, the loading history for numerical fatigue calculations is defined with respect to 0.2 mm depth.

Table 6.3 Equivalent von Mises Stress for different ball positions at the observed location

	Depth From Surface (mm)				
Angle From Azimuth, ψ	0	0.1	0.2	0.3	0.4
0°	1283.71	1537.74	1609.15	1401.27	1379.85
0.25°	1191.08	1450.45	1547.05	1362.17	1373.90
0.51°	1083.36	1305.88	1379.01	1225.76	1261.13
0.77°	597.82	848.88	1062.42	1024.55	1112.18
1.02°	177.11	403.30	704.41	791.15	927.55
1.28°	104.20	223.52	439.35	579.21	745.50

Hence, for a fixed inner ring and rotating outer ring during a ball pass on the azimuth region, the stress variation within the observed point is given in Figure 6.11. For the fatigue calculations stress history is taken into account with respect to this variation.

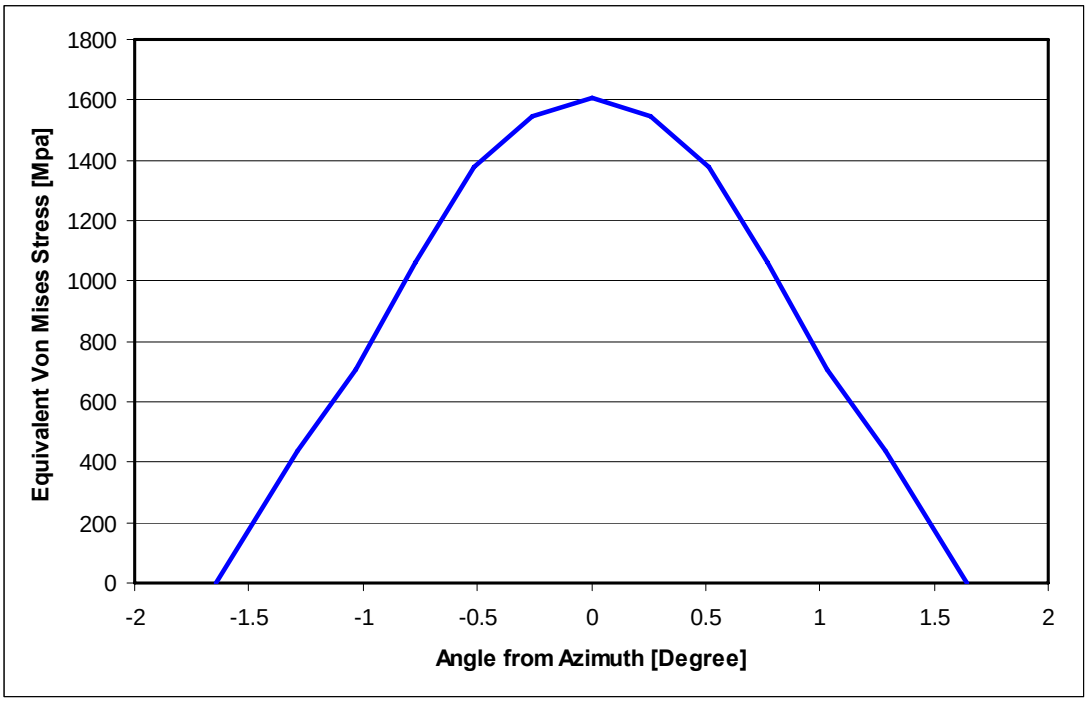

Figure 6.11 Numerically determined stress variation at Azimuth

6.3.4 Fatigue Analysis

Fatigue life of the bearing is also calculated via commercially available package program MSC. Fatigue (MSC. Software, 2005) with following assumptions:

- Since it is proposed by several sources (Harris, 2001, ASME, 2003) the von Mises stress is selected as the criterion for fatigue calculations.
- Because of the purely compressive stress, for the ε-N method calculations Morrow correction and for the S-N method calculations Goodman correction is used.
- The lubrication effects and hoop stresses in the bearing are not taken into account.
- Temperature effects are neglected.
- All the calculations conducted for L_{10} life of the inner ring.
- For the Neuber Method K_t is assumed to be 1.2.

The material properties of the 100Cr6 steel are given in Table 6.4. The S-N and ε-N curve of the material are also given in Figure 6.12 and Figure 6.13. The endurance properties of the material are obtained from the push-pull test.

Table 6.4 Material properties of 100Cr6 steel (MSC Software, 2005)

Material Name:SAE5210_517_H, DIN 100Cr6	Designation	
UTS: Ultimate Tensile Strength (MPa)	S_u	2647
Fatigue Strength Coefficient (MPa)	S'_f	2647
Elastic Modulus (MPa)	E	2.1E+05
Fatigue Ductility Coefficient	ε'_f	0.16
Cyclic Strain Hardening Exponent	n'	0.15
Fatigue Strength Exponent	t	-0.09
Fatigue Ductility Exponent	g	-0.58

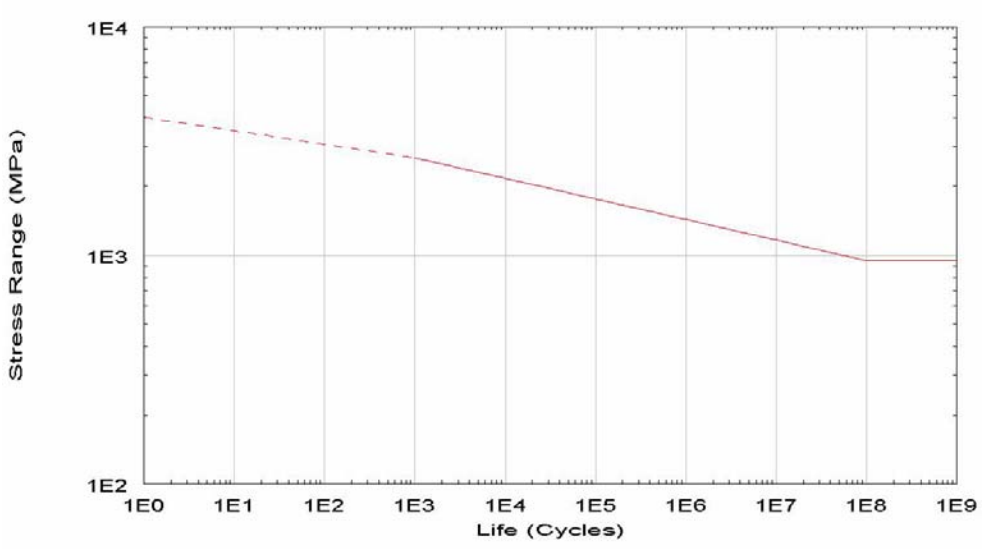

Figure 6.12 S-N Curve of 100Cr6 Steel (MSC Software, 2005)

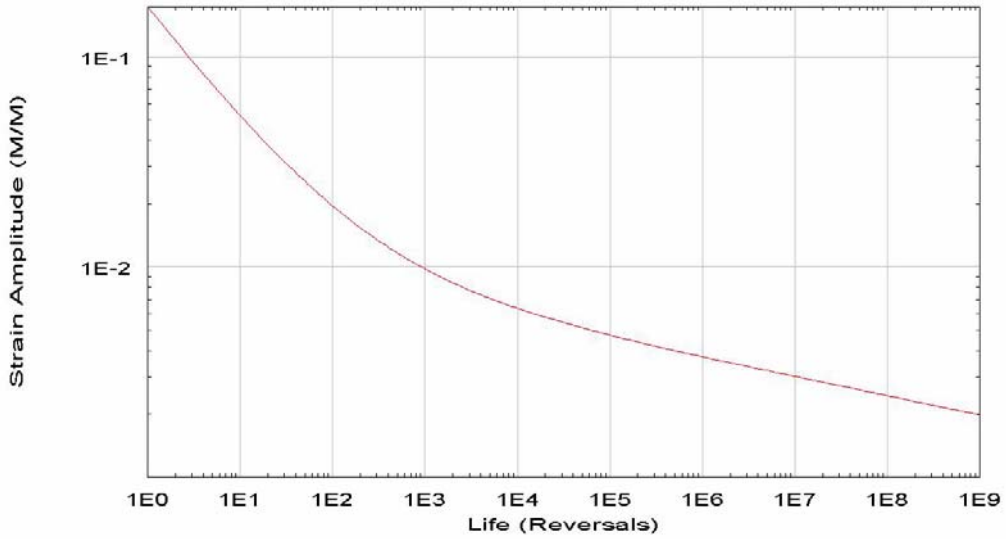

Figure 6.13 ε-N Curve of 100Cr6 Steel (MSC Software, 2005)

The material properties are used for the 100Cr6 steel are provided by the material library of the program which are referenced on a SAE Paper, No: 820682, by B.E. Broardman.

6.3.4.1 Consideration of reliability

The standard S-N and ε-N curves are based on mean values that correspond to a 50 percent of probability of failure. Since the bearing fatigue calculations based on 90 percent of survival the modification of the data from the fatigue tests should be taken into consideration. It is necessary to add probability parameter P to the fatigue life curves (Figure 6.14). MSC. Fatigue considers the probability of survival with respect to material data in its material library.

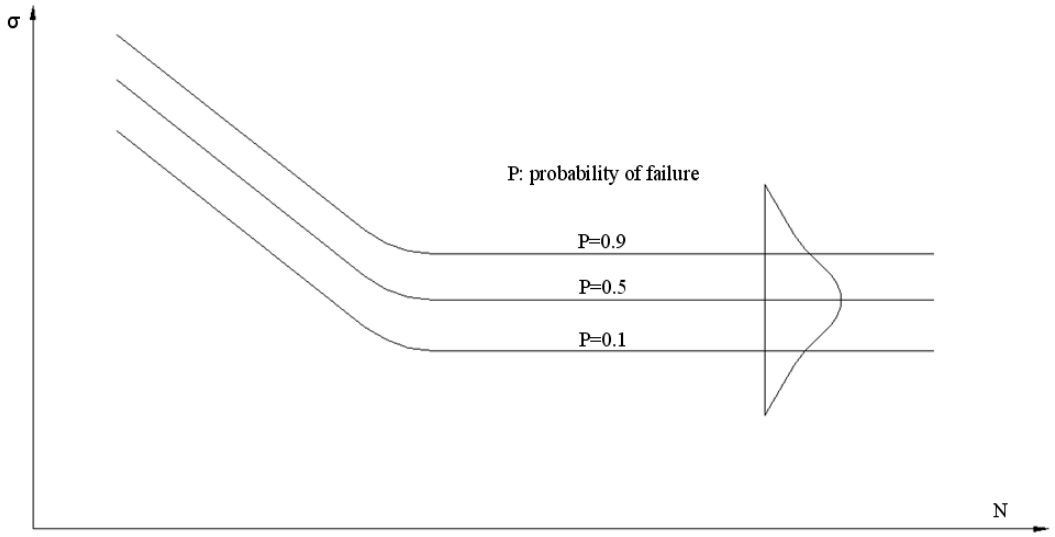

Figure 6.14 Schematic illustration of probability distribution on S-N curve

6.3.4.2 Comparison of ε-N, S-N and ISO Methods under Constant Operating Load Conditions

Several fatigue life calculations for different bearing loads are conducted for which the results are graphically illustrated in Figure 6.15. As seen in the figure the ε-N method gives the most conservative results. This can be explained by the fact that the required time for crack initiation is less than the time for first flaking particle from the raceway surface which is found by S-N method. The ε-N Method does not give a fatigue limit and since the material data is only provided till 2.0E+8 cycles the maximum life for ε-N calculation is limited to 2.0E+8 cycles. The S-N method give a

fatigue limit load of 4200 N where ISO method gives an endurance life even if the applied load decreases.

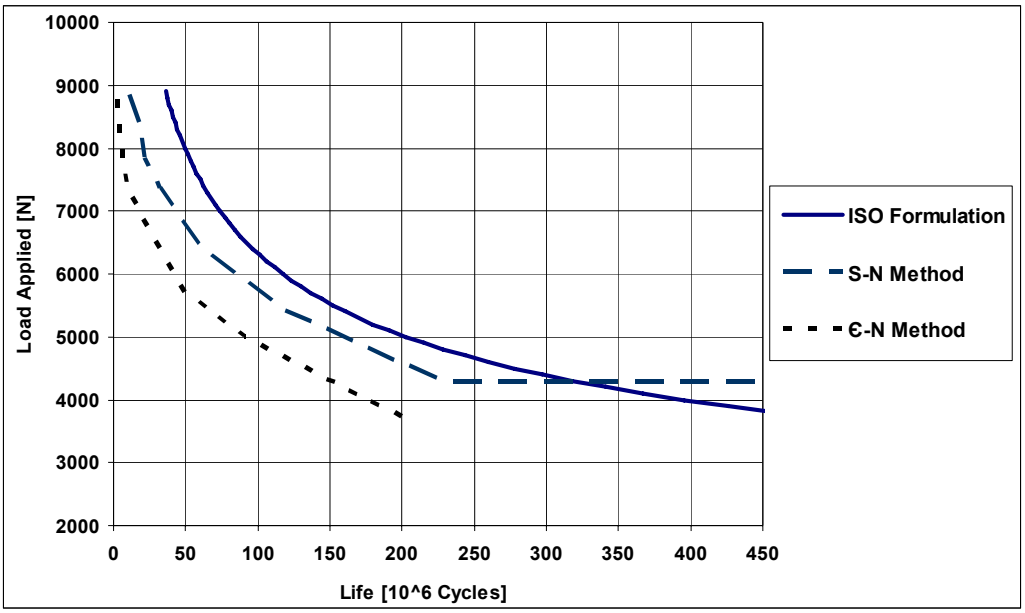

Figure 6.15 Comparison of the inner ring life results from S-N and ε-N methods vs. ISO formulation

6.3.4.3 Comparison of S-N, ε-N and ISO Methods under Variable Operating Load Conditions

ISO formulation is widely used to predict the bearing endurance life in the industry which is given in Equation (5.3). The ISO formulation for variable load conditions is also given in Equation (5.6). These formulations are depends simply on the dynamic capacity of the bearing and the load applied on bearing and the load selection is always done for the worst case condition, e.i. the maximum load that applied on bearing during the service life. In this part of the study several different loading conditions are inspected to compare the ISO methods and structural fatigue life calculations.

Firstly, 3 different loading cases are inspected. The assumptions for 3 cases which are graphically given in Figure 6.16 as follows:

Case 1: The bearing operates under 7100 N on the half of the operating life, and under 6200 N on the other half of the service life.
Case 2: The bearing operates under 7100 N on 20%, and under 6200 N on the 80% of the service life.
Case 3: The bearing operates under 7100 N on 2%, and under 6200 N on the 98% of the service life.

The inner ring fatigue life can be calculated according to ISO method with use of the formulations given in Chapter 5. From structural fatigue point of view, according to Palmgren-Miner rule, the damage effect of the load of 7100 N and 6200 N are different. If the operating time with 6200 N increases the life of the inner ring would be higher. The results of calculations with the ISO formulations S-N and ε-N method are given in Table 6.5.

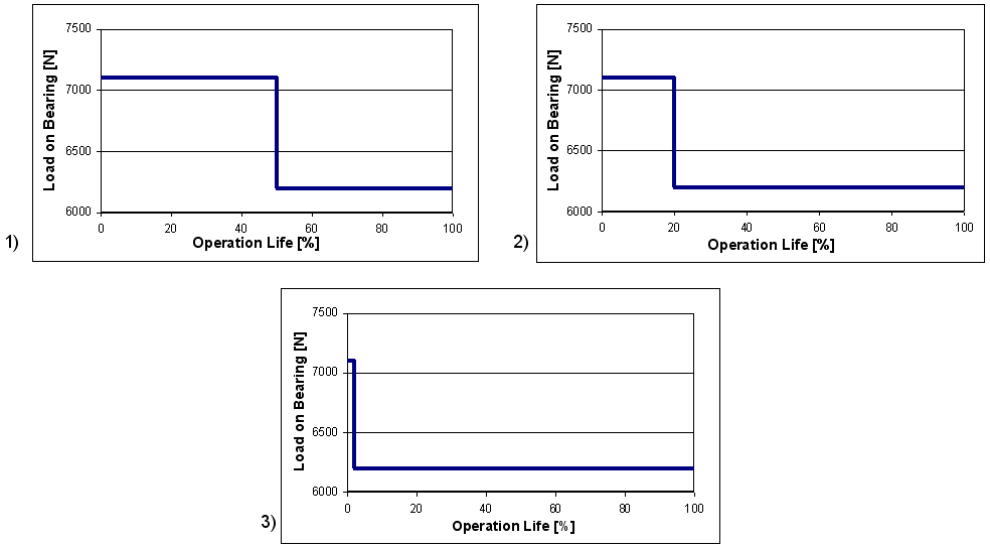

Figure 6.16 Loads and operation percentages for Case 1 through Case 3

Table 6.5 Endurance values for Case 1 through Case 3

	ISO Formulation	ISO Formulation for variable loading	S-N Method	ε-N Method
Case 1	7.10E+07	8.5E+07	7.20E+07	2.50E+07
Case 2		9.6E+07	7.46E+07	3.20E+07
Case 3		1.1E+08	7.50E+07	3.90E+07

Both of the 7100 N and 6200 N creates von Mises stress of approximately 1600 MPa and 1520 MPa respectively which are higher than the endurance limit of the material. If the load decreases to a level during operating which creates stress lower than the fatigue limit of the material, more significant differences can be found between the ISO formulation and S-N method. For the next three cases the bearing assumed to operate between 7100 N and 4000 N (Figure 6.17) with the following assumptions:

Case 4: The bearing operates under 7100 N on the half of the operating life, and under 4000 N on the other half of the service life.
Case 5: The bearing operates under 7100 N on 20%, and under 4000 N on the 80% of the service life.
Case 6: The bearing operates under 7100 N on 2%, and under 4000 N on the 98% of the service life.

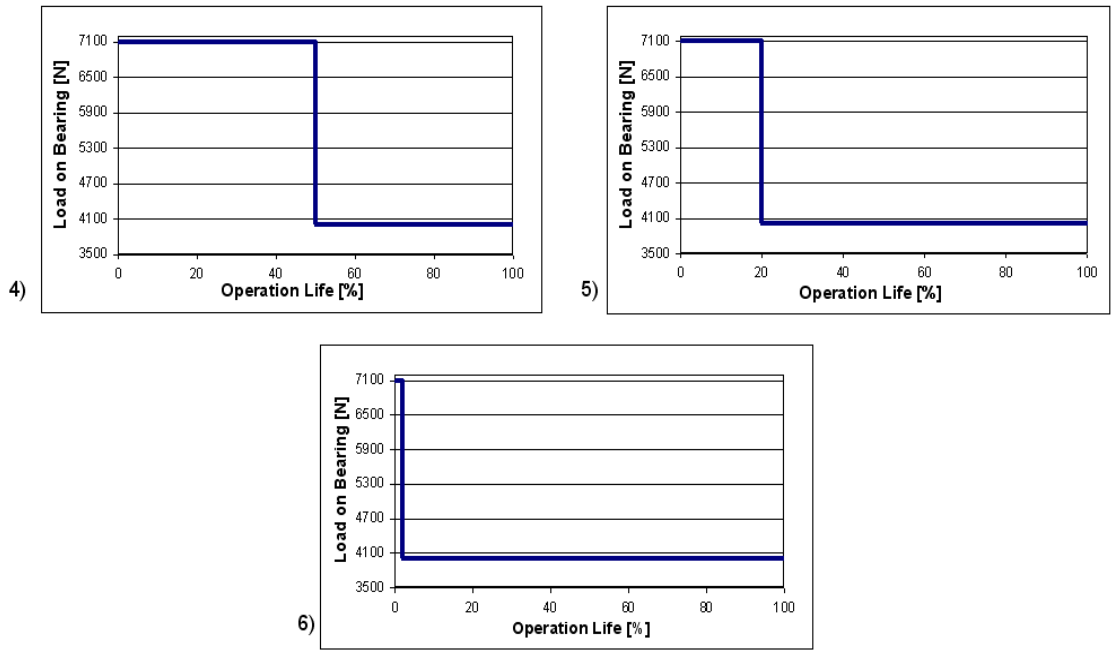

Figure 6.17 Loads and operation percentages for Cases 4, 5, and 6

Since the loading of 4000 N is bellow the fatigue limit load of the ring, the endurance life of the inner ring significantly increased with decreased operation percentage of the load of 7100 N. The calculated fatigue life values are given in Table 6.6.

Table 6.6 Endurance values for Case 4 through Case 6

	ISO Formulation	ISO Formulation for variable loading	S-N Method	ε-N Method
Case 4	7.10E+07	1.2E+08	1.36E+08	3.30E+07
Case 5		2.1E+08	3.40E+08	6.50E+07
Case 6		3.6E+08	3.40E+09	1.50E+08

Lastly for case 7, a more complex loading condition is defined where the loads varies between 7200 N and 1000 N as given in Figure 6.18. The fatigue lives are given in Table 6.7. For such kind and more complex loading conditions the MSC. Fatigue tool is useful to calculate fatigue life.

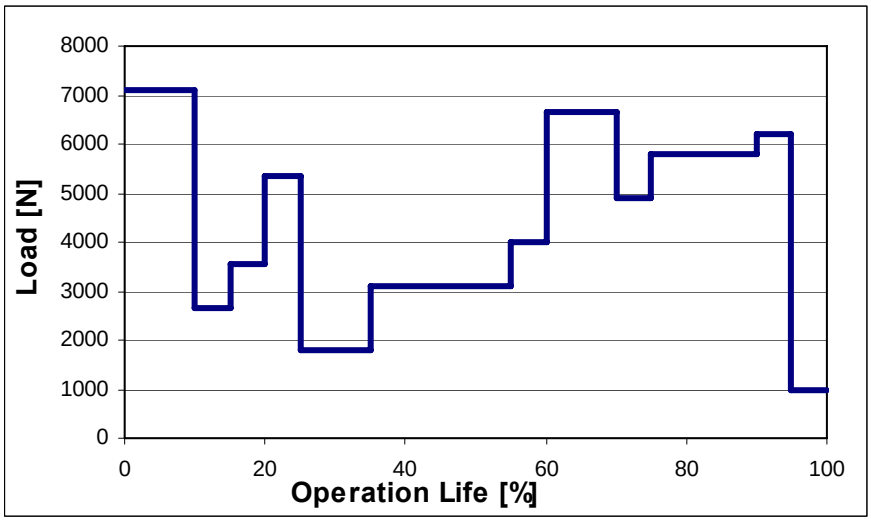

Figure 6.18 Loads and operation percentages for Case 7

Table 6.7 Endurance values for Case 7

	ISO Formulation	ISO Formulation for variable loading	S-N Method	ε-N Method
Case 7	7.10E+07	2.7E+08	1.60E+08	4.50E+07

The ISO formulation is widely used for fatigue life prediction in industry. However the method does not take into account the fatigue limit of the material. In this the S-N and ε-N methods are used to estimate the fatigue life of an inner ring of a rolling element bearing for various load conditions.

With the use of three-dimensional finite element analysis, models of a rolling element bearing inner ring and ball have been developed and variation in the stress field within the inner ring has been obtained numerically under the given load. The stress field is used in the fatigue analysis by S-N and ε-N methods. Results compared with ISO formulation.

The ε-N method is observed to give shorter fatigue lives compared to S-N method. That difference can be explained by the fact that the required time for crack initiation is less than the time necessary for first flaking particle from the raceway surface which is found by S-N method.

As a result of the study, the fatigue calculations are determined to give more conservative results than ISO method for higher loads that cause stresses higher than fatigue limit of the material. By use of S-N and ε-N methods for bearing endurance predictions, it is become possible to consider the fatigue limit stress of the bearing material. It is determined that, if the stresses within an operating bearing do not exceed the limit stress, the bearing can achieve infinite life. The variation of loading is evaluated to have a direct influence on bearing life. With the use of damage summation method, it is determined that if the stress values within the bearing changes from the higher levels to lower that bellow the fatigue stress limit of the material, the fatigue life of the inner ring significantly extends which is not recognized by ISO method.

CHAPTER 7

CONCLUSIONS AND FURTHER RECOMMENDATIONS

7.1 CONCLUSION

In this thesis, to predict the fatigue life of the inner ring of a rolling element ball bearing, stress field within the bearing is obtained by using finite element method. Endurance estimations are done with the use of Total Life (S-N) and Crack Initiation (ε-N) Analysis methods, which are used for fatigue life analysis in the industry. At the end of the studies, following results are obtained;

1. For the loads that create stresses higher than the fatigue limit of the material, S-N and ε-N methods are found to give more conservative results than ISO formulation.
2. Since the ISO formulation method does not take into account the fatigue limit of the material, it is observed that the formulation underestimates the fatigue life of the bearing.
3. S-N and ε-N methods consider the fatigue limit of the material hence, below the limit load these methods give unlimited service life.
4. The variation of loading, which is determined by the Palmgren-Miner Damage Summation Method is evaluated to have a direct influence on bearing life.

7.2 SUGGESTIONS FOR FURTHER WORK

In this study, the main parameter that has been taken into account in fatigue analysis was the stress distribution in the inner ring caused by the contact between raceway and rolling element. Although the contact between raceway and inner ring has an important role in rolling element bearing fatigue life, there are several additional aspects that should be put into consideration.

The elastohydrodynamic lubrication is one of the important parameters in rolling contact fatigue. The thickness of the lubricant film provides separation between rolling element and raceway and prevents the asperity interaction between the rolling surfaces and improves the fatigue life of the bearing. Therefore consideration of the lubrication effects would be increase the accuracy of the analysis.

Besides the contact of rolling element and raceway, there are several forms of imposed stress combinations which effects the generalized stress field that exist in rolling element bearing applications like surface shear stress, interference fit induced stress, centrifugal load stresses, contaminant caused stresses. The thermal effects, surface finishes of the raceway and rolling element, and residual stresses within the material are also other parameters influencing the fatigue life of a bearing and could be included the analysis.

REFERENCES

1. Arıduru, S., "Fatigue Life Calculation by Rainflow Cycle Counting Method", Master of Science Thesis, Middle East Technical University, (2003).

2. ASME, "Life Ratings for Modern Rolling Bearings, A Design Guide for the Application of International Standard ISO 281/2", ASME International, (2003).

3. Brändlein, J., Eschmann, P., Hasbargen, L., and Weigand, K., "Ball and Roller Bearings: Theory, Design and Application", 3rd Edition, New York, John Wiley & Sons, (1999).

4. Changsen, W., "Analysis of Rolling Element Bearings", Mechanical Engineering Publications Limited, (1991).

5. Dambaugh, P.E., "Fatigue Consideration of High Strength Rolling Bearing Steels", (2008),
   www.simulia.com/download/pdf/BearingSteelFatigue_AUC.pdf
   (Download date: 10.09.2008)

6. Eschmann, P., Hasbargen, L., and Weigand, K., "Ball and Roller Bearings: Theory, Design and Application", 2nd Edition, New York, John Wiley & Sons, (1985).

7. FAG, "Rolling Bearing Damage, Recognition of damage and bearing inspection", Publ. No. WL82102/2EA., FAG Kugelfisher AG, (2003), www.pheltom.pl/katalogi/FAG%20uszkodzenia%20lozysk.pdf
   (Download date: 05.12.2008)

8. Forrest, P.G., "Fatigue of Metals", Pergamon Press, (1962).

9. Fuchs, H.O., and Stephens R.I., "Metal Fatigue in Engineering", John Wiley & Sons, (1980).

10. Harris, T.A. and McCool, J. I., “On the Accuracy of Rolling Bearing Fatigue Life Prediction”, Journal of Tribology, Vol. 118, pp. 297-310, (1996).

11. Harris, T.A. and Yu, W.K., “Lundberg-Palmgren Fatigue Theory: Considerations of Failure Stress and Stressed Volume”, Journal of Tribology, Vol. 121, pp.85-89, (1999).

12. Harris, T.A., “Rolling Bearing Analysis”, 4th Edition, John Willey&Sons, Inc., (2001).

13. Ioannides, E. and Harris, T. A., “A New Fatigue Life Model for Rolling Bearings”, ASME Journal of Tribology, Vol. 107, pp. 367-378, (1985).

14. Ioannides, E., Harris, T. A., and Ragen, M., “Endurance of Aircraft Gas Turbine Mainshaft Ball Bearings-Analysis Using Improved Fatigue Life Theory: Part 1- Application to a Long-Life Bearing”, ASME Journal of Tribology, Vol. 112, pp. 304-308, (1990).

15. Kotzalas, M. N. and Harris, T. A., “Fatigue Failure Progression in Ball Bearings” ASME Journal of Tribology, Vol. 123, pp. 238-242, (2001).

16. Lamagnere, P., Fougeres, R., Lormand, G., Vincent, A., Dirodin, D., Dudragne, G., and Vergne, F., “A Physically Based Model for Endurance Limit of Bearing Steels”, Journal of Tribology, Vol. 120, pp. 421-426, (1998).

17. Lee, Y. and Taylor, D., “Stress Based Fatigue Analysis”, Testing and Analysis, pp. 103-180, (2005)

18. Lee, Y. and Taylor, D., “Strain Based Fatigue Analysis”, Testing and Analysis, pp. 181-236, (2005).

19. MSC. Software, “MSC. Fatigue, User Manual”, MSC. Software Corporation, (2005).

20. MSC. Software, “MSC. Fatigue, Quick Reference Guide”, MSC. Software Corporation, (2005).

21. MSC. Software, “MSC. Marc, User’s Guide”, MSC. Software Corporation, (2005).

22. Murakami, Y., “Metal Fatigue: Effects of Small Defects and Nonmetallic Inclusions”, Elsevier, (2002).

23. Music, O, “Analysis of Cold Ring Rolling Process”, Master of Science Thesis, Middle East Technical University, (2005).

24. Norton, R.L., “Machine Design: An Integrated Approach” 3rd Edition, Pearson Prentice Hall, (2006).

25. ORS Bearing, “Interactive Catalogue (CD)”, Ortadoğu Rulman Sanayi ve Ticaret A.S., (2005).

26. Parker, R., J., Zaretsky, E. V., “Reevaluation of the Stress-Life Relation in Rolling-Element Bearings”, NASA, (1972), http://ntrs.nasa.gov/archive/nasa/casi.ntrs.nasa.gov/19720012807_1972012807.pdf
(Download date: 17.11.2008)

27. Peterson, R.E., “Stress Concentration Factors: Charts and Relations Useful in Making Strength Calculations for Machine Parts and Structural Elements”, John Wiley& Sons Inc., (1974).

28. Pook, L. P., “Metal Fatigue, What It Is, Why It Matters”, Springer, (2007).

29. Shigley, J.E., “Mechanical Engineering Design”, 5th Edition, McGraw Hill, (1989).

30. Sraml, M., Flasker, J., and Potrc, I., “Numerical procedure for predicting the rolling contact fatigue crack initiation”, International Journal of Fatigue, pp. 585-595, (2003).

31. Stella, T., “Comparison of Bearing Life Theories and Life Adjustment Factors”, Mechanics of Contact and Lubrication Department of Mechanical and Engineering, Northeastern University, (2006), http://www1.coe.neu.edu/~smuftu/docs/MTMG2006/Group-8.pdf (Download date: 15.09.2008)

32. Suresh, S., “Fatigue of Materials”, Cambridge University Press, (1991).

33. Tallian, T. E., “Simplified Contact Fatigue Life Prediction Model-Part II: New Model”, Journal of Tribology, Vol. 114, pp. 214-222, (1992).

34. Wangquan (Winston), C. and Cheng, H. S., “Semi-Analytical Modeling of Crack Initiation Dominant Contact Fatigue Life for Roller Bearings” Journal of Tribology, Vol. 119, pp. 233-240, (1997)

35. Zahavi, E., “Fatigue Design Life Expectancy of Machine Parts”, CRC Press Inc., (1996).

36. Zaretsky, E. V., Poplawsky, J. V., Steven, M. P., “Comparison of Life Theories for Rolling-Element Bearings”, NASA, (1995), http://ntrs.nasa.gov/archive/nasa/casi.ntrs.nasa.gov/19950020354_1995120354.pdf (Download date: 19.12.2008)

37. Zaretsky, E. V., Poplawsky, J. V., Miller, C. R., “Rolling Bearing Life Prediction-Past, Present, and Future”, NASA, (2000), ntrs.nasa.gov/archive/nasa/casi.ntrs.nasa.gov/20010018968_2001018997.pdf (Download date: 19.07.2008)